Analysis and Experiments for Contra-Rotating Propeller

by
Eyal Kravitz

Bachelor of Science in Mechanical Engineering
Tel-Aviv University, 2005
Submitted to the Department of Mechanical Engineering
in Partial Fulfillment of the Requirements for the Degrees of

Master of Science in Naval Architecture and Marine Engineering
and
Master of Science in Mechanical Engineering

at the
MASSACHUSETTS INSTITUTE OF TECHNOLOGY
February 2011

Signature of Author_____
~~Department of~~ Mechanical Engineering
January 8, 2011

Certified by_____
Chryssostomos Chryssostomidis
Doherty Professor of Ocean Science and Engineering
Professor of Mechanical and Ocean Engineering
Thesis Supervisor

Accepted by_____
David E. Hardt
Professor of Mechanical Engineering
Chairman, Departmental Committee on Graduate Students

This page intentionally left blank

Analysis and Experiments for Contra-Rotating Propeller

by
Eyal Kravitz

Submitted to the Department of Mechanical Engineering on January 8, 2011
in Partial Fulfillment of the Requirements for the Degrees of

Master of Science in Naval Architecture and Marine Engineering
and
Master of Science in Mechanical Engineering

Abstract

Contra-rotating propellers have renewed interest from the naval architecture community, because of the recent development of electric propulsion drives and podded propulsors. Contra-rotating propulsion systems have the hydrodynamic advantages of recovering part of the slipstream rotational energy which would otherwise be lost utilizing a conventional screw propeller system. The application of this type of propulsion becomes even more attractive with the increasing emphasis on fuel economy and the improvement of the propulsive efficiency.

OPENPROP is an open source propeller design and analysis code that has been in development at MIT since 2007. This thesis adds another feature to the project with the off design analysis of a contra-rotating propeller set. Based on this code, the thesis offers a comparative analysis of two types of propulsors: a single propeller and a contra-rotating propeller set, which were designed for the DDG-51 destroyer class vessel. This thesis also presents the method for using these off-design analysis results to estimate ship powering requirements and fuel usage.

The results show the superiority of the contra-rotating propeller over the traditional single propeller, with increased propeller efficiency of about 9% at the design point and up to 20% at some of the off design states. The annual fuel consumption savings for the DDG-51 equipped with a CRP was a total of 8.8% fuel savings.

Thesis Supervisor: Chryssostomos Chryssostomidis
Title: Doherty Professor of Ocean Science and Engineering
Professor of Mechanical and Ocean Engineering

This page intentionally left blank

Acknowledgements

I would like to express my gratitude to my thesis advisor, and director of the MIT Sea Grant College Program, Professor Chryssostomos Chryssostomidis, for supporting me during the period I was working on this project, and for giving me the opportunity to work on such an interesting and significant topic.

I would also like to express a special thanks to Dr. Brenden Epps for his guidance during the preparation of my thesis; he has been a significant contributor for the enjoyment and satisfaction I experienced while working on this project.

For their mentoring and support during the time of my studies I am grateful to:
Captain Mark S. Welsh, USN
Commander Trent R. Gooding, USN
Commander Pete R. Small, USN

I would also like to thank the Israeli Navy for giving me the opportunity to experience the academic life at MIT and for sponsoring my graduate studies during this period.

This page intentionally left blank

Table of Contents

List of Figures

List of Tables

This page intentionally left blank

Introduction

The concept of contra rotating propellers is a very old one nearly as old as the invention of the screw propeller itself. However, the complex shafting and gearing associated with this propulsion system has prevented the wide use of this concept. Only relatively few modern applications are known.

The development of the electric propulsion in general and the podded propulsors in particular in the recent years, bring to mind of the naval architecture this type of propulsors .Contra rotating propulsion systems have the hydrodynamic advantages of recovering part of the slipstream rotational energy which would otherwise be lost to a conventional screw propeller system. The application of this type of propulsion becomes even more attractive with the increasing emphasis on the last years on fuel economy and the improvement of the propulsive efficiency. A design tool and a thorough study of the contra rotating propeller performance are in great demand.

OPENPROP is an open source propeller design and analysis code that has been in development since 2007 at MIT (Kimball and Epps, 2010). The theory contribution of this thesis is by adding another feature to this source with the implementation of the off design analysis for contra rotating propeller.

The history of contra-rotating propellers and the design theory behind the contra-rotating code are introduced in chapter one. Chapter two presents the CRP off design theory. Illustration of a contra-rotating design procedure for the DDG-51 ship class, using the off design code with the inclusive of a comparison of the two propulsors; single and contra rotating propeller are presented in chapter three. Once the efficiency superiority of the contra-rotating propeller over the conventional single propeller was studied in chapter three, the consequence with respect to the ship fuel consumption was investigated in chapter four. The propeller model design and manufacturing procedures for future experiments is described in chapter five. Conclusions and future work recommendation are presented in the last chapter of this thesis. All the supplementary calculations as well as the Matlab codes are shown in the appendices for a full completion of this work.

Chapter 1- Propeller Design Background

1.1 The history of marine propeller development

Along the marine ship design history people have always looked for new technologies to improve the ship propulsion efficiency. Whenever presenting any new novel propeller technology, the history of the predecessor evolution types is important to be introduced as well. Therefore, despite the essence of this work is the contra-rotating propeller design methodology, the development of the marine propeller over the history which leads to the contra-rotating propeller idea, will introduced in this chapter.

1.1.1 Screw propeller

The concept of screw propeller dates back to the 950 BC; the Egyptians used a screw-like device for irrigation purposes. Archimedes (287-212 BC) and later Leonardo da Vinci (1452-1519) created and drew water screws devices for pumping purposes (Taggart, 1969). However, only at the mid-17th century, the development of steam engines contributed to effective use of screw propellers and only at that time the concept of screw propeller transformed to marine propeller. Nevertheless, the screw propeller was still considered as a second mover to the paddle wheel at this time. The acknowledgment for the invention of the modern style propeller goes to Smith and Eriksson who acquired patents in 1836 for screw propellers (John Ericson RINA affairs, 2004), marking the start of its contemporary development. Eriksson's propeller design took advantage of benefits of the bladed wheel. The final step to what is now recognizable as a screw propeller was made by George Rennie's conoidal screw, Rennie combined the ideas of increased pitch, multiple blades, and minimum convolutions in what he called a Conoidal propeller, patented in 1840 (Taggart,1969). Screw propellers installed in the late of the 19th century lacked sophistication, but their performance exceeded all other devices conceived up to that time. During 1880 to 1970 Basic shape of propellers remained unchanged. Ever since, marine propeller technology has made some advancements toward greater efficiency, more reliable design, better performance, improved materials, and cavitation resistance. Marine engineers are still looking for new developments of unconventional propellers to improve the propeller efficiency and consequently the total ship fuel consumption. Among these new

developments count up the controllable pitch propeller (CPP), Skewback propeller, ducted propeller, Cycloidal propellers, water jet propulsion, and podded and Azimuth podded propulsion systems.

1.1.2 Contra-rotating propeller

The concept of having two consecutive propellers behind each other, rotating in different directions is not new. In fact, this concept is as old as the screw propeller itself, as John Ericsson's patent of 1836 included single, twin, as well as contra-rotating propellers (John Ericson RINA affairs, 2004).Although the high efficiency obtained with contra-rotating propellers has long been known, until fairly recently material technology and the need for long concentric shafts running in different directions, made the concept both technically and economically unfeasible. However, in the mid 1980's contra-rotating propellers were successfully introduced in azimuth thrusters for, utilizing the short propeller shaft and bevel gear. In the late 1980's, a distinct concept has made its way into the marine world. This new concept is referred to as podded propulsor and is distinguished from the original thruster in that its prime mover is an electric motor, situated in the hub, directly driving the propeller. The idea of placing the electric propulsion motor inside a submerged azimuthing propulsor arose by Kvaerner Masa-Yards, together with ABB Industry. Over the last decade since, podded propulsors have become more and more important, particularly on cruise liners.

In the new millennium, efforts have been concentrated on development of a novel propulsion plant using the pod unit; it has been found that the "CRP-POD propulsion system," combining the conventional propeller propulsion system with pod propulsion, is sufficiently economic and competitive in general merchant ships. The combined high efficiency of CRP and the excellent maneuverability of podded propulsors make the hybrid CRP system extremely attractive.

The concept of contra-rotating propellers can be found also in aeronautics industry, Contra-rotating aircraft propellers came into service at the end of WW II. This configuration offered a number of advantages including lower asymmetrical torque, higher efficiency, and smaller propeller disk (allowing shorter landing gear), (Carlton, 2008). But the complexity caused by the gearing mechanisms and the expensive maintenance costs resulted in the delay of contra-rotating propeller entering into service. Other fields the contra-rotating propellers are used are in the wind turbine field and in tide turbine for ocean energy utilization.

1.2 Propeller design methods developments

From the beginning of the screw propeller concept till the 19th century(the Industrial Revolution) the propeller design were based upon trial and errors ;i.e., the propeller designer produced a baseline propeller while utilizing its geometry to detect the performances changes until the best results (from their point of view) are achieved. Only at 1865, with the introduction of the Momentum theory by Rankine, the propeller design methods began to evolve.

Momentum theory, Rankine (1865-1887): This theory is based on the axial motion of the water passing through a propeller disc. The propeller thrust can be estimated by calculating the change in the waters momentum across the two faces of the disk. This theory did not concern with the propeller geometry, since the propeller is replaced by an actuator disk. Hence, this method is not useful for blade design purposes. His result, however, leads to some general conclusions about propeller actions, in particular the optimum efficiency which can be delivered by a screw propeller, named as the "Actuator disk efficiency", (Rankine, 1865).

Blade element theory, Froude (1878): In contrast to Rankin's theory, Froude developed a method which takes into account the propeller blade geometry (Froude, 1889). In his model, the propeller blade was divided up to a large number of elements; each element can be regarded as an aerofoil subject to an incident velocity. This model allows the propeller thrust and torque to be calculated provided the appropriate values of the aerofoil drag and lift coefficients are known. Although Froude's work failed to predict the propeller performance accurately, since the blade elements drag and lift coefficient were hard to find, it contained the basic principles upon modern theory is founded (Carlton,2008) .

Propeller theoretical development (1900-1960): Lanchester and Prandtl (1919) were the first who put forward the concept that the lift on a wing was due to the development of circulation around the blade elements and that a system of trailing free vortices shed from each section. The application of this theory was the understanding of the axial and tangential velocities induced by the free vortices on the blade element. Bets (1919) and followed by Lerbs (1952) established conditions for formatting the optimum circulation along the propeller blade. Lerbs introduced the lifting line method which can produce a great prediction for the moderately loaded propeller performance working in an inviscid flow At these time many lifting line procedures were formed to numerically calculate the propeller performance also for light

and heavy loaded base on different assumptions, such as Burrill (1944), and Morgan and Eckhardt (1955).The lifting line methods mostly used for preliminary design since its highly computational efficient. For a detail design and analysis, however, more accurate methods were developed.

Lifting surface model (1960-1995): In this model the blade is replaced by an infinitely thin surface which take the form of the blade camber line and upon which a distribution of vorticity is place in both spanwise and chordwise directions. Later, the sectional thicknesses could be modeled by adding a distribution of sources and sinks in the chordwise direction. In the early 1960s many lifting surface procedures made their appearance mainly due to the various computational capabilities that became available at that time. Pien (1960) is generally credited with producing the first lifting surface theories. The vortex lattice method, Kerwin and Lee (1978) is a subclass of the lifting surface method. In this approach the continuous circulation distribution (as well as the source and sinks distribution) is replaced with discrete values along the blade (or chordwise).This method found to be mostly efficient with respect of the propeller performance predictions. The basic lifting surface, however, with respect to computational efforts this method is not satisfactory efficient. Therefore, is mostly used for detail design propeller and performance analysis.

Boundary element methods (1980: recent years): This method was developed in the recent years to overcome two problems with the lifting surface models. First, is the occurrence of local errors nearby the leading edge, and the second is the errors which occur near the hub where the blades are closely spaced and relatively thick. In this method the surfaces of the propeller blades and the hub are approximate by a number of small hyprboloidal quadrilateral panels having constant source and doublet distribution. The trailing sheet is also represented by the same panel geometry. The strength of the source and doublet values are determined by solving the boundary problem at each control point which are located at each panel. Using methods of this type, good correlation between theoretical and experimental results for pressure distribution along the blade and propeller performances has been achieved.

Computational Fluid Dynamics (21st century): In the last decade, considerable advances have been made in the application of computational fluid dynamics to the analysis and design of marine propellers. A number of approaches for modeling the flow around the propeller plane have been developed. These approaches are the Reynolds Averaged Navier-Stokes (RANS) method, Large Eddy Simulation (LES), and direct numerical simulations (DNS).However, the

application of many of these methods is limited by the amount of computational effort required to derive a solution. The RANS codes were found to be the most efficient with regarded the computational effort. For this reason, these methods are currently used for research purposes rather than a practical propeller design. The usage of these method will increased in the following years with the developments of fast computers (the computer processors speeds double itself, in general, every two years)

.

1.3 Single propeller lifting line theory

What follows is a summary of propeller lifting line theory; following the formulations of Kerwin and Hadler (2010).The lifting line which used in marine propeller is by representing the Z number of blades by straight, radial, lifting lines. The bound vorticity distribution along each of the blade radial chords $\gamma_{(r,x)}$, is replaced by a concentrate single circulation $\Gamma_{(r)}$. Since all blades are equal loading and consequently have the same circulation distribution in circumferentially uniform flow, we can select one blade (or lifting line) and designate it as the key blade. The blade geometry: camber, pitch, chord, thickness etc., are represented by this radial circulation distribution. The lifting lines start at the propeller hub r_{hub} and extended to the maximum propeller radius, R. Figure 1-1 demonstrates the propeller blades as a lifting line.

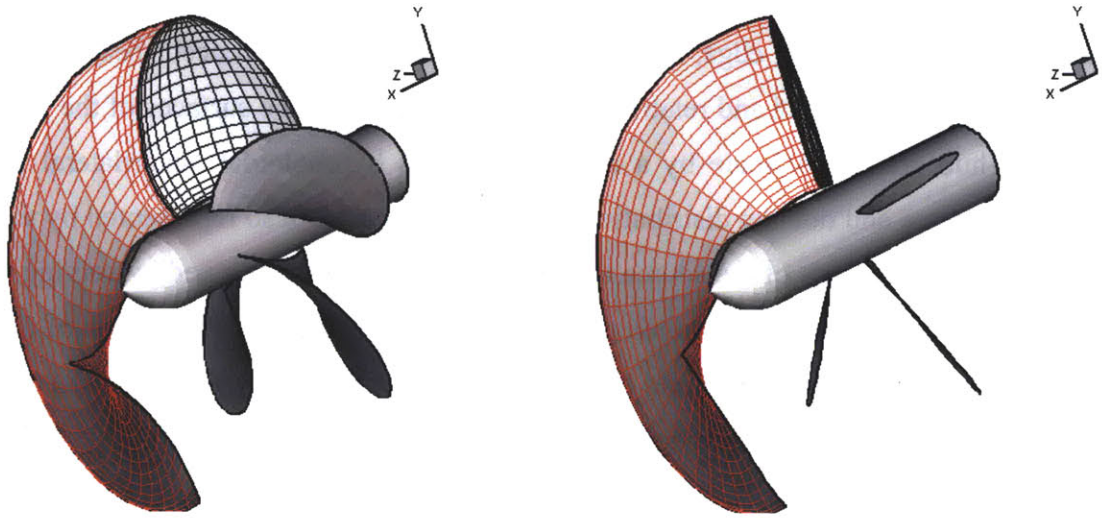

Figure 1-1: Representation of the propeller blade as a lifting line, reproduced from (Kerwin and Hadler, 2010).

Since the inflow is unsteady relative to the ship fixed coordinate system the chosen coordinate system is cylindrical (x, r, θ) with the x axis coincident with the axis of rotation of the propeller. The origin of the coordinate is in the plane of the propeller, which serves as the reference point for all axial dimensions of the propeller blade surfaces. The radial coordinate is denoted by 'r', and the angular coordinate by 'θ', which is measured in a clockwise (right-handed) sense when looking downstream with θ = 0 being at 12 o'clock. In most cases we would find that the variation in inflow velocity would be slight in the x direction, it is therefore customary to assume that the inflow field is independent of x, and that the inflow stream tubes are therefore cylindrical. To be consistent with this assumption, conservation of mass then requires that the circumferential mean radial inflow velocity be considered to be zero. However, tangential inflow velocities may be present. The coordinate system and velocity notation are describes in figure 1-2.

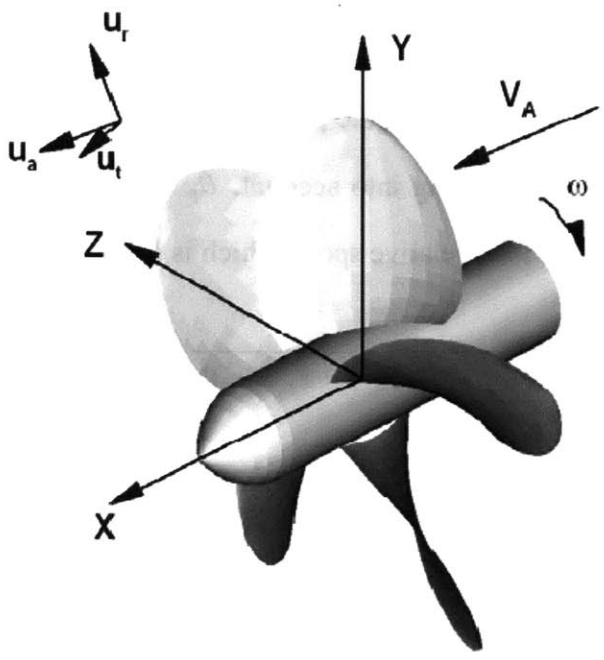

Figure 1-2: Propeller coordinate system and velocity notation, reproduced from (Kerwin and Hadler, 2010).

The velocities and forces diagram at a radial lifting line point are described in figure 1-3.

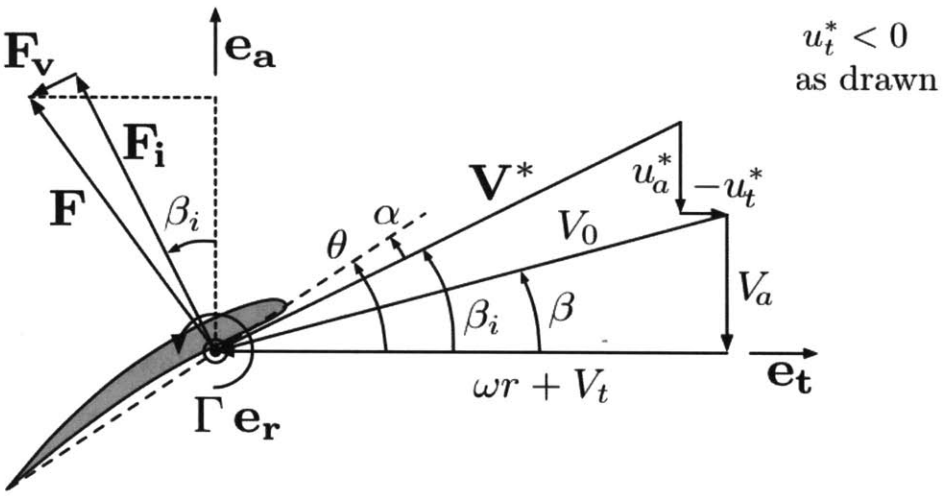

Figure 1-3 : Velocity and force diagram at a radial position on a lifting line, reproduced from (Epps, 2010b).

V_A and V_T are the axial and tangential inflows velocities, respectively. r is the lifting line radial location, wr is the propeller rotational speed, u_a^*, u_t^* are the axial and tangential induced velocities, respectively. β_i is the hydrodynamic pitch angle ,and β is the same angle when the propeller induced velocities are not taking into account. θ_P is the geometric pitch angle , α is the angle of attack ,and V^* is the total relative speed which is calculated by the next equation,

$$V^* = \sqrt{(V_a + u_a^*)^2 + (w\,r + V_t + u_t^*)^2} \tag{1.1}$$

and its orientation with respect to the plane of rotation - the hydrodynamic pitch angle is,

$$\beta_i = \arctan\left(\frac{V_a + u_a^*}{w\,r + V_t + u_t^*}\right) \tag{1.2}$$

Expression of the inviscid force (lift) acting on a vortex locates at radius r, can be calculated using the local Kutta-Joukowski's law:

$$F_i = \rho V^* \Gamma \tag{1.3}$$

and is directed at right angle to the total relative velocity (V^*).

The effect of the viscous drag force on the radial section can be determined by 2D experimental data or by theoretical means of the two dimensional drag coefficients. The radial viscous force can be expressed as:

$$F_v = \tfrac{1}{2}\rho\left(V^*\right)^2 C_D \cdot c \tag{1.4}$$

where c is the radial chord length and C_D is the 2D drag coefficient. This force acts with direction parallel to V^*.

To produce the total propeller thrust and torques, the lift and viscous forces are parted into two forces; axial (thrust) and tangential torque). The radial forces are then integrated along the blade (from the hub radius to the max blade radius), and multiple with the number of blades Z. The total thrust (T) and torque (Q) will then be:

$$T = \rho Z \int_{R_{hub}}^{R} [V^* \Gamma \cos\beta_i - \frac{1}{2}\left(V^*\right)^2 c C_D \sin\beta_i] dr \tag{1.5}$$

$$Q = \rho Z \int_{R_{hub}}^{R} [V^* \Gamma \sin\beta_i + \frac{1}{2}\left(V^*\right)^2 c C_D \cos\beta_i] dr \tag{1.6}$$

where $V^* \cdot \cos\beta_i$ is the tangential velocity equal to $w\,r + V_t + u_t^*$,and $V^* \cdot \sin\beta_i$ is the axial velocity equal to $V_a + u_a^*$.

After formulating the required equations for computing the propeller thrust and torque, the propeller efficiency is then can calculated. However, the circulation distribution and the radial induced velocities are still unknown. The following sections will introduce the Vortex lattice

model theory, which estimates a solution for the induced velocities and then, the optimum circulation distribution methods will be presented. However, because these theories are not the main subject of this work and they are well studied and presented in many works since the established of the lifting line theory (e.g. Kerwin and Hadler, 2010; Epps, 2010b) only a general review of the basic concepts, which are important to understand the contra-rotating propeller design method, will be introduced.

1.3.1 Vortex lattice model

In this model, each lifting line is divided to M panels of length dr. The induced velocities are calculated at control points located at the mid of each panel. The continuous bound circulation distribution is replaced with a discrete distribution lengthwise each of the lifting lines panels with strength $\Gamma_{(m)}$, located at radius $r_{(m)}$. The helical free vortex sheet is replaced with a concentrated helix vortices shed from each panel boundary. Therefore, the discrete circulation distribution can be thought as a set of vortex horseshoes, each assembles one bound vortex segment with two free trailing helix vortices. The strength of each free trailing vortices is equal to the strength difference of two adjacent bound vortex along the blade $\Gamma_{(m+1)} - \Gamma_{(m)}$.

The velocity induced from this vortices system are computed with the asymptotic formula developed by Wrench (1957), appendix A.1.The total induced velocities at each control point is the summation of the velocity induced from an individual horseshoe vortex at that point,

$$u^*_{a(n)} = \sum_{m=1}^{M} \Gamma_{(m)} \bar{u}^*_{a(n,m)} \tag{1.7}$$

$$u^*_{t(n)} = \sum_{m=1}^{M} \Gamma_{(m)} \bar{u}^*_{t(n,m)} \tag{1.8}$$

where $u^*_{a(n)}, u^*_{t(n)}$ are axial and tangential total induced velocities at control point n, respectively. $\Gamma_{(m)}$ is the strength of horseshoe vortex locate at radius $r_{v(m)}$. $\bar{u}^*_{a(n,m)}, \bar{u}^*_{t(n,m)}$ are the axial and tangential influence functions; velocity induced by a unit strength horseshoe vortex surrounding the control point at $r_{c(n)}$.

The integrations of equations 1.5 and 1.6 under the discrete form are replaced in by summations over the number of panels (M):

$$T = \rho Z \sum_{m=1}^{M} \{ [V_{t(m)} + wr_{(m)} + u^*_{t(m)}] \cdot \Gamma_{(m)} \Delta r - \frac{1}{2} V^*_{(m)} [V_{a(m)} + u^*_{a(m)}] c_{(m)} C_{D(m)} \Delta r \} \quad (1.9)$$

$$Q = \rho Z \sum_{m=1}^{M} \{ [V_{a(m)} + u^*_{a(m)}] \cdot \Gamma_{(m)} r_{(m)} \Delta r + \frac{1}{2} V^*_{(m)} [V_{t(m)} + wr_{(m)} + u^*_{t(m)}] c_{(m)} C_{D(m)} r_{(m)} \Delta r \} \quad (1.10)$$

All characteristics at equations 1.9, 1.10 are computed at control point located at radius $r_{(m)}$. These equations can now be solved if the discrete circulation distribution is known.

1.3.2 Optimum circulation

To design the most efficient propeller for a specified design point, an optimum circulation distribution method should apply. After successfully computing this distribution, the other essential propeller characteristics could analyze. During the design process, however, the circulation distribution might depart from its optimum while other considerations, such as; inception of tip vortex cavitation, are taking into account.

Betz (1919) developed an optimum condition for propeller in uniform flow based on the variational principles and Munks theorem; which states that the total force on a lifting line is unchanged if an element of bound vorticity is displaced in the streamwise direction. His result suggested that the ultimate forms of the vortices far downstream for an optimum circulation distribution are true helices and is expressed as:

$$\frac{\tan \beta_i}{\tan \beta} = const \quad (1.11)$$

The unknown constant is a function of the required propeller thrust. Lerbs (1952) expanded Betz criteria to non-uniform axial flow:

$$\frac{\tan \beta_i}{\tan \beta} = const \cdot \sqrt{1 - w_{x(r)}} \quad (1.12)$$

here, $w_{x(r)}$ is the radial wake fraction and the constant is a function of the propeller thrust.

Different procedure for calculating the optimum circulation distribution is suggested by Kerwin, Coney and Hsin (1986). In their procedure the optimum distribution is achieved by minimizing the propeller torque (equ.1.10) subjected to a constraint of a given thrust T_r. The required auxiliary function can, then, be formulated:

$$H = Q - \lambda(T - T_r) \tag{1.13}$$

λ is the Lagrange multiplier. When partial differentiate this function with respect to the unknowns circulation $\Gamma_{(m)}$ and the Lagrange multiplier and set to equal zero, the solution will provide the desirable optimum circulation distribution as well as the Lagrange multiplier.

1.3.3 Propeller geometry

Once computing the optimum circulation distribution, the required radial lift coefficient is calculated,

$$C_{L(m)} = \frac{2 \cdot \Gamma_{(m)}}{V^*_{(m)} \cdot c_{(m)}} \tag{1.14}$$

$C_{L(m)}$ is the required radial lift coefficient. The problem now is diminished to find a suitable blade section geometry which provides the required lift coefficient. The lifting theory, by itself, does not provide any method to determine the lift generated by a particular foil shape, since the details of the flow over the actual surface are completely lost in the idealization of the lifting line. The NACA serious is, hence, should be introduced.

A series of foils geometry were developed and tested by the NACA in the 30's and 40's, Abbott & Von Doenhoff (1959) tabulated all this data, and is known as the 'a' series, where the "a" denotes the fraction of the chord over which the circulation is constant. In this source many foils geometry (meanlines and thicknesses) were examined by a set of experiments and the resulted flow data were tabulated, amongst is the foil ideal lift coefficient and angle of attack. All it is necessary to complete the propeller design is to linearly scale the required lift coefficient with the chosen foil's one ,and do the same for the angle of attack to find the required radial section geometry; meanline and orientation. One foil type, the NACA meanline a=0.8 and the NACA 65A (TBM) basic thickness form was widely adopted by propeller designers for marine propeller and is also used in this work.

In summary, the first step of the lifting line linearization process was to find the required radial lift coefficients by computing the optimum circulation distribution and the velocities induced by these circulations on the lifting line. Then, the 3D problem is diminished by choosing a proper 2D foil geometry which can provide the required lift by linearly scale its characteristics

with the desired lift coefficient. These characteristics; the ideal angle of attack and the foil geometry are the base for the propeller design.

1.4 Lifting line method for CRP

The first lifting line design method for two coaxial open propellers separated apart with some distance and rotate in different directions is refer to Lerbs (1955).His contra-rotating design scheme was an extension of the single propeller lifting line with the inclusive of the interaction velocities induced by each propeller on the other. Lerbs first modeled an "equivalent" propeller while assuming no axial separation between components, compute the required characteristics of this propeller while considering the desirable thrust to be one half of the total thrust . Then, he decomposed the equivalent propeller to two separate ones. In his work the two propellers have the same number of blades. Morgan (1960) derived again Lerbs' theorem for a free running and a wake adopted inflow with the extension of any combination of number of blades. Morgan and Wrench (1965) rederived the differential equation for the equivalent circulation distribution of the CRP set, and most important derived accurate equations to calculate the interactive induced velocities.

Contrary to Morgan *et al* (1965) who decoupled the CR propellers to two different units and then designed the required characteristics by coupling two single propellers code in an iterative way, Kerwin,Coney and Hsin (1986) considered the CRP set as an integrated unit. This method was the extension of the variational scheme of the single propeller. According to them, the lifting line method for designing a contra-rotating propeller takes into account the two propellers as an integrated propulsive unit .Next; an iterative procedure is established to calculate the optimum circulation distribution at each propeller. Laskos (2010) integrated both of these methods, referring to them methods as "coupled" and "uncoupled". A major distinguish between the two is that in the "uncoupled" method, two separate sets of equations are established and then are optimized. The parameters which bond the two sets of equations, unlike from being two separated single propellers, is the consideration of the mutual velocities induced by each propeller on the other. In the "coupled" method, on the other hand, one complete set of equations is formulated and then is optimized. One of the advantages of the last method is the ability to design a multi component propeller.

The next sections will introduce the system of equations formulating the self and interaction velocities induced by each propeller component. The optimization process of the circulation distribution over each propeller lifting line will introduce as well.

In this work, the "coupled" design procedure of Kerwin, Coney, and Hsin (1986), as implemented by Laskos (2010) is used.

1.4.1 Self and mutual Induced Velocities

As mentioned in section 1.3.1, the discrete horseshoe vortex surrounding each of the m'th control point on the lifting line, consist one segment of bound vortex and two free trailing vortices shed from the panel boundary. For straight, radial, lifting lines with equal angular spacing and identical loading, the self-induced velocity at each propeller is only due to the free trailing vortices. For a purely helical wake geometry, these velocities can calculated using the asymptotic formulas developed by Wrench (1957) as same as for the single propeller case.

The mutual induced velocities on each of the lifting lines component's plane are the velocity induced by the other components' lifting lines vortices. Contrary to the self-induced velocity, the interaction velocities come from both; the bound and free vortex sheet. It can be seen from a simple geometric relationship that the circumferential mean interaction velocities induced by the bound vortices contribute only in the tangential direction. The circumferential mean interaction velocities induced by the free vortices, on the other hand, consist of axial, tangential and radial velocities. For calculating the steady forces delivered by each component the time–averaged interaction velocities are those of interest.

The contra-rotating velocity and forces diagram on one component of the CRP set is presented in figure 1-4.

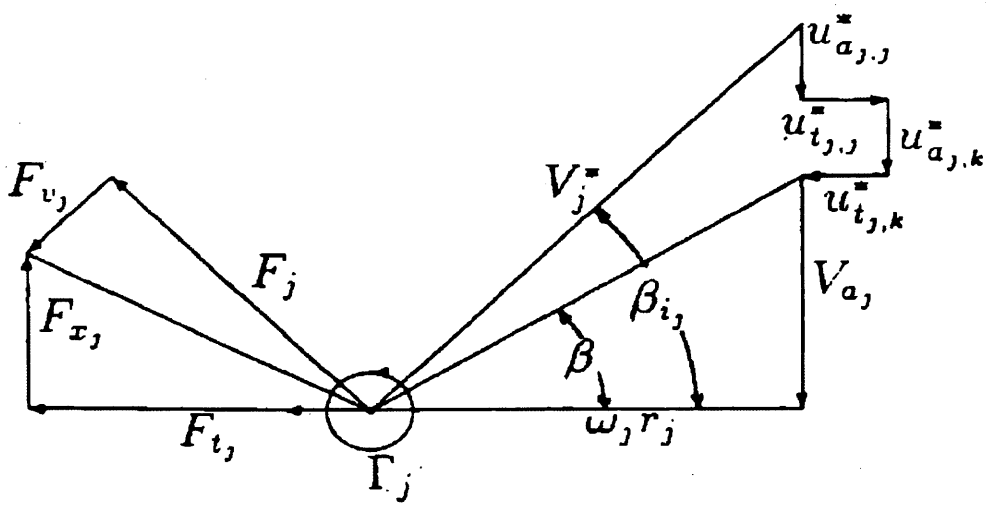

Figure 1-4: CRP velocities and forces diagram on one component of the set, reproduced from (Coney, 1989).

here, j indicates one of the components ($j = 1,2$),k is another component indicator. $u^*_{a_{j,j}}, u^*_{a_{j,k}}$ are axial self and interaction induced velocity on component j. $u^*_{t_{j,j}}, u^*_{t_{j,k}}$, are the tangential self and induced velocities on component j, respectively.

The radial interaction velocity component induced by each component is not of interest since it is not contribute to the total forces acting on the blade. Moreover, a basic assumption of the CRP code is that the slipstream is not contract, thus, the radial velocity is set to zero (by default).

Hsin (1987) compared several of methods to compute the circumferential mean interaction velocities and he found that the method developed by Hough and Ordway (1965) was the most computationally efficient way to do so. For the part due to the free trailing vorticity, the tangential induced velocities by the bound vorticity can be computed directly from the circulation conservation application of Kelvins theorem. The set of equation formulating both the free and bound induced interaction velocity are introduced in Appendix A.

1.4.2 Optimum CRP circulation distribution process

As already mentioned, the CRP code employs the described "coupled" method. In this approach one set of differential equation is formulated and is solve simultaneously to produce the loading and the circulation distribution at each component of the unit. Following Kerwin, Coney, and Hsin (1986) ,the goal is to find the discrete circulation strength values $\Gamma_1 \ldots \Gamma_{M1}, \Gamma_2 \ldots \Gamma_{M2}$ .that minimizes the total power absorbed by the propeller unit ; $p = w_1 Q_1 + w_2 Q_2$,when subjected to two constraints; the propeller needs to deliver thrust T_r for a specified moment ratio absorbed by each propeller $q = Q1/Q2$.

The auxiliary function consists the three conditions can now be formed:

$$H = (w_1 Q_1 + w_2 Q) + \lambda_T (T_1 + T_2 - T_r) + \lambda_Q (q Q_1 - Q_2) \tag{1.15}$$

From now and on, subscript "1" denotes to the forward propeller and "2" refer the aft propeller.M_1 and M_2 are the number of panels dividing the key lifting line on each component. T_1, T_2 are the thrust carried by each component, respectively.

The thrust and moment forces acting on each component are the sum of the inviscid and the viscous forces acting on all control points along the propeller lifting lines.

$$T = \rho Z \sum_{n=1}^{M_j} \{ [V_{t\,j(n)} + w_j r_{j_{(n)}} + u^*_{tj(n)}] \cdot \Gamma_{j(n)} \Delta r_j - \frac{1}{2} V^*_{j(n)} [V_{aj(n)} + u^*_{aj(n)}] c_{j(n)} C_{Dj(n)} \Delta r_j \} \tag{1.16}$$

$$Q = \rho Z \sum_{n=1}^{M} \{ [V_{aj(n)} + u^*_{aj(n)}] \cdot \Gamma_{j(n)} r_{j(n)} \Delta r_j + \frac{1}{2} V^*_{j(n)} [V_{tj(n)} + w_j r_{j(n)} + u^*_{tj(n)}] c_{j(n)} C_{D(jn)} r_{(jn)} \Delta r_j \} \tag{1.17}$$

here, $_{j(n)}$ represents, the control point 'n' at component j ,were j=1,2.

The axial and tangential velocities induced on a given control points are the sum of the self and interaction velocities induced from each of the horseshoe vortex on the lifting lines can be written as:

$$u^*_{a_j}(n) = \sum_{k=1}^{K} \sum_{m=1}^{M} \Gamma_k(m) \cdot \bar{u}^*_{a_{j,k}}(n) \tag{1.18}$$

$$u^*_{t_j}(n) = \sum_{k=1}^{K} \sum_{m=1}^{M} \Gamma_k(m) \cdot \bar{u}^*_{t_{j,k}}(n) \tag{1.19}$$

j,k=1,2

$\bar{u}^*_{a_{j,k}}(n)$ and $\bar{u}^*_{t_{j,k}}(n)$ are the axial and tangential velocities induced at control point 'n' of component j by horseshoe vortex of unit strength surrounding control point m of component k. $\Gamma_k(m)$ is the horseshoe vortex strength surrounding control point 'm' of component k. Whenever j=k, the velocity is the self-induced velocity, otherwise it is the interaction induced velocities.

After determining all the constituents in the auxiliary function with respect to the discrete circulation strengths Γ_i, the optimum circulation values can now be computed. While computing a partial derivative of the auxiliary function with respect to the unknown circulation and the unknown Lagrange multipliers λ_T, λ_Q and equal set to zero, the results provide the required optimum circulation values at each propeller. The partial derivative can be written as follows:

$$\frac{\partial H}{\partial \Gamma_j(i)} = 0 = w_1 \frac{\partial Q_1}{\partial \Gamma_j(i)} + w_2 \frac{\partial Q_2}{\partial \Gamma_j(i)} + \lambda_T[\frac{\partial T_1}{\partial \Gamma_j(i)} + \frac{\partial T_2}{\partial \Gamma_j(i)}] + \lambda_Q[\frac{\partial Q_1}{\partial \Gamma_j(i)} - \frac{\partial Q_2}{\partial \Gamma_j(i)}]$$

$$= (w_1 + q\lambda_Q)\frac{\partial Q_1}{\partial \Gamma_j(i)} + (w_2 - \lambda_Q)\frac{\partial Q_2}{\partial \Gamma_j(i)} + \lambda_T[\frac{\partial T_1}{\partial \Gamma_j(i)} + \frac{\partial T_2}{\partial \Gamma_j(i)}] \quad (1.20)$$

$$\frac{\partial H}{\partial \lambda_T} = 0 = T_1 + T_2 - T_r \quad (1.21)$$

$$\frac{\partial H}{\partial \lambda_Q} = 0 = qQ_1 - Q_2 \quad (1.22)$$

This is a system of M1+M2+2 nonlinear equations, and the same number of unknowns;M_1 circulation values on the forward key lifting line, M_2 circulation values on the aft key lifting line, and two unknown Lagrange multipliers. Kerwin (1986) sets-up an iterative procedure to solve this nonlinear problem. The Lagrange multipliers λ_T, λ_Q and the induced velocities u^*_a, u^*_t are frozen and then updated at each of the iteration set. This procedure found to converge rapidly when the initial values for the induced velocities and the multiplier λ_Q are set to zero and the multiplier λ_T is set to -1.This process is implemented in the CRP analysis code by Laskos (2010).

This page intentionally left blank

Chapter 2 – Off Design Analysis

2.1 Chapter introduction

The general propeller design procedure generates the optimum propeller characteristics for the required ship on design demands which commonly restricted by several constraints such as; hull geometry, speed engine etc. The output of the optimization process is the necessitated radial circulation distribution over the blade span (Γ) corresponded to the radial hydrodynamic pitch angle (β_i), at each propeller. This procedure is generally suitable for both; single and contra-rotating propellers and will describe in the following chapters. Once the required circulation distribution was computed, the required sectional lift coefficient (C_{Lo}) is calculated using equation 1.14.Based on this required lift coefficient and a 2D foil shape parameters $\{\tilde{f}_o/c, \tilde{\alpha}_I\}$, a determination of the blade geometry parameters; required sectional camber ratio (f_o), and the required radial ideal angle of attack (α_I) which produces the desired characteristics, is linearly scale to produce the propeller blade required geometry.

The above procedure demonstrates the design process for single and contra-rotating propeller. In order to analyze the propeller performances at off design state an additional analysis is required. The subject of this chapter is to establish a numeric procedure to analyses the contra-rotating off design states. This procedure is an extension of the single propeller off design analysis Epps (2010).

2.2 CRP off design analysis -theory

From this point until the end of this chapter, the on design characteristics will be added with the following subscription: $C_{LO}, \alpha_O, \beta_{iO}, C_{DO}$, while the off design unknowns will remain without any particular subscription: $C_L, \alpha, \beta_i, C_D$.In addition, subscripts k=1,2 are correspond to the forward and aft propeller, respectively.

After the propeller geometry was defined at the design process, a method to determine the contra-rotating propeller off design states performances is required to be established. The objective is to comprehend the propeller performance in a range of off design states (advance ratios); various propeller rotational speeds with different ship speeds.

The basic concept to cope with the off design problem is to find a method to solve a system of nonlinear equations with the same number of unknowns. The method described herein follows that of the single propeller analysis developed by Epps (2010a). The off design (OD) operating state is defined by the propellers advance coefficient,

$$Js_{1OD} = \frac{Vs}{n_{1OD}D_1} = \frac{\pi Vs}{w_{1OD}R_1} \tag{2.1}$$

$$Js_{2OD} = \frac{Vs}{n_{2OD}D_2} = \frac{\pi Vs}{w_{2OD}R_2} \tag{2.2}$$

where $J_{S_{1OD}}, J_{S_{2OD}}$ are the advance coefficients; V_S is the ship speed [m/s]; n_{1OD}, n_{2OD} are the propellers rotation speed [rps] ; w_{1OD}, w_{2OD} are the rotation rate[1/rad]; and D_1, D_2 are the propellers diameter [m].

For a given advance coefficient, the hydrodynamics unknowns are,

$\left\{V_1^*, \alpha_1, C_{L1}, G_1, u_{a1}^*, u_{t1}^*, \beta_{i1}, \overline{u}_{a11}^*, \overline{u}_{a12}^* \overline{u}_{t11}^*, \overline{u}_{t12}^*\right\}$, for the forward propeller,

$\left\{V_2^*, \alpha_2, C_{L2}, G_2, u_{a2}^*, u_{t2}^*, \beta_{i2}, \overline{u}_{a22}^*, \overline{u}_{a21}^* \overline{u}_{t22}^*, \overline{u}_{t21}^*\right\}$, for the aft propeller.

The unknown are vectors of size [1, Mp], where Mp is the number of control points lengthwise the blade.

Contradicting to the single propeller off design state, the CRP off design state is depended by the rotation rates of both propellers; fore and aft, which makes the process to be more complicated.

2.2.1 The system of nonlinear equations

Before continuing, an equations for determine the angles of attack α_1, α_2 and the lift coefficient C_{L1}, C_{L2} are required. The other equations which complete the system of equations were already introduced in chapter two for the on-design analysis.

To achieve a shock free at the leading edge, the angle of attack at the design state is forced to be the ideal angle of attack, which is straightforwardly computed from the 2D foil shape. At the off design states, on the other hand, the radial angle of attack is not the ideal one, therefore, additional equations are required. Nevertheless, after the propeller geometry was found, the radial pitch angle (θ_p) is fixed, hence the radial pitch angle at the off design state is the same as at on design state;

$$\theta_{p(k)} = \beta_{io(k)} + \alpha_{I(k)} = \beta_{i(k)} + \alpha_{(k)}$$

$$\Downarrow$$

and the net angle of attack: $$\Delta\alpha_{(k)} = \alpha_{(k)} - \alpha_{I(k)} = \beta_{iO(k)} - \beta_{i(k)} \tag{2.3}$$

The 2D section lift and drag coefficient are given in closed form by equations,

$$C_{L(k)} = C_{LO(k)} + \frac{dC_{L(k)}}{d\alpha_{(k)}}\Delta\alpha_{(k)} - \frac{dC_{L(k)}}{d\alpha_{(k)}}(\Delta\alpha_{(k)} - \Delta\alpha_{STALL})\cdot F(\Delta\alpha_{(k)} - \Delta\alpha_{STALL}) + \\ + \frac{dC_{L(k)}}{d\alpha_{(k)}}(-\Delta\alpha_{(k)} - \Delta\alpha_{STALL})\cdot F(-\Delta\alpha_{(k)} - \Delta\alpha_{STALL}) \tag{2.4}$$

$$C_{D1} = C_{DO(k)} + A(\Delta\alpha_{(k)} - \Delta\alpha_{STALL})F(\Delta\alpha_{(k)} - \Delta\alpha_{STALL}) + \\ + A(-\Delta\alpha_{(k)} - \Delta\alpha_{STALL})F(-\Delta\alpha_{(k)} - \Delta\alpha_{STALL}) - 2A(-\Delta\alpha_{STALL})F(-\Delta\alpha_{STALL}) \tag{2.5}$$

Where, $\Delta\alpha_{(k)} = \alpha_{(k)} - \alpha_{I(k)}[rad]$ is the net angle of attack, $\Delta\alpha_{STALL} = 8^o = 8\cdot\frac{\pi}{180}[rad]$ is the stall angle; $F_{(x)} = \frac{\arctan(Bx)}{\pi} + \frac{1}{2}$ is the auxiliary function; $B = 20$ is the stall sharpness parameter; $A = \frac{2 - C_{D01,2}}{\frac{\pi}{2} - \Delta\alpha_{STALL}}$ is the drag coefficient post stall slope ;and the lift curve slope $\frac{dC_{L1,2}}{d\alpha_{1,2}} = 2\pi$,which is consistent with the linear foil theory.

This model is also used for the single propeller off design analysis at OPENPROP (Epps 2010b).The drag coefficient is not required for solving the system ,but it will be valuable when introducing the calculations of the off design forces.

Another set of equations which join all the other unknowns are not unique to the off design analysis, and were also used to find the optimum dimensionless circulation distribution, and to determine the propellers geometry at the design state. At that procedure the optimum circulation distribution (G_1, C_2) was first optimized and then the lift coefficient was computed through equations 1.14. In the off design analysis, on the other hand, the lift coefficient is computed first using equation 2.4 afterwards the circulation is computed,

$$C_{L(k)} = \frac{2\Gamma_{(k)}}{V^*_{(k)} c_{(k)}} \Rightarrow \Gamma_{(k)} = \frac{C_{L(k)} V^*_{(k)} c_{(k)}}{2} \tag{2.6}$$

the relative velocity,

$$V^*_{(k)} = \sqrt{(V_a + u^*_{a(k)})^2 + (w_{OD(k)} r + V_t + u^*_{t(k)})^2} \tag{2.7}$$

and the hydrodynamic pitch angle,

$$\beta_{i(k)} = \arctan\left(\frac{V_a + u^*_{a(k)}}{w_{OD(k)} r + V_t + u^*_{t(k)}}\right) \tag{2.8}$$

where, V^* is the relative velocity; V_a is the speed of advance, which in this work is equal to the ship speed; V_t is the transverse inflow speed; $u^*_{a(k)}$ is the axial induced velocity at the fore and aft propellers; $u^*_{t(k)}$ is the tangential induced velocity; and β_i is the hydrodynamic pitch angle.

The induced velocities at each propeller are the sum of the self and interaction induced velocities, the equations for calculating these induced velocities are described in chapter one, equations 1.181 and 1.19.

Up to now, the unknown and the system of equation for the off design states were introduced, in the next paragraph the numerical method for solving this nonlinear system will be presented.

2.2.2 Newton solver method

For a linear system of equations numerous analytical and direct procedures for solving the system are accessible in the literature, such as; the Newton's method, the bisection method, and the Jacobi iteration.

In this thesis the Newton's method was selected to be used for solving the off design states. This method can often converge remarkably quickly especially if the initial guess is sufficiently near the desired root. Newton's method can fail to converge with little warning so a smart initial guess is very important.

The idea of the method is as follows:
For a set of n nonlinear equations with n unknown,

$$F(X)=\begin{bmatrix} f_1(x_1,x_2,x_3.....x_n) \\ f_2(x_1,x_2,x_3.....x_n) \\ f_3(x_1,x_2x_3.....x_n) \\ \vdots \\ f_n\ (x_1,x_2,x_3.....x_n) \end{bmatrix}=0$$

A linearization of the system, using the Taylor series expanded, can be done with the following conditions; if f is differentiable at the iterations guess ($\hat{x}$) and x is near $\hat{x}$ then,

$$f_i(x)\approx f_i(\hat{x})+\frac{\partial f_i(\hat{x})}{\partial x_1}(x_1-\hat{x}_1)+\frac{\partial f_i(\hat{x})}{\partial x_2}(x_2-\hat{x}_2)+\quad\dots\quad+\quad\frac{\partial f_i(\hat{x})}{\partial x_n}(x_n-\hat{x}_n)$$

and, in a vector form,

$$f(x)\approx f(\hat{x})+J(\hat{x})(x-\hat{x})=f(\hat{x})+J(\hat{x})dx$$

where $f(x)$ is called the residual vector, and the derivative matrix (or Jacobian matrix) $J(\hat{x})$ evaluated at $\hat{x}$ is defined as follow,

$$J(\hat{x}) = \begin{bmatrix} \frac{\partial f_1(\hat{x})}{\partial x_1} & \frac{\partial f_1(\hat{x})}{\partial x_2} & \cdots & \frac{\partial f_1(\hat{x})}{\partial x_n} \\ \frac{\partial f_2(\hat{x})}{\partial x_1} & \frac{\partial f_2(\hat{x})}{\partial x_2} & \cdots & \frac{\partial f_2(\hat{x})}{\partial x_n} \\ \vdots & \vdots & \vdots & \vdots \\ \frac{\partial f_n(\hat{x})}{\partial x_1} & \frac{\partial f_n(\hat{x})}{\partial x_2} & \cdots & \frac{\partial f_n(\hat{x})}{\partial x_n} \end{bmatrix}$$

In order to derive the residual vector to zero the desired change in the state vector is found by solving,

$$f(\hat{x}) + J(\hat{x})dx = 0$$
$$dx = -J^{-1}(\hat{x})f(\hat{x})$$

and continuing , the next guess for the next iteration is,

$$\hat{x}^{+} = \hat{x} + dx$$

$\hat{x}^{+}$ is the new guess ,while $\hat{x}$ is the current guess. The new guess is installed back to the system of equation and the procedure is repeated until convergence.

2.2.3 Implementation of the Newton's solver

2.2.3.1 Final configuration

This paragraph demonstrate the implementation of the Newton's solver to find the off design states; solving the system of the off design nonlinear equations. Deciding which equations are added to the Newton's solver and which are left out is a very challenges task. Several Newton solver configurations were examined, in a manner of computer time consumption and a convergence of the system. A discussion of the options which were not integrated in the solver will be follow after introducing the final set up.

Since the system of equations are coupled through the parameters $\{ \beta_{i1}, \bar{u}^{*}_{a11}, \bar{u}^{*}_{a12} \bar{u}^{*}_{t11}, \bar{u}^{*}_{t12} \}$ and $\{ \beta_{i2}, \bar{u}^{*}_{a22}, \bar{u}^{*}_{a21} \bar{u}^{*}_{t22}, \bar{u}^{*}_{t21} \}$they can be decoupled by considering two states vectors:

$$x = \left\{ \quad V_1^*, \alpha_1, C_{L1}, G_1, u_{a1}^*, u_{t1}^*, V_2^*, \alpha_2, C_{L2}, G_2, u_{a2}^*, u_{t2}^* \quad \right\}, \text{ and}$$

$$y = \left\{ \beta_{i1}, \overline{u}_{a11}^*, \overline{u}_{a12}^*, \overline{u}_{t11}^*, \overline{u}_{t12}^*, \beta_{i2}, \overline{u}_{a22}^*, \overline{u}_{a21}^* \overline{u}_{t22}^*, \overline{u}_{t21}^* \right\}$$

During each iteration vector state x is updated at each control point (every unknown is actually a vector of M_p control points), using the Newton solver method .With the updated x and equations: 1.18 and 1.19 vector y is then updated. A convergence test is then calculated, and if necessary, the procedure is repeated until convergence of the system.

The final residual vector consist the following equations:

$$R_m = \begin{bmatrix} V_1^* - \sqrt{(V_a + u_{a1}^*)^2 + (w_{1OD} r + V_t + u_{t1}^*)^2} \\ \Delta\alpha_1 - (\beta_{i1O} - \beta_{i1}) \\ C_{L1} - C_{L1(\alpha_1)} \\ \Gamma_1 - \frac{1}{2} \cdot C_{L1} V_1^* c_1 \\ u_{a1(m)}^* - \left(\sum_{j=1}^{M1} \Gamma_{1(j)} \overline{u}_{a11(m,j)}^* + \sum_{j=1}^{M2} \Gamma_{2(j)} \overline{u}_{a12(m,j)}^* \right) \\ u_{t1(m)}^* - \left(\sum_{j=1}^{M1} \Gamma_{1(j)} \overline{u}_{t11(n,j)}^* + \sum_{j=1}^{M2} \Gamma_{2(j)} \overline{u}_{t12(m,j)}^* \right) \\ V_2^* - \sqrt{(V_a + u_{a2}^*)^2 + (w_{2OD} r + V_t + u_{t2}^*)^2} \\ \alpha_2 - \alpha_{2ideal} - (\beta_{i2O} - \beta_{i2}) = \Delta\alpha_2 - (\beta_{i2O} - \beta_{i2}) \\ C_{L2} - C_{L2(\alpha_2)} \\ \Gamma_2 - \frac{1}{2} \cdot C_{L2} V_2^* c_2 \\ u_{a2(m)}^* - \left(\sum_{j=1}^{M1} \Gamma_{2(j)} \overline{u}_{a22(m,j)}^* + \sum_{m=1}^{M2} \Gamma_{1(j)} \overline{u}_{a21(m,j)}^* \right) \\ u_{t2(m)}^* - \left(\sum_{m=1}^{M1} \Gamma_{2(j)} \overline{u}_{t22(m,j)}^* + \sum_{m=1}^{M2} \Gamma_{1(j)} \overline{u}_{t21(m,j)}^* \right) \end{bmatrix}_{12*1}$$

where, each of the unknowns is evaluated at the $r_{c(m)}$ control point, for each propeller; assuming both propellers have an equal number of panels (control points). This set up of the residual vector found to be the most efficient vector to lead the system to a finite solution. In order to drive the residual vector to zero, the desired change in the state vector dx_m is found by solving the matrix equation:

$$R_m + J_m dx_m = 0$$

where the Jacobian matrix, as was mentioned in the previous paragraphs, is the derivatives of each unknowns with respect to the unknowns others in the matrix.

$$J_{m(i,j)} = \frac{\partial R_{m(i)}}{\partial X_{m(j)}}$$

This matrix is complicated since all the variables in vector x are dependent to each other, and some are also dependent threw the other unknowns (vector y); which were not included in the residual vector. The way to put together this matrix is by using the chain rule derivatives for two unknowns in the residual vector that are dependent by other unknowns which are not included in the residual vector. For all the others, the direct derivatives are computed.

The non-zero elements of the Jacobian matrix are,

$$
J_{m(i,j)}=\left[\begin{array}{l}
J_{(i,i)}=\dfrac{\partial R_{V_1^*}}{\partial V_1^*}=\dfrac{\partial R_{\alpha_1}}{\partial \alpha_1}=\dfrac{\partial R_{C_{L1}}}{\partial C_{L1}}=\dfrac{\partial R_{G_1}}{\partial G_1}=\dfrac{\partial R u_{a1}^*}{\partial u_{a1}^*}=\dfrac{\partial R u_{t1}^*}{\partial u_{t1}^*}=\dfrac{\partial R_{V_2^*}}{\partial V_2^*}=\dfrac{\partial R_{\alpha_2}}{\alpha_2}=\dfrac{\partial R_{C_{L2}}}{\partial C_{L2}}=\dfrac{\partial R_{G_2}}{\partial G_2}=\dfrac{\partial R u_{a2}^*}{\partial u_{a2}^*}=\dfrac{\partial R u_{t2}^*}{\partial u_{t2}^*}=1,(i=1\ldots12)\\
J_{(1,5)}=\dfrac{\partial R_{V_1^*}}{\partial u_{a1}^*}=-\dfrac{V_a+u_{a1}^*}{\sqrt{\left(V_a+u_{a1}^*\right)^2+\left(w_{OD1}r_{c1}+V_t+u_{t1}^*\right)^2}}\\
J_{(1,6)}=\dfrac{\partial R_{V_1^*}}{\partial u_{t1}^*}=-\dfrac{w_{OD1}r_{c1}+V_t+u_{t1}^*}{\sqrt{\left(V_a+u_{a1}^*\right)^2+\left(w_{OD1}r_{c1}+V_t+u_{t1}^*\right)^2}}\\
J_{(2,5)}=\dfrac{\partial R_{\alpha_1}}{\partial u_{a1}^*}=\dfrac{\partial R_{\alpha_1}}{\partial \beta_{i1}}\cdot\dfrac{\partial \beta_{i1}}{\partial u_{a1}^*}=\dfrac{\partial R_{\alpha_1}}{\partial \beta_{i1}}\cdot\dfrac{\partial \tan(\beta_{i1})}{\partial \tan(\beta_{i1})}\cdot\dfrac{\partial \tan(\beta_{i1})}{\partial u_{a1}^*}=\dfrac{1}{1+\tan^2(\beta_{i1})}\cdot\dfrac{1}{w_{OD1}r_{c1}+V_t+u_{t1}^*}\\
J_{(2,6)}=\dfrac{\partial R_{\alpha_1}}{\partial u_{t1}^*}=\dfrac{\partial R_{\alpha_1}}{\partial \beta_{i1}}\cdot\dfrac{\partial \beta_{i1}}{\partial u_{t1}^*}=\dfrac{\partial R_{\alpha_1}}{\partial \beta_{i1}}\cdot\dfrac{\partial \tan(\beta_{i1})}{\partial \tan(\beta_{i1})}\cdot\dfrac{\partial \tan(\beta_{i1})}{\partial u_{t1}^*}=\dfrac{1}{1+\tan^2(\beta_{i1})}\cdot\dfrac{-\tan(\beta_{i1})}{w_{OD1}r_{c1}+V_t+u_{t1}^*}\\
J_{(3,2)}=\dfrac{\partial R_{C_{L1}}}{\partial \alpha_1}=-\dfrac{\partial C_{L1(\alpha_1)}}{\partial \alpha_1}\\
J_{(4,1)}=\dfrac{\partial R_{\Gamma_1}}{\partial V_1^*}=-\dfrac{1}{2}C_{L1}c_1\\
J_{(4,3)}=\dfrac{\partial R_{\Gamma_1}}{\partial C_{L1}}=-\dfrac{1}{2_S}V_1^*c_1\\
J_{(5,2)}=\dfrac{\partial R_{a1}}{\partial \alpha_1}=\sum_{j=1}^{M1}\Gamma_{1(j)}\dfrac{\partial \overline{u}_{a11(m,j)}^*}{\partial \beta_{i1}}\\
J_{(5,4)}=\dfrac{\partial u_{a1}^*}{\partial \Gamma_1}=-\overline{u}_{a11(m,m)}^*\\
J_{(5,8)}=\dfrac{\partial u_{a1}^*}{\partial \alpha_2}=\sum_{j=1}^{M1}\Gamma_{2(j)}\dfrac{\partial \overline{u}_{a12(m,j)}^*}{\partial \beta_{i2}}\\
J_{(5,10)}=\dfrac{\partial u_{a1}^*}{\partial \Gamma_2}=-\overline{u}_{a12(m,m)}^*\\
J_{(6,2)}=\dfrac{\partial u_{t1}^*}{\partial \alpha_1}=\sum_{j=1}^{M1}\Gamma_{1(j)}\dfrac{\partial \overline{u}_{t11(m,j)}^*}{\partial \alpha_1}=\sum_{j=1}^{M1}\Gamma_{1(j)}\dfrac{\partial \overline{u}_{t11(m,j)}^*}{\partial \beta_{i1}}\cdot\dfrac{\partial \beta_{i1}}{\partial \alpha_1}=\sum_{j=1}^{M1}\Gamma_{1(j)}\cdot\dfrac{\partial \overline{u}_{t11(m,j)}^*}{\partial \beta_{i1}}\\
J_{(6,4)}=\dfrac{\partial u_{t1}^*}{\partial \Gamma_1}=-\overline{u}_{a11(m,m)}^*\\
J_{(6,8)}=\dfrac{\partial u_{t1}^*}{\partial \alpha_2}=\sum_{j=1}^{M1}\Gamma_{2(j)}\dfrac{\partial \overline{u}_{t12(m,j)}^*}{\partial \alpha_2}=\sum_{j=1}^{M1}\Gamma_{2(j)}\dfrac{\partial \overline{u}_{t12(m,j)}^*}{\partial \beta_{i2}}\cdot\dfrac{\partial \beta_{i2}}{\partial \alpha_2}=\sum_{j=1}^{M1}\Gamma_{2(j)}\dfrac{\partial \overline{u}_{t12(m,j)}^*}{\partial \beta_{i2}}\\
J_{(6,10)}=\dfrac{\partial u_{t1}^*}{\partial \Gamma_2}=-\overline{u}_{a12(m,m)}^*
\end{array}\right]
$$

$$
J_{m(i,j)=}\left[\begin{array}{l}
J_{(7,11)}=\dfrac{\partial R_{V_2^*}}{\partial u_{a2}^*}=-\dfrac{V_a+u_{a2}^*}{\sqrt{\left(V_a+u_{a2}^*\right)^2+\left(w_{OD2}r_{c2}+V_t+u_{t2}^*\right)^2}} \\
J_{(7,12)}=\dfrac{\partial R_{V_2^*}}{\partial u_{t2}^*}=-\dfrac{w_{OD2}r_{c2}+V_t+u_{t2}^*}{\sqrt{\left(V_a+u_{a1}^*2\right)^2+\left(w_{OD2}r_{c2}+V_t+u_{t2}^*\right)^2}} \\
J_{(8,11)}=\dfrac{\partial R_{\alpha 2}}{\partial u_{a2}^*}=\dfrac{\partial R_{\alpha_2}}{\partial \beta_{i2}}\cdot\dfrac{\partial \beta_{i2}}{\partial u_{a2}^*}=\dfrac{\partial R_{\alpha 2}}{\partial \beta_{i2}}\cdot\dfrac{\partial \beta_{i2}}{\partial \tan(\beta_{i2})}\cdot\dfrac{\partial \tan(\beta_{i2})}{\partial u_{a2}^*}=\dfrac{1}{1+\tan^2(\beta_{i2})}\cdot\dfrac{1}{w_{OD2}r_{c2}+V_t+u_{t2}^*} \\
J_{(8,12)}=\dfrac{\partial R_{\alpha 2}}{\partial u_{t2}^*}=\dfrac{\partial R_{\alpha_2}}{\partial \beta_{i2}}\cdot\dfrac{\partial \beta_{i2}}{\partial u_{t2}^*}=\dfrac{\partial R_{\alpha 2}}{\partial \beta_{i2}}\cdot\dfrac{\partial \beta_{i2}}{\partial \tan(\beta_{i2})}\cdot\dfrac{\partial \tan(\beta_{i2})}{\partial u_{t2}^*}=\dfrac{1}{1+\tan^2(\beta_{i2})}\cdot\dfrac{-\tan(\beta_{i2})}{w_{OD2}r_{c2}+V_t+u_{t2}^*} \\
J_{(9,8)}=\dfrac{\partial R_{C_{L2}}}{\partial \alpha_2}=-\dfrac{\partial C_{L2(\alpha 2)}}{\partial \alpha_2} \\
J_{(10,7)}=\dfrac{\partial R_{\Gamma_2}}{\partial V_2^*}=-\dfrac{1}{2}C_{L1}c_1 \\
J_{(10,9)}=\dfrac{\partial R_{\Gamma_1}}{\partial C_{L1}}=-\dfrac{1}{2}V_2^*c_2 \\
J_{(11,2)}=\dfrac{\partial u_{a2}^*}{\partial \alpha_1}=\sum_{j=1}^{M1}\Gamma_{1(j)}\dfrac{\partial \overline{u}_{a12(m,j)}^*}{\partial \beta_{i1}} \\
J_{(11,4)}=\dfrac{\partial u_{a2}^*}{\partial \Gamma_1}=-\overline{u}_{a12(m,m)}^* \\
J_{(11,8)}=\dfrac{\partial u_{a2}^*}{\partial \alpha_2}=\sum_{j=1}^{M1}\Gamma_{2(j)}\dfrac{\partial \overline{u}_{a22(m,j)}^*}{\partial \beta_{i2}} \\
J_{(11,10)}=\dfrac{\partial u_{a2}^*}{\partial \Gamma_2}=-\overline{u}_{a22(m,m)}^* \\
J_{(12,2)}=\dfrac{\partial u_{t2}^*}{\partial \alpha_1}=\sum_{j=1}^{M1}\Gamma_{1(j)}\cdot\dfrac{\partial \overline{u}_{t21(m,j)}^*}{\partial \beta_{i1}} \\
J_{(12,4)}=\dfrac{\partial u_{t2}^*}{\partial \Gamma_1}=-\overline{u}_{t11(m,m)}^* \\
J_{(12,8)}=\dfrac{\partial u_{t2}^*}{\partial \alpha_2}=\sum_{j=1}^{M1}\Gamma_{2(j)}\dfrac{\partial \overline{u}_{t22(m,j)}^*}{\partial \beta_{i2}} \\
J_{(12,10)}=\dfrac{\partial u_{t2}^*}{\partial \Gamma_2}=-\overline{u}_{t12(m,m)}^*
\end{array}\right]
$$

To visualizes the Jacobin matrix, the matrix elements are in the following format; non-zeros elements are represented with X,

$$J_{m(i,j)} = \begin{bmatrix} 1 & 0 & 0 & 0 & X & X & 0 & 0 & 0 & 0 & 0 & 0 \\ 0 & 1 & 0 & 0 & X & X & 0 & 0 & 0 & 0 & 0 & 0 \\ 0 & X & 1 & 0 & 0 & 0 & 0 & 0 & 0 & 0 & 0 & 0 \\ X & 0 & X & 1 & 0 & 0 & 0 & 0 & 0 & 0 & 0 & 0 \\ 0 & X & 0 & X & 1 & 0 & 0 & X & 0 & X & 0 & 0 \\ 0 & X & 0 & X & 0 & 1 & 0 & X & 0 & X & 0 & 0 \\ 0 & 0 & 0 & 0 & 0 & 0 & 1 & 0 & 0 & 0 & X & X \\ 0 & 0 & 0 & 0 & 0 & 0 & 0 & 1 & 0 & 0 & X & X \\ 0 & 0 & 0 & 0 & 0 & 0 & 0 & X & 1 & 0 & 0 & 0 \\ 0 & 0 & 0 & 0 & 0 & 0 & X & 0 & X & 1 & 0 & 0 \\ 0 & X & 0 & X & 0 & 0 & 0 & X & 0 & X & 1 & 0 \\ 0 & X & 0 & X & 0 & 0 & 0 & X & 0 & X & 0 & 1 \end{bmatrix}$$

Once finding the required change increment for the new guess, vector state x is then updated,

$$x^{new} = x^{current} + dx$$

Next, vector y is updated through equations 1.18 and 1.19. This process is repeated until convergence of the system to a finite solution.

The prescribed off design analysis for the CR propellers is implemented in the **CRP_Analyzer.m** function file. This function can be found in appendix B.1.

2.2.3.2 Not selected configurations

In the last paragraph the final configuration for the states vectors x and y was presented. However, other configurations to form these vectors were examined and are briefly presenting next.

The first configuration is included two different vectors; x_1 and x_2; each vector consists only one of the different propellers unknowns. And a third vector y which consists the other unknowns.

$$x_1 = \left\{V_1^*, \alpha_1, C_{L1}, G_1\right\}$$
$$x_2 = \left\{V_2^*, \alpha_2, C_{L2}, G_2\right\}$$
$$y = \left\{\beta_{i1}, u_{a1}^*, u_{t1}^*, \overline{u}_{a11}^*, \overline{u}_{a12}^*, \overline{u}_{t11}^*, \overline{u}_{t12}^*, \beta_{i2}, u_{a2}^*, u_{t2}^*, \overline{u}_{a22}^*, \overline{u}_{a21}^* \overline{u}_{t22}^*, \overline{u}_{t21}^*\right\}$$

at each iteration, state vectors x_1 and x_2 are updates using the Newton solver,

$$dx_{1m} = -J_{1m}^{-1} R_{1m} \rightarrow X_{1m}^{new} = x_{1m}^{current} + dx_{1m}$$
$$dx_{2m} = -J_{2m}^{-1} R_{2m} \rightarrow X_{2m}^{new} = x_{2m}^{current} + dx_{2m}$$

where, R_{1m}, J_{1m} and $R_{2m,} J_{2m}$ are the residual vectors and Jacobian matrices for the forward(x_1) and aft (x_2)propellers unknowns, respectively.

The two propellers unknowns are then combined in vector y which is updated using equations 1.18 and 1.19.This method was not established a solution since the system of equations was not converged.

Another configuration, which indeed gives a finite solution, formed by combining the two vectors x_1 and x_2 to one vector x with the same vector x,

$$x = \left\{V_1^*, \alpha_1, C_{L1}, G_1, V_2^*, \alpha_2, C_{L2}, G_2\right\}$$
$$y = \left\{\beta_{i1}, u_{a1}^*, u_{t1}^*, \overline{u}_{a11}^*, \overline{u}_{a12}^*, \overline{u}_{t11}^*, \overline{u}_{t12}^*, \beta_{i2}, u_{a2}^*, u_{t2}^*, \overline{u}_{a22}^*, \overline{u}_{a21}^* \overline{u}_{t22}^*, \overline{u}_{t21}^*\right\}$$

However, the final configuration that was presented in the last paragraph generates the most efficient result for the system of the nonlinear equations.

2.3 CRP open water diagrams

Before presenting the open water diagrams in the next chapter, several equations are needed to be introduced to understand the scheme of the curves. This paragraph includes the CRP equations and theory which are required for establishing the open water diagrams.

Once the off design states computation is completed, the off design thrust and torque can be computed, at each state, using equations 1.9 and 1.10.The thrust coefficient C_{T1}, C_{T2} ,and the torque coefficient C_{Q1}, C_{Q1} are calculated as well , here k=1,2 for the fore and aft propeller, respectively.

$$C_{T(k)} = \frac{T_{(k)}}{\frac{1}{2}\rho V_{(k)}^{*2} \pi R^2} \tag{2.11}$$

$$C_{Q(k)} = \frac{Q_{(k)}}{\frac{1}{2}\rho V_{(k)}^{*2} \pi R^3} \tag{2.12}$$

the propeller thrust coefficient K_{T1}, K_{T2} and torque coefficient K_{Q1}, K_{Q2} are computed next,

$$K_{T(k)} = C_{T(k)} \cdot \frac{\pi}{8} J_{S(k)}^2 \tag{2.13}$$

$$K_{Q(k)} = C_{Q(k)} \cdot \frac{\pi}{16} J_{S(k)}^2 \tag{2.14}$$

$$\begin{aligned} K_T &= K_{T1} + K_{T2} \\ K_Q &= K_{Q1} + K_{Q2} \end{aligned} \tag{2.15}$$

2.3.1 CRP open water propeller efficiency

Efficiency of a two stage propulsors is given as,

$$\eta_{0(CRP)} = \frac{T_1 \cdot V_{A1} + T_1 \cdot V_{A1} - T_h \cdot V_S}{w_1 \cdot Q_1 + w_2 \cdot Q_2} \tag{2.16}$$

where, T, Q, w are the thrust, torque and rotational speed ratio for each of the propellers. V_{A1}, V_{A2} are the volumetric mean effective inflows for the forward and aft propellers ,respectively, defined as,

$$V_A = \frac{2}{(R^2 - r_h^2)} \int_{r_h}^{R} r V_{a(r)} dr \tag{2.17}$$

The hub drag can be approximated as follows,

$$T_h = \frac{\rho}{16} (\ln \frac{r_h}{r_0} + 3)[Z_1 \Gamma_1(1) - Z_2 \Gamma_2(1)]^2 \tag{2.18}$$

and in non-dimensional form:

$$CT_h = 0.5(\ln \frac{r_h}{r_0} + 3)[Z_1 G_1(1) - Z_2 G_2(1)]^2 \tag{2.19}$$

r_h is the hub radius ; r_0 is the core radius of the hub vortex; Z_1, Z_2 are the number of blades for each propeller; and $\Gamma_1, \Gamma_2; G_1, G_2$ are the circulation and non-dimensional circulation at the blade root for each propeller, respectively.

The hub drag formed as a result of a concentrated hub vortex. This force is not the focus of this work and is explained in details by Wang (1985). However, the problem of the hub drag can be overcome with the contra-rotating propeller at the design process, if the circulation distribution is well designed so that $Z_1 \Gamma_1(1) = Z_2 \Gamma_2(1)$, than the hub drug force can be eliminated.

This page intentionally left blank

Chapter 3- Illustration Example for DDG-51

3.1 Chapter introduction

The objective of this chapter is to demonstrate a physical contra-rotating propeller design for an existing ship. For this work, the well-studied DDG-51 was chosen to be situated as a case study. The goal is to evaluate a new propulsur for the DDG-51 propulsion configuration; from two single controllable pitch propellers to two sets of contra-rotating propeller. The design procedure for both; single and contra-rotating propellers is the interest of this chapter. When propeller designer lunch the process of a propeller designing for a given ship, some essential information is required before starting the design process. First, the on design data; i.e. ship required thrust for a specified ship speed, is delivered by the ship naval architecture. This information is based on a model ship resistance experiments at the tow tank and the ship predicted operational profile. In addition, the wake fraction at the propeller disk is required for computing the actual radial inflow velocity; which in most cases is not the ship speed (depend on the location of the propeller and the propulsur method). Any constraints which can affect the propeller design process must introduce to the designer, such as: propeller maximum diameter, propeller hub diameter, propeller speed, etc. Then, a parametric study is conducted to find the optimum geometric and hydrodynamics parameters which produce the best propeller efficiency, and as a result less fuel consumption. After presenting the contra-rotating propeller design theory in the last chapter, the on design DDG-51 requirements and a parametric study for both; single and contra-rotating propeller are introduced in this chapter. Furthermore, the manufacturing process of the full scale propeller will introduce as well.

An off design analysis for these propellers as well as a detailed comparison between the two types of propulsors will present in this chapter as well. Before continuing with the parametric study, the discussed ship; the DDG-51 basic naval characteristics are introduced.

3.2 DDG-51-Overview

3.2.1 DDG-51-background

As mentioned in the introduction to this chapter, the objective of this thesis is to analyze a comparison between two different propulsors type; single and contra-rotating propellers. To do so, it was decided to design these propulsors to an existent ship that is already well studied. An overview the case study ship will present next.

The USS Arleigh Burke (DDG-51) is a guided missile destroyer class ship, which has a full load displacement of 8,350 tons, length of 506 feet, and has a 62 foot beam. The ship is driven by two shafts powered by four LM2500 engines to produce 100,000 total shaft horsepower. The ship's maximum speed is in excess of 30 knots, and its endurance speed is 20 knots. Tables 3-1 and 3-2 show the main geometric and propulsion parameters of the ship, respectively.

Displacement [L-ton]	8350	**Block Coefficient**	0.519
LBP[ft]	466	**Prismatic Coeff**	0.626
Beam[ft]	62	**Waterplane Coefff**	0.788
Draft[ft]	20.7	**Midship section coeff**	0.828
L/B	7.898	**Waterplane area(sq ft)**	21665

Table 3-1: DDG-51 geometric parameters of the underwater hull

Propeller type	Controllable pitch
Number of propellers	2
Number of blades	5
Propeller Diameter [ft]	17
Design Pitch at 0.7R[ft]	29.2
P/D=Pitch Ratio at 0.7R	1.72
Disk Area[sq ft]	227

Table 3-2: DDG-51 Propeller parameters (Tsai,1994)

3.2.2 DDG-51- propeller design requirements

The designed thrust is based on 15% redundant above the ship required thrust at the design speed (20 knts).The ship required thrust is required to be divided evenly by the number of propellers (Kp), which in this design is the same number as for the existing DDG-51.The ship required thrust, as measured at the sea trials at August 1991 is shown in figure 3-1.

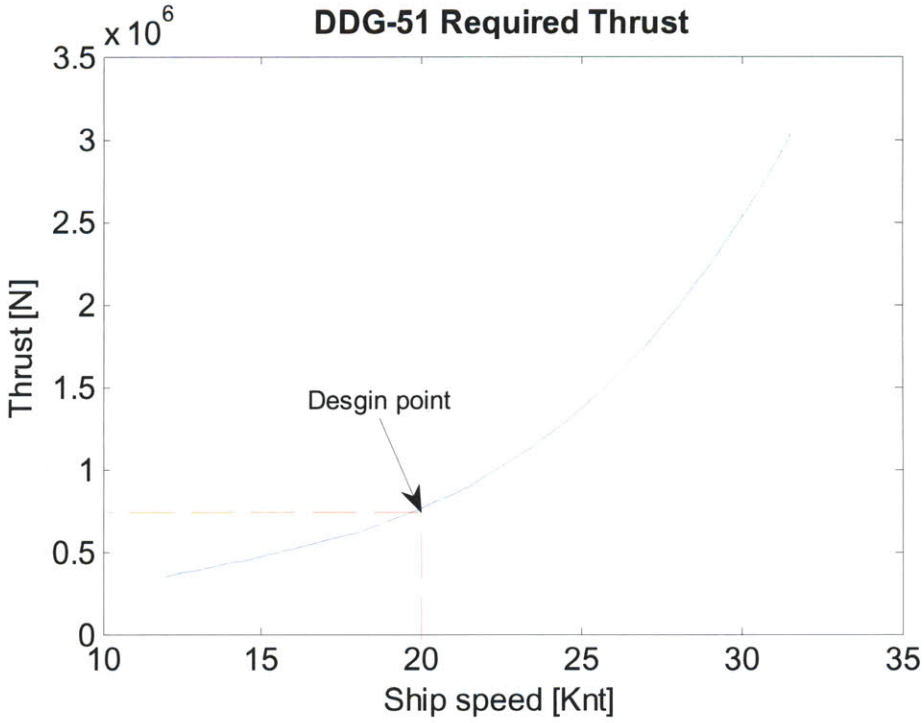

Figure 3-1: DDG-51 total required thrust (Tsai,1994))

The DDG-51 design characteristics are presented in table 3-3.

	Metric	English
Ship required thrust [Tr] at design speed (20 knt)	753 [kN]	169,400[lbf]
Additional 15% thrust	866 [kN]	194,810 [lbf]
Total Required thrust per propeller	433 [kN]	97,405 [lbf]
Ship speed [Vs]	10.36 [m/s]	20.14 [knt]
2D drag coefficient	Cd=0.01	Cd=0.01

Table 3-3 : DDG-51 design characteristics

Besides the design characteristics several external constrains are additionally considered. The maximum propeller diameter is limit by the hull clearance and the ship minimum draft .The hub diameter is constraint, in this thesis, by the model hub diameter. The number of propellers was selected to be the same number as for the existing ship since the propulsion modification concept is to increase efficiency with minimum alterations in the ship. The constraints values are presented in table 3-4.

	Metric	English
Max diameter [D]	5.1816 [m]	17'
Number of propellers [Kp]	2	2
Hub diameter	(3.25/14) D	(3.25/14) D

Table 3-4 : Propeller geometric restrictions

The 2D blade geometry are shown in table 3-5 .These sections are commonly used by marine propellers because of their flat pressure distribution on the suction side which results in relatively wide cavitation-free envelops.

Meanline	NACA a=0.8 (modified)
Thickness	NACA 65A010 (modified)

Table 3-5 : 2D blade geometry

3.3 Parametric design for the DDG-51

As already mentioned, in order to compare the contra-rotating propeller performance with the single propeller configuration, an optimum SR and CR propellers for the DDG-51 should be designed. The design tool for the single propeller case is the OPENPROP program which developed at MIT (Kimball and Epps, 2010), and for the CRP case is the code developed by Laskos (2010). The input for the program is the design requirements and constraints. In this section, a parametric study to determine the propeller characteristics which derive the most efficient propeller, for both cases, is performed.

3.3.1 Single propeller (SP) parametric study

3.3.1.1 Chord length distribution

A parametric study for a range of number of blades (Z), range of propeller speed (N), for a different chord length distribution was made and is presented in the following figures.

Figure 3-2 presents the parametric study using the blade chord distribution of US Navy propeller 4119, follows by figures 3-3 and 3-4 for chord distribution of US Navy propellers 4381 and 4148, respectively. The selection of the chord length distribution is a tradeoff between propeller efficiency on one hand, and cavitation performance as well as the blade structural strength on the other hand. Small chord length is expected to improve the propeller efficiency by inducing low viscous losses. However, the blades would be more vulnerable to the occurrence of cavitation due to increased loading on the shorter blade section. The chord length distribution is a direct input by the user in the propeller design code. For the purpose of this work, the chord length distribution was taken from current US naval propellers. The characteristics of the 4119, 4381 and 4148 propellers are presented in appendix C.

In the following figures the y axis represent the propeller efficiency while the x axis is the propeller speed [rpm], the data cursor indicates the best efficiencies for the top three propeller blade configurations.

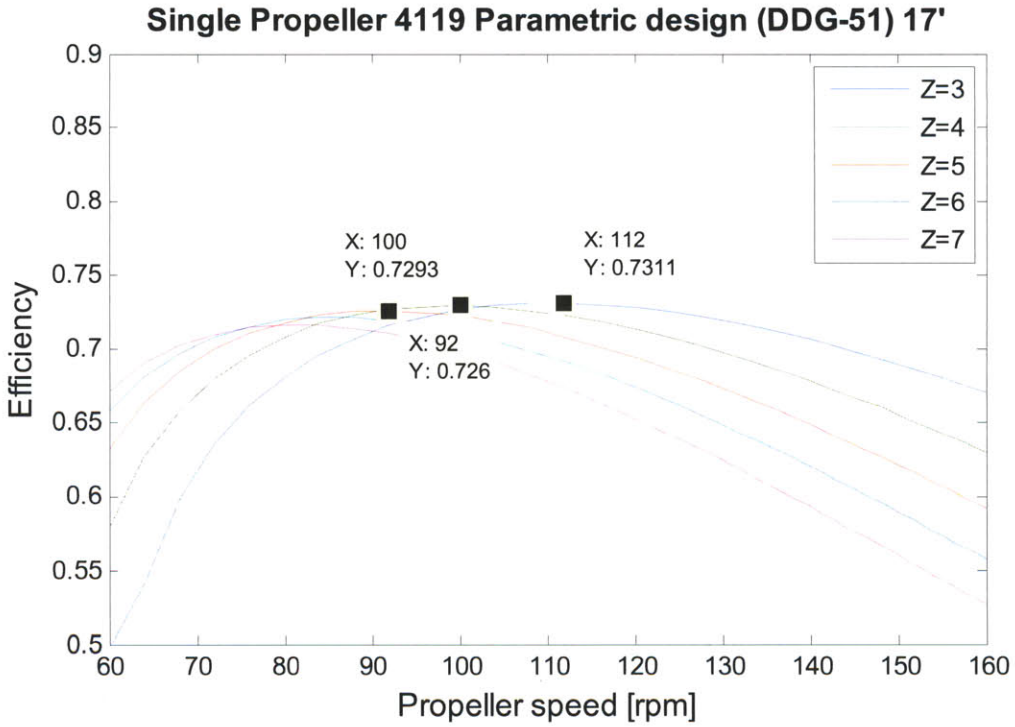

Figure3-2: Parametric study using the blade chord distribution of US Navy propeller 4119

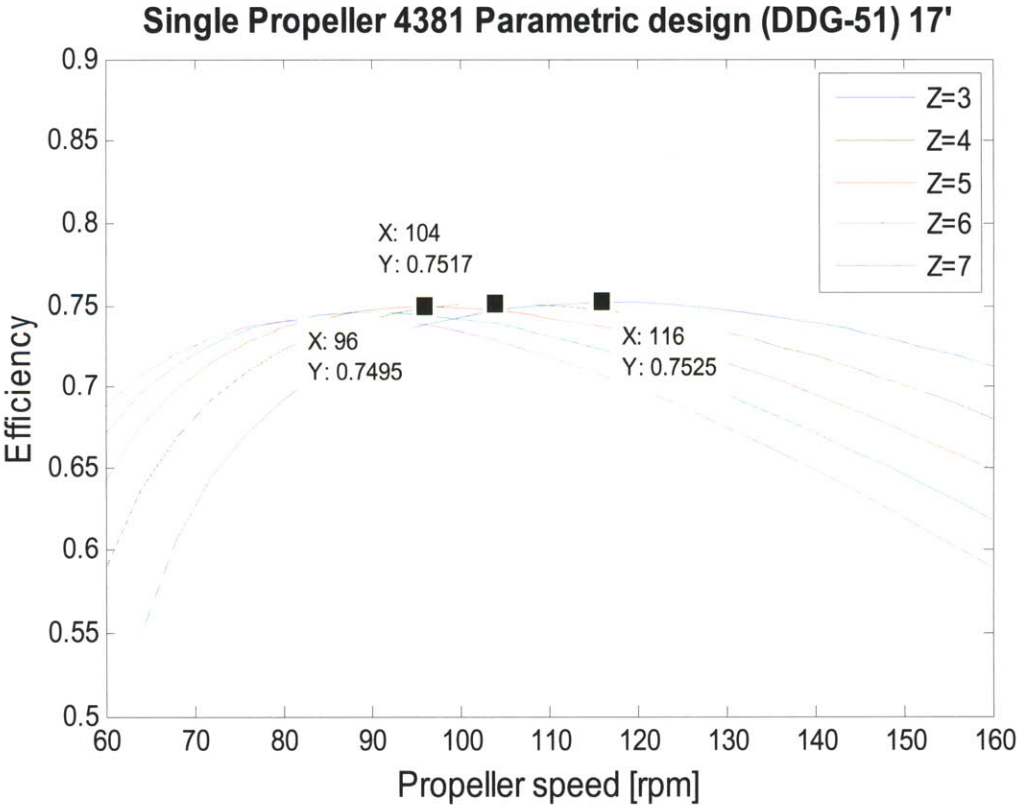

Figure 3-3: Parametric study using the blade chord distribution of US Navy propeller 4381

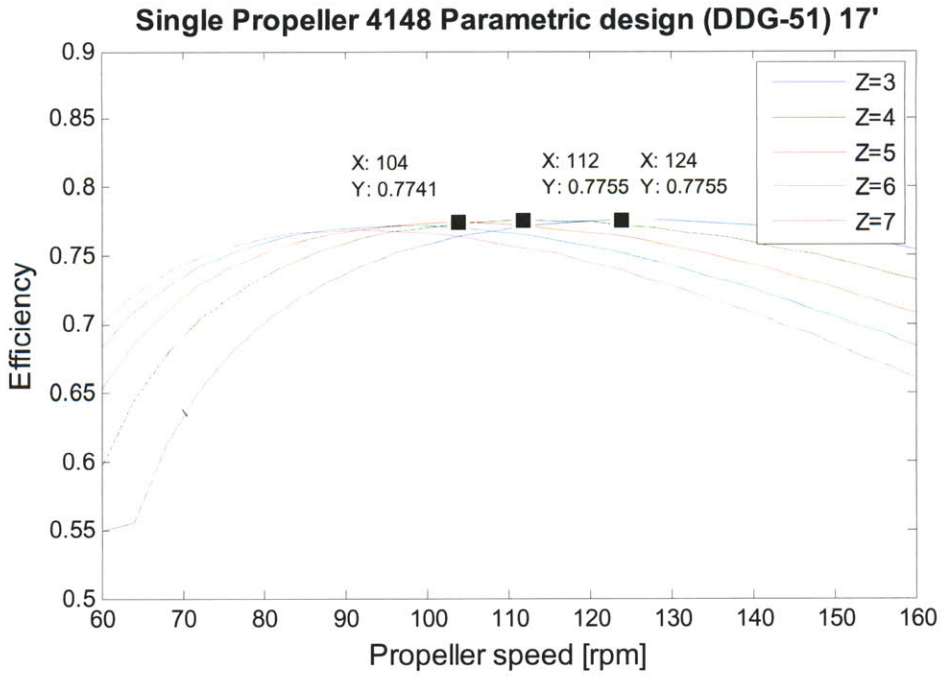

Figure 3-4: Parametric study using the blade chord distribution of US Navy propeller 4148

The parametric study which was presented in these figures were made for hub diameter ratio of 3.25/14.Additioal study was made to hub diameter ratio of 3.25/16.This ratio will be lately constraint by the model motor diameter (3.25") and the propeller model. However, at this stage of the parametric study, the hub diameter is open for selection.

The most efficient single propellers for each case are shown in table 3-6:

Propeller\Hub Radius	3.25/16			3.25/14		
	Z	N	EFFY	Z	N	EFFY
4119	3	108	0.7351	3	112	0.7311
4381	3	116	0.7563	3	116	0.7525
4148	4	112	0.7791	3,4	112,124	0.7755

Table 3-6: Single propeller parametric study summery

As expected, the most efficient propeller with respect to chord length distribution is 4148 which has the shortest chords length among the three types. However, as explained, this propeller will, probably, be more vulnerable to cavitation occurrence.

3.3.1.2 Propeller diameter

As a rule of thumb, the most efficient propeller is achieved with the maximum diameter limit, this is why the previous propeller's performances study were made for propeller diameter of 17 [ft]. To verify this assumption additionally study was done for propeller 4148 with different propeller diameters. It can be seen at figure 3-5 that this assumption is validated for the single propeller case; the best propeller efficiency is achieved with the largest propeller diameter (D=17'). In addition, the best efficiency which is achieved in the maximum diameter is performed at the lowest propeller speed, an advantage tribute for a cavitation point of view.

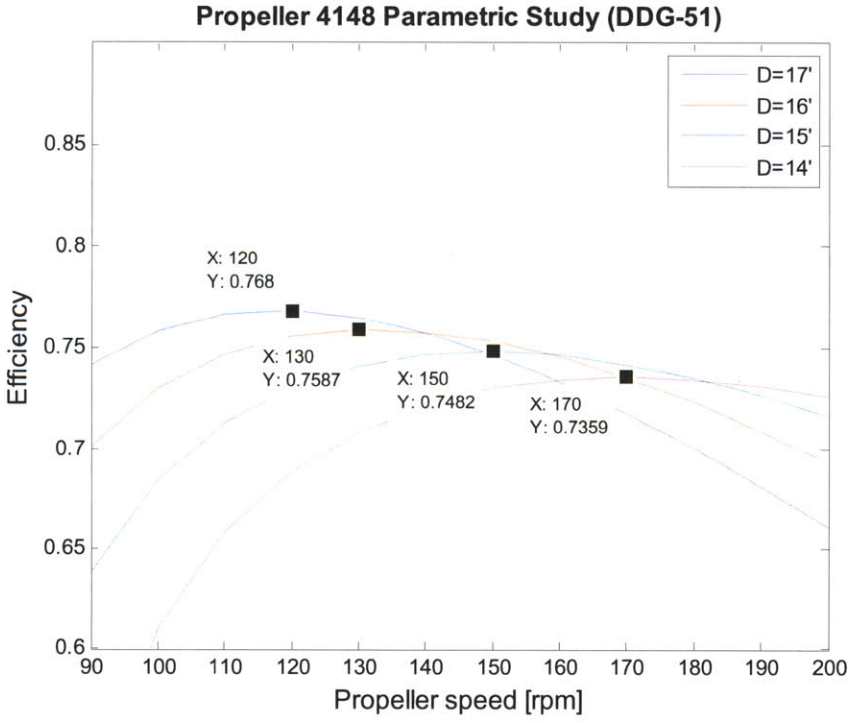

Figure 3-5 : Single propeller efficiency for a range of propeller diameters

The objective of this work is to design and manufacture a set of CRP and make a test plan matrices for future experiments. The single three blades propeller parametric study that was done for a range of propeller diameters, included a blade shape modification for better printing the propeller models (3D printing), this is the reason for dissimilarity of the propeller maximum

efficiency from the chord length study and the final model. The modification was made by enlarging the tip blade section (chord and thickness); the variations are presented in appendix C.

3.2.2 Contra-rotating propeller parametric study

The parametric study and a detail design for the DDG-51 contra-rotating propeller are the subject of this section. In addition to the restrictions mentions in table 3-4 for the single propeller, several distinctive restrictions for the contra-rotating propeller case are added. The torque required by the propeller is divided equally between the two propellers; this is a demand from the electric motors (will discussed in particulars in the next sections). The propellers are powered by an electric motor which requests the two propeller's delivered torques to be equal. Furthermore, the code is not taking into account the contraction of the slipstream behind the forward propeller, so the aft propeller should not require to be designed smaller than the forward propeller; in fact, the code demands equal propeller diameters. Moreover, the chord length distribution for both propeller among with the 2D thickness and meanline are the same as for the single propeller case. CRP additional required restrictions are shown in table 3-7.

Propeller diameters [ft]	D1=D2=17
Torque ratio [q=Q2/Q1]	1
Axial separation Coeff. [Xf=spacing/R1]	0.5
2D drag coefficient	0.008

Table 3-7 : Contra-rotating additional requirements

3.3.2.1 Number of propellers' blades

The parametric study for CRP is not as straight forward as for the single propeller. The optimum propeller characteristics depend on both propellers; therefore, there are many propellers configuration which can be considered. The first parametric study is to find the number of blades for each propeller which produces the most efficient propeller set. From the single propeller parametric study we figured that propeller 4148 chord length distribution bring together the best efficiencies, thus, this chord length distribution was chosen to the CRP set study. The propellers axial separation of Xf=0.5 and diameter of 17[ft] are an input to the code. The study was done

for a range of propeller speeds, assuming, at this stage, both propellers rotates at the same speeds N1=N2=N [rpm]. The results for the number of blade study are presented in figure 3-6.

The most efficient propellers configurations with respect to number of blades are summarized in table 3-8.

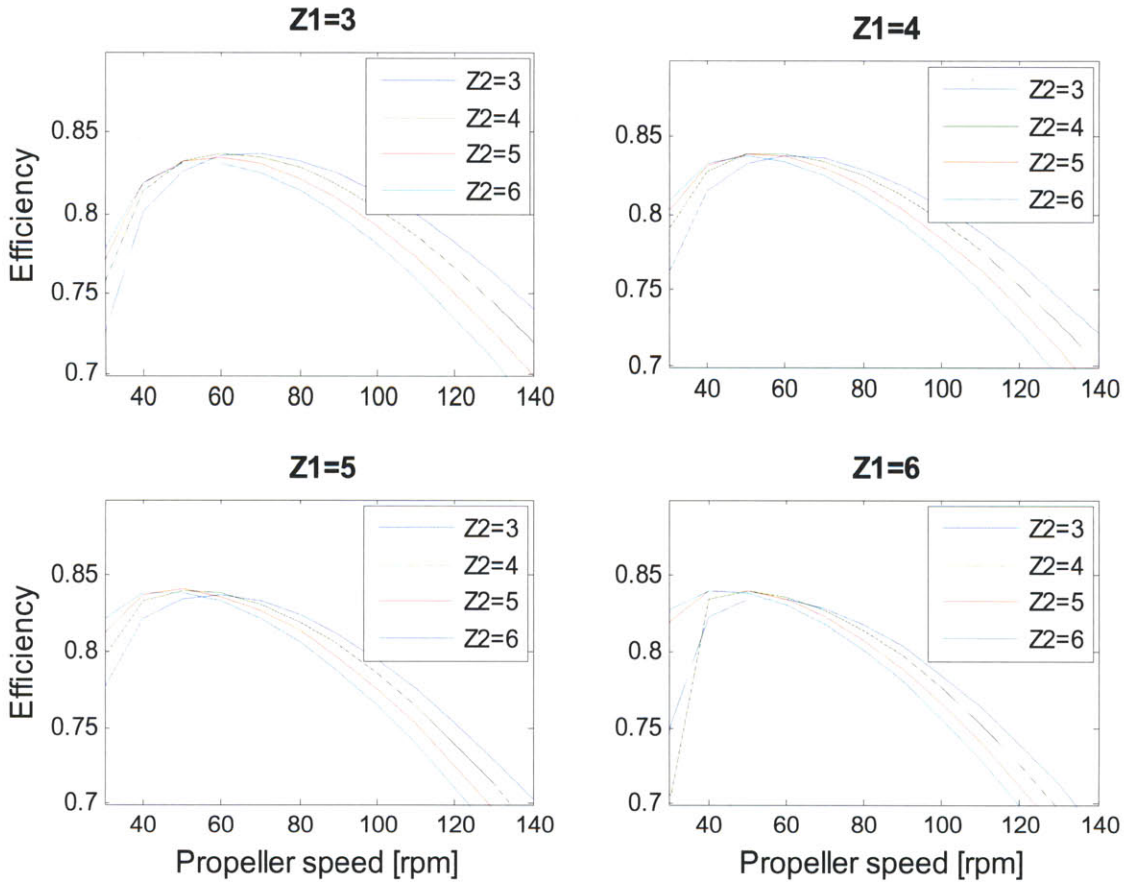

Figure 0-6: Contra-rotating propeller parametric study - range of propeller blades

# of blades for prop Z1	# of blades aft prop Z2	EFFY	N[rpm]
3	4	0.8369	60
4	4	0.8397	60
5	5	0.841	50
6	5	0.8404	50

Table 3-8 : Contra-rotating propeller parametric study summery for a range of propeller blades

To continue with the parametric study, the constraint for both propellers being rotate at the same speed will discharge, and the best configurations will be analyzed for a range of different propeller speeds.

3.3.2.2 Range of different propeller speed

In contra-rotating propeller there is no essential limit that the two propellers must rotate at the same speed. At the previous section the best number of blades configuration were found with the assumption that both propellers rotate at the same speed. In this study, however, the best number of blades configuration were inspected for a range of different propellers speed. In figure 3-7 the x axis is the forward propeller speed (N1) and the y axis is the total CRP set efficiency for different numbers of aft propeller speed (N2).

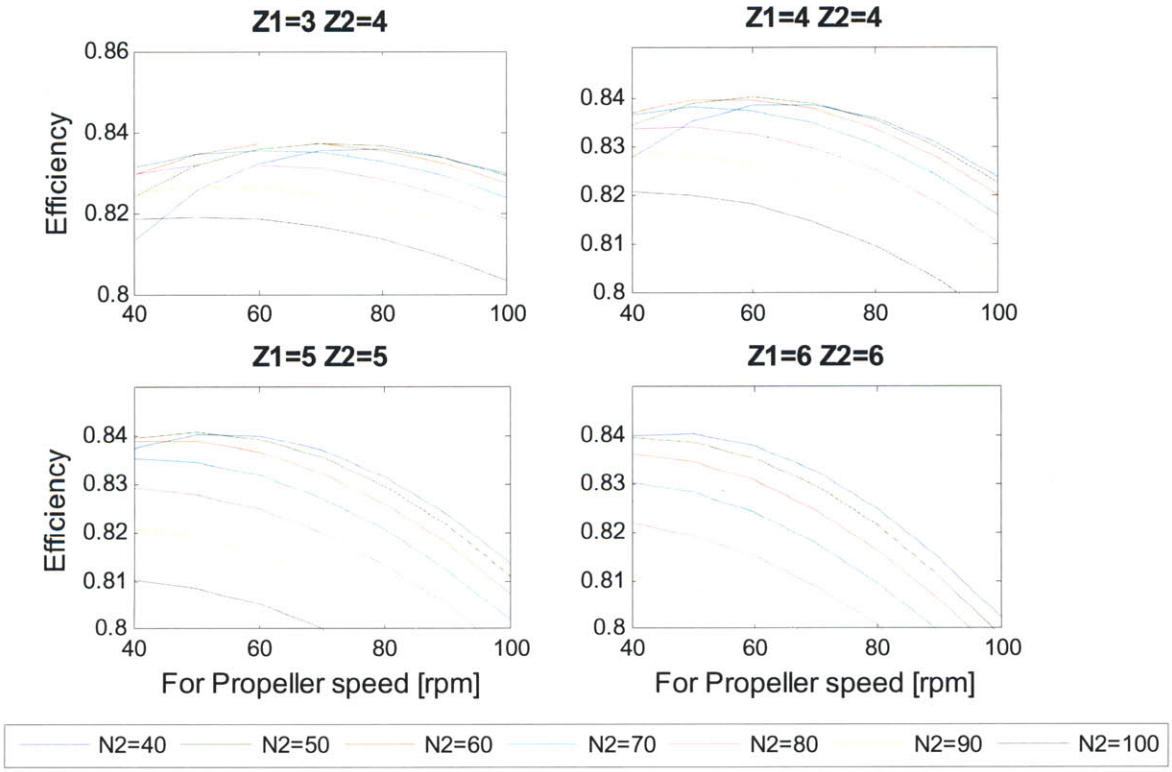

Figure 3-7: Contra-rotating propeller parametric study - range of propeller's speed

The propellers' speeds that obtain the best efficiencies for each number of blade configurations are summarized in table 3-9.

# of blades for prop Z1	# of blades aft prop Z2	For propeller speed N1	Aft propeller speed N1	EFFY	N[rpm]
3	4	70	50	0.8373	60
4	4	60	50	0.8401	60
5	5	50	50	0.841	50
6	5	50	40	0.8405	50

Table 3-9 : Contra-rotating propeller parametric study summery for a range of propellers' speeds

It is interesting to see that giving the propellers the freedom to rotate whatever speed they want, the variation of the speed between the two does not considerably alter, and the gain of the efficiency is not significant. In addition, the most efficient propeller configuration Z1=Z2=5 maintain the same rotational speed for both propellers to achieve the optimum efficiency. One important conclusion that can be made at this study; that under the assumptions of the CRP design program ,whenever a different propellers' speeds ($N1 \neq N2$) make the CRP construction more expensive and complicated, the marine engineer could consider to find the best efficiency for an equal speeds without reducing significantly (or in some cases, at all) the maximum achievable efficiency.

3.3.2.3 Axial separation

At this point, one can have a broad appreciative of how the CRP efficiency is influenced by vary of several propeller characteristics. At all the previous parametric studies the axial separation; i.e., the axial spacing between the two propellers, was not discussed and was assumed to be Xf=0.5.

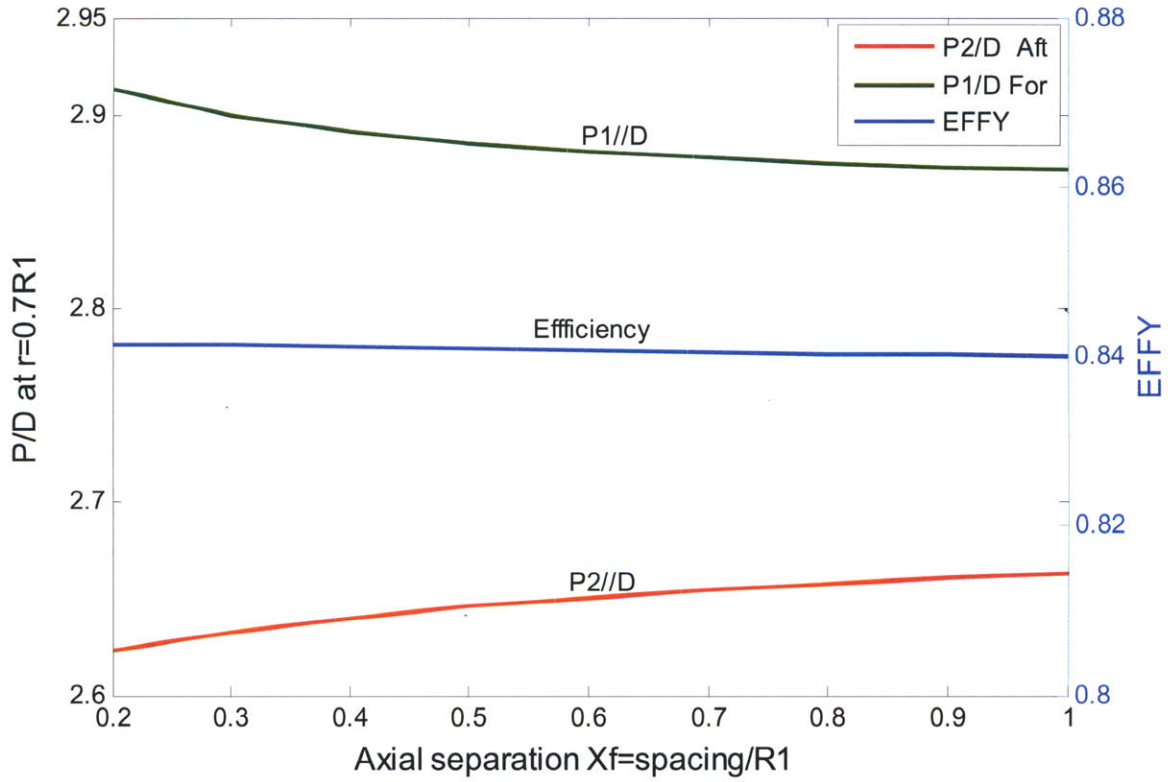

Figure 3-8: Axial separation parametric study

Figure 3-8 shows the propeller set efficiency in a range of axial spacing normalized by the propellers' radius. It can be seen that the effects of the spacing between the propellers is almost negligible with respect to the CRP efficiency. The particulars design conditions input were for the best propeller configuration from the previous sections; Z1=Z2=5 and N1=N2=50 [rpm] with the same characteristics as presented at tables 3-4 and 3-5.The geometric pitch ratio at blade radius of 0.7R ,for both components, are given as well in the figure. In order to maintain the CRP performances the designed pitch ratio of the aft propeller is increased to adapt to the higher axial interaction velocities induced on the forward propeller. Conversely, the propellers pitch ratio decreases as a result of lower axial velocities induced by the aft propeller, as the axial separation increases.

3.4 Final design

3.4.1 Single propeller final design

Before continuing with the scheme, a summary for the single propeller parametric study is required. The most efficient SR propeller characteristics are shown in table 3-10.

Chord distribution	Propeller 4148
Propellers diameters [ft]	D=17
Propeller speed [rpm]	N=120
Hub diameter /prop diameter	3.25/14
Number of blades	Z=3
2D Thickness	NACA 65A010 (modified)
2D Meanline	NACA a=0.8 (modified)
Designed advance coefficient	Js=0.9998
Blade tip modification	Yes
Efficiency	**0.7647**

Table 3-10 : Single propeller design specifications

After concluding the parametric study, the next step is a detailed design which is analyzing the propeller performance for the following: caivation inception, noise, vibrations and blade strength. If the propeller does not stand with these criteria a modification in the propeller characteristics is sometimes essential. At this work, however, only the cavitation criteria will be examined. After analyzing the cavitation criteria the geometry presentation for the DDG-51 single propeller will introduce.

The OPENPROP design optimizer computes the optimum circulation distribution using the Lagrange multiplier from variational calculus. This method is described in details at OPENPROP v2.4 theory, (Epps 2010b).

The final single propeller non dimensional circulation distribution with respect to the blade radial location is presented in figure 3-9. The circulation distribution begins at the first radial section on the hub.

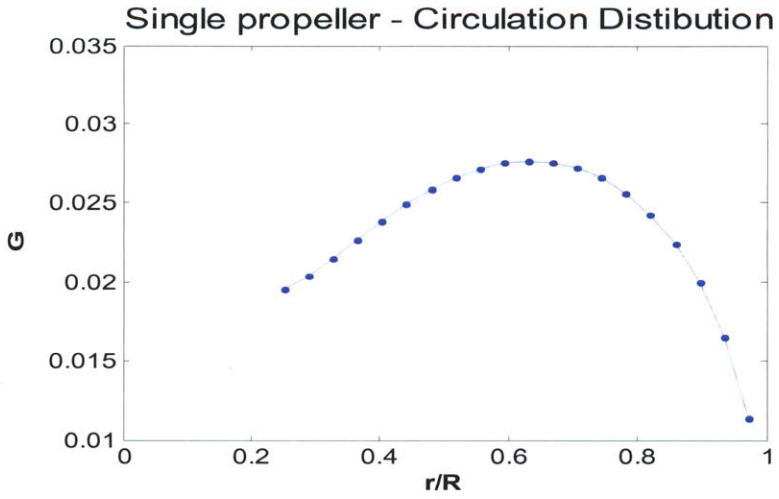

Figure 3-9: Non dimensional circulation distribution

In this work the cavitation inception analysis does not take into account the unsteadiness in the propeller disk inflow speed and assume that the propeller speed of advance equals to the ship speed. The cavitation free blade for the final single propeller design can be seen in figure 3-10. For this propeller design, the propeller is cavitated free in both sides; pressure and suction.

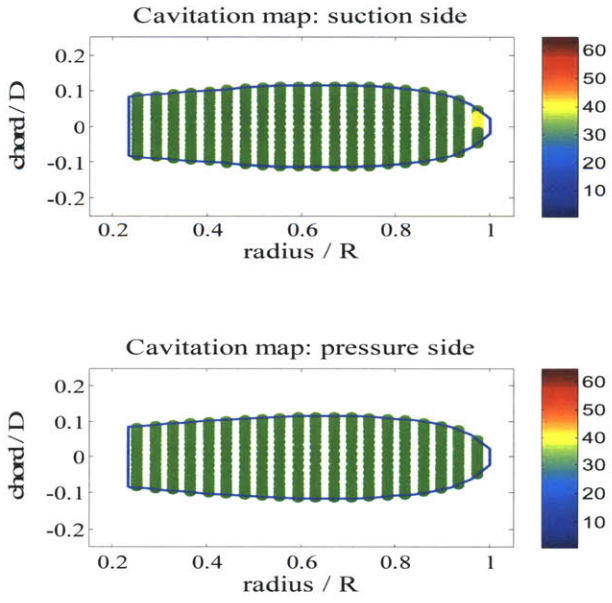

Figure 3-10: DDG-51 final Single propeller design cavitation map (for steady inflow speed)

3.3.2 Contra-rotating propeller final design

A summary of the most efficient DDG-51 contra-rotating propellers' design characteristics are introduced in table 3-11.

DDG-51 design speed [knt]	Vs=20.14
Required thrust [lbf]	Tr=97,405
Propeller type	4148
Propellers diameters [ft]	D1=D2=17
Propeller speed [rpm]	N1=N2=50
Hub diameter /prop diameter	3.25/14
Number of blades	Z1=Z2=5
Axial separation	Xf=0.5
Designed advance coefficient	Js1=Js2=2.3994
2D Thickness	NACA 65A010 (modified)
2D Meanline	NACA a=0.8 (modified)
Efficiency	**0.841**

Table 3-11 : Final DDG-51 CRP specifications

The non-dimensional circulation distribution for both components is presented in figure 3-11. The CRP set consist two five bladed propellers with the same diameter free running at the same speed. The circulation distribution for the optimum single propeller is shown on the graph as well. It can be seen that the CRP loading is lower than the single propeller for the all range along the propeller blade, except in the vicinity of the hub root. Note that The CRP blade is less tip loaded than the SR propeller which is significant attribute when cavitation inception is considered.

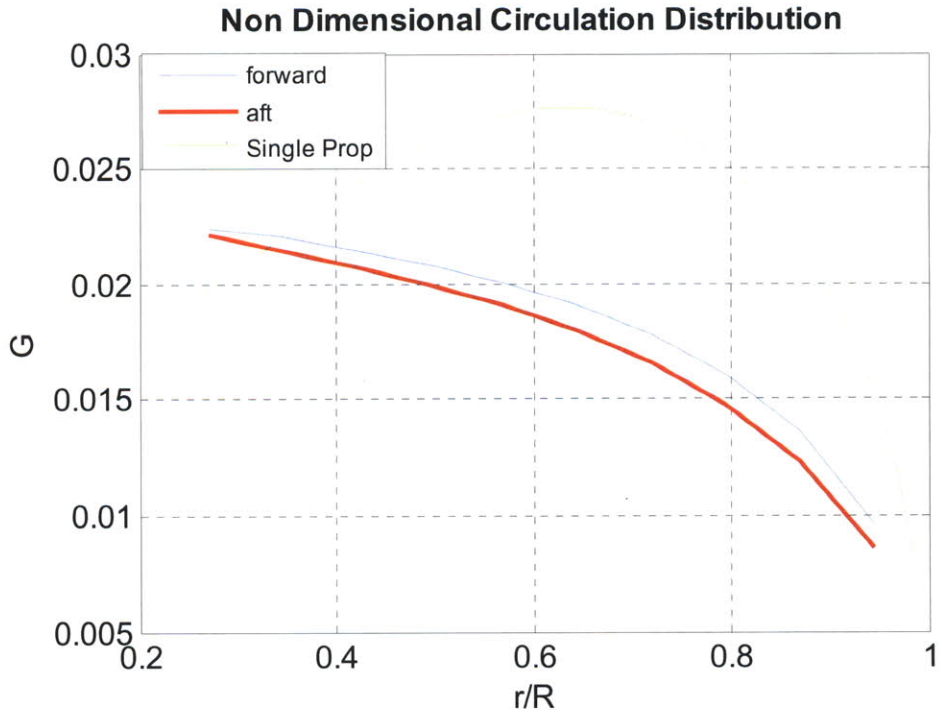

Figure 3-11: Non dimensional circulation distribution

The final CRP geometry is shown in figure 3-12.

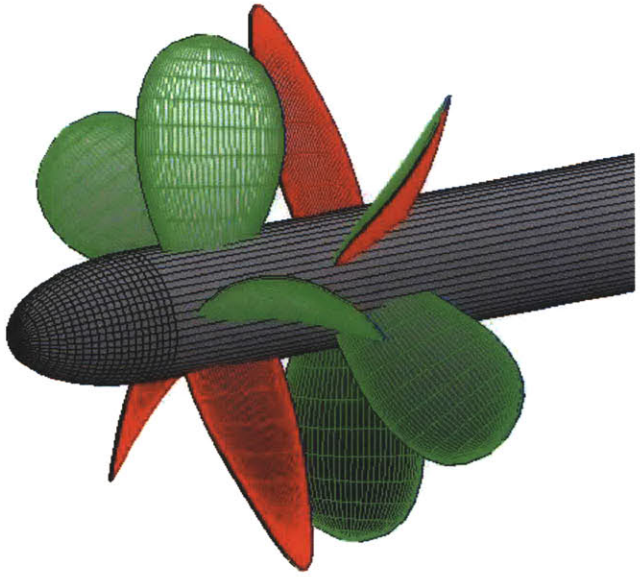

Figure 3-12: Final contra-rotating propeller 3D image

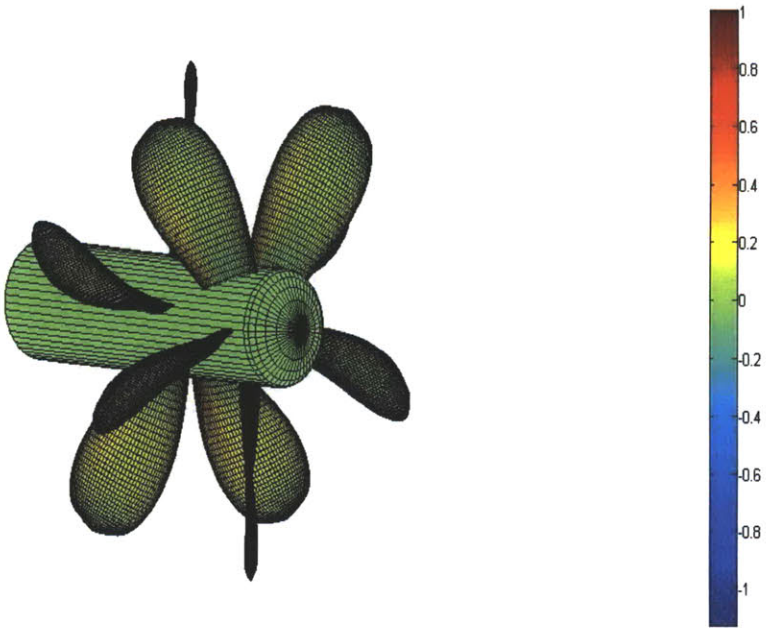

Figure 3-13: CRP cavitation map

In figure 3-13 the cavitation map at the contra-rotating propeller blades is shown. It can be seen that at the design point under uniform inflow velocity, the propellers' blades are cavitated free.

Ones concluding the design study for both; single and contra-rotating propellers, the next step is to analyze the propellers at off design states which is the basically one of the foremost theoretical contributions of this thesis.

3.5 Off-design analysis for DDG-51

3.5.1 Single propeller off design analysis

The final step to conclude the DDG-51 single propeller design is the analyzing its performance at the off design states. The propeller is designed for a certain requirements, however, the speed of advanced and the propeller rotational speed are vary with the ship operational profile and accordingly the propeller performances. This is why an off design analysis is required. The theory of the single propeller off design analysis is presented in details in the OPENPROP theory document, Epps (2010b). The different propeller performance (Thrust coefficient, torque coefficient and efficiency) are shown in figure 3-14, the dashed line represent the on design state.

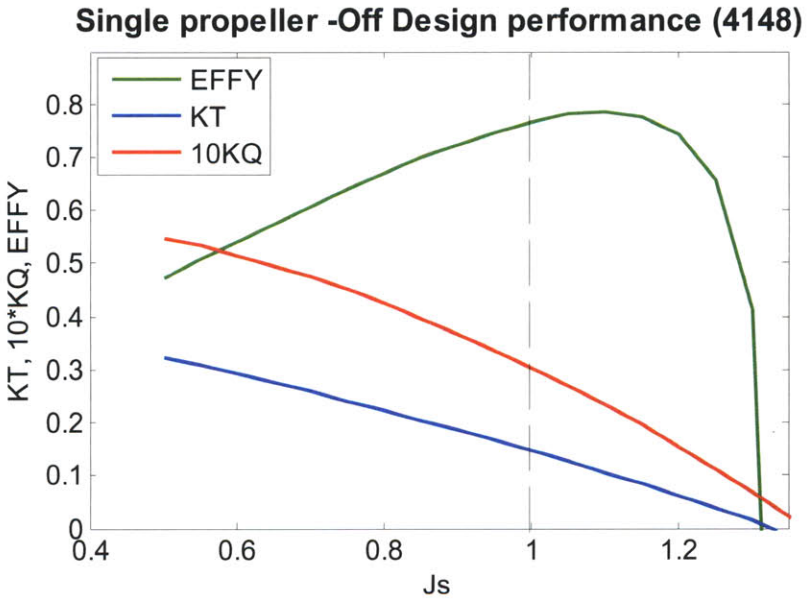

Figure 3-14: Single propeller off design performance

3.5.2 Contra-rotating propeller off design analysis

The theory behind the off design analysis was described in the previous chapter. The practice application of that analysis to the DDG-51 contra-rotating designed propeller is introduced in this paragraph.

3.5.2.1 Contra-rotating propeller-open water diagrams

In the single propeller case the non-dimensional propeller performance; efficiency (η_0), thrust coefficient (K_T) and torque coefficient (K_Q) are presented as a function of the off design advance coefficients (J_{OD}) in one diagram; the open water diagram (OPD), as demonstrated in for the single propeller case, figure 3-14. This presentation is an excellent tool to visualize the propeller performances for a range of advance coefficients (J_{OD}).

In contra-rotating propeller, on the other hand, the off design state is dependent on two different advance coefficient of both propellers ($J_{s1,}J_{s2}$), since both propellers are not constrained to rotate at the same rotational speed and have the same diameter.

Therefore, the open water diagram for the contra rotting propeller case is needed to be modified. In addition, each propeller as its own performance curves($K_{T1},K_{T2}K_{Q1},K_{Q2},\eta_{O1,}\eta_{O2}$) , and a total performance for the whole unit K_T,K_Q,η_O .The open water diagram for contra rotting propeller, in this thesis, is divided to three separate diagrams .Each diagram presents a different performance curves K_T,K_Q,η_O . The x axis, in each diagram, relates to the advance coefficient of the forward propeller (J_{S1}), and the y axis associates with the propeller's selected performance. Furthermore, several curves are shown ,in each diagram, for a different aft propeller advance coefficient (J_{S2}).This presentation of the contra-rotating open water diagram, from a perspective of the author of this paper, seems to be the most sufficient way to demonstrate the CRP performance curves, as will be shown next for the CRP1.

3.5.2.2 Propeller thrust and torque coefficient

In order to understand the K_{T1}, K_{T2} behavior with respect to the change of the advance ratio, the ship thrust coefficients C_{T1}, C_{T2} behavior is need to be demonstrated and explained first. Figures 3-15(A and B) demonstrates C_{T1}, C_{T2} with respect to the change of advance ratios. It is clearly shown that when the advanced ratio tends to zero the thrust loading reaches its maximum. It can be thought that when the advance ratio tends to zero it likes the propeller rotational speed tends to infinity $(J \to 0 = w \to \infty)$, where in this case, for the same ship speed, the thrust is definitely lean towards its maximum. It can also be shown from figure 3-15 that the forward propeller thrust coefficient is not influence from the change of the aft propeller advance ratio .On the other hand, the aft propeller thrust coefficient is slightly reliant on the forward advance ratio.

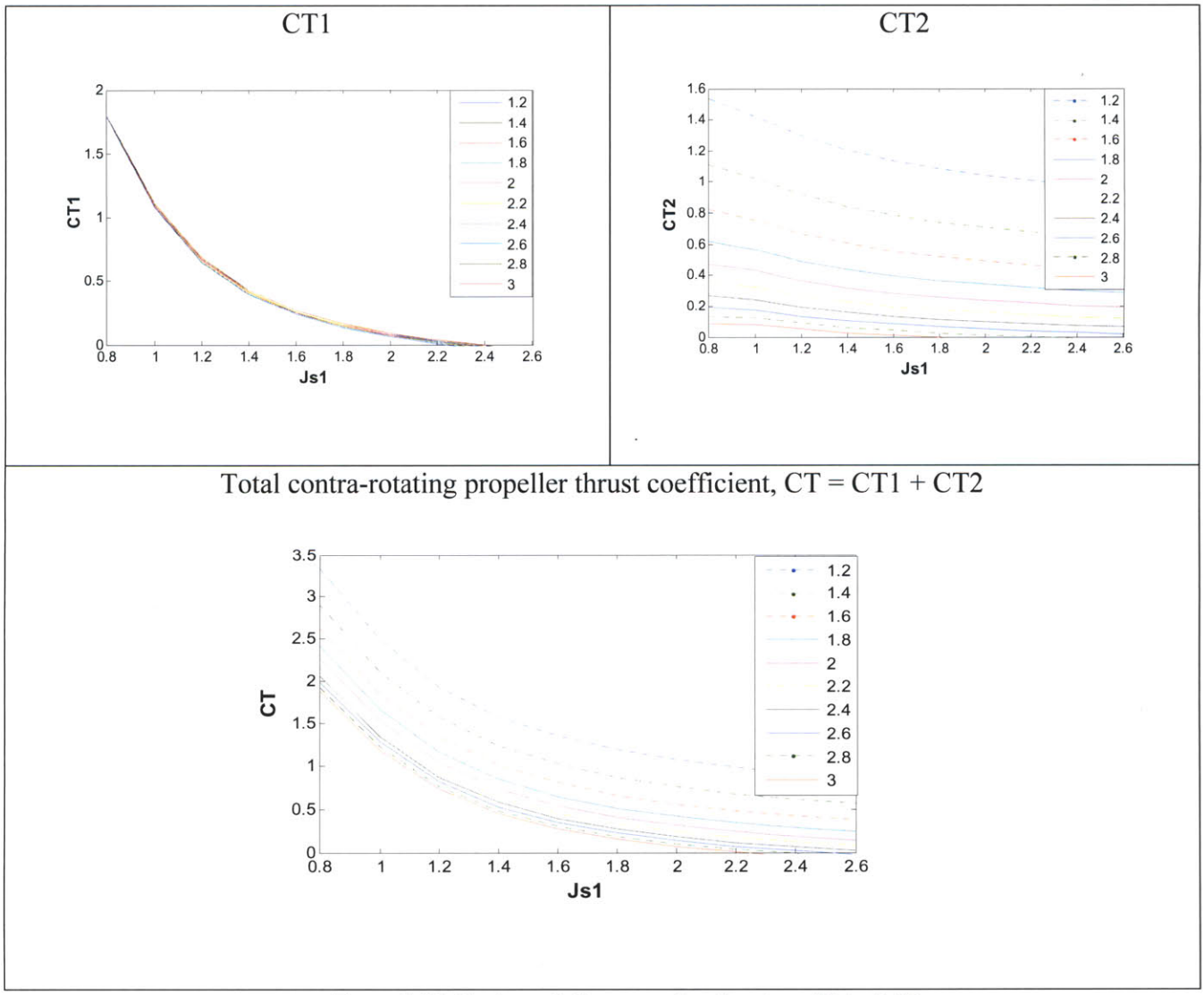

Figure 3-15: Contra-rotating propeller thrust coefficient, CT

Following, the propeller thrust coefficient K_T is presented. This coefficient is depend on both; thrust loading coefficient C_T, and the square of the advance ratio, as already introduced in equation 2.13. The total K_T is sum K_{T1} and K_{T2} (equ. 2.15) so the total curves inclination will follow by the most dominant coefficient between the two. Since K_T curves for the CRP is much different from the single propeller case, and therefore, at first glance it looks quite odd to marine engineers who familiar with the single propeller open water diagrams , the phenomenon will described for a particular Js2 before the final diagram is introduced for the full range .

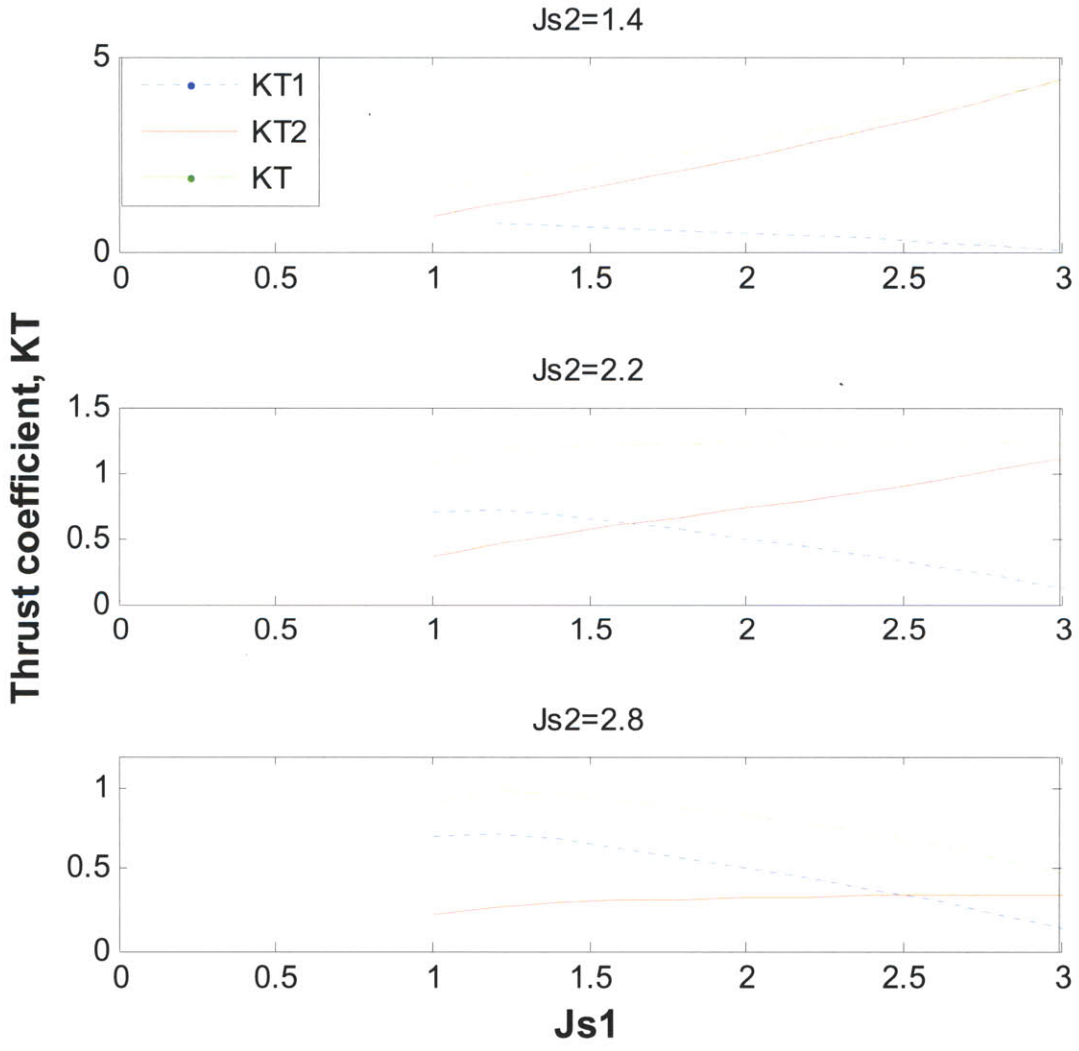

Figure 3-16: Evolution of the propeller thrust coefficient

The behavior of the propeller torque coefficient (C_Q) with respect to the advance coefficient is similar and is presenting next in figure 3-17.

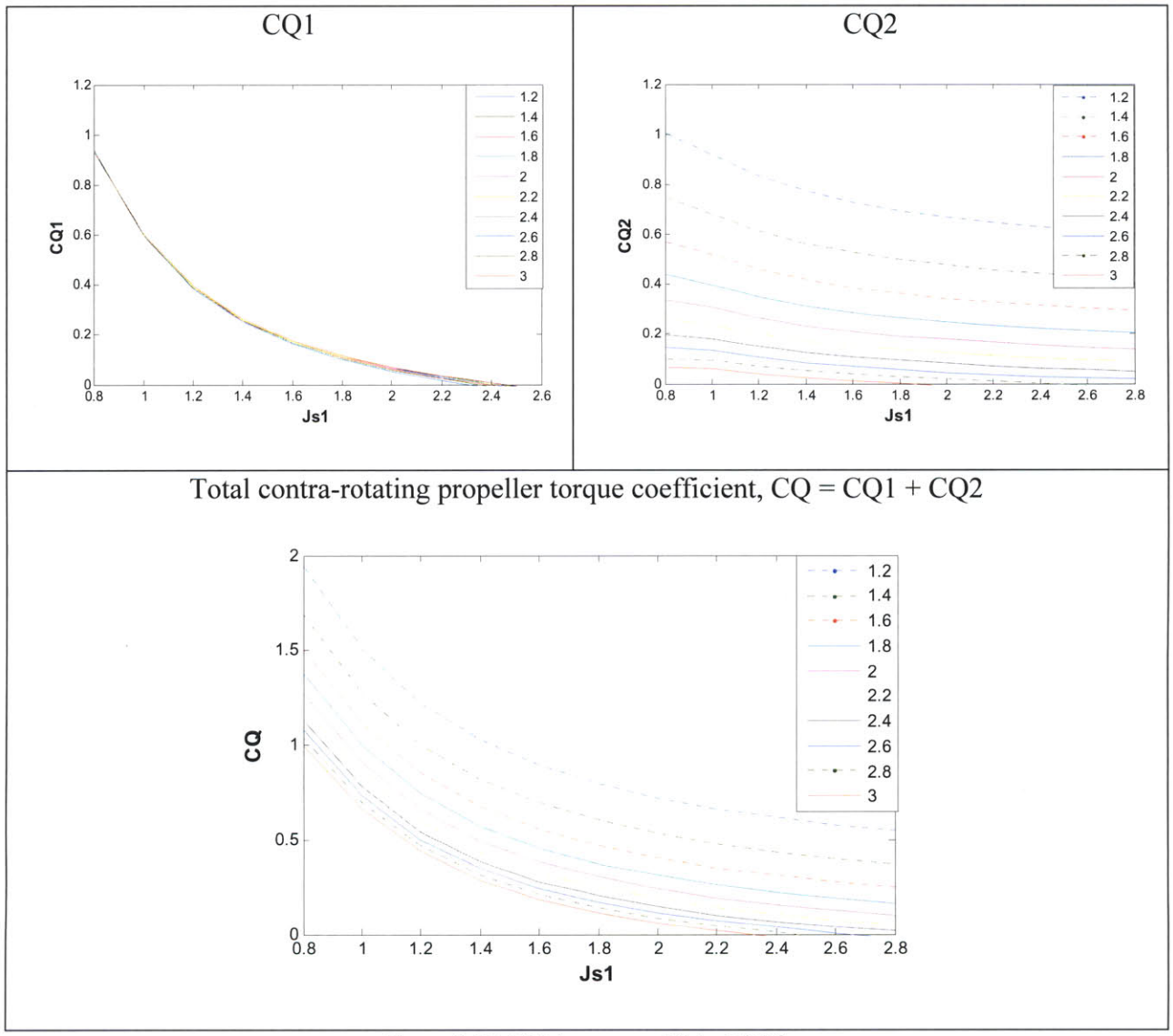

Figure 3-17: CRP torque coefficient (CQ)

Similar to the propeller thrust coefficient, the total trend of the propeller torque coefficient K_Q is affected by the dominancy of K_{Q1}, K_{Q2} which each is vary with the propeller advance ratio as demonstrated in figure 3-18.

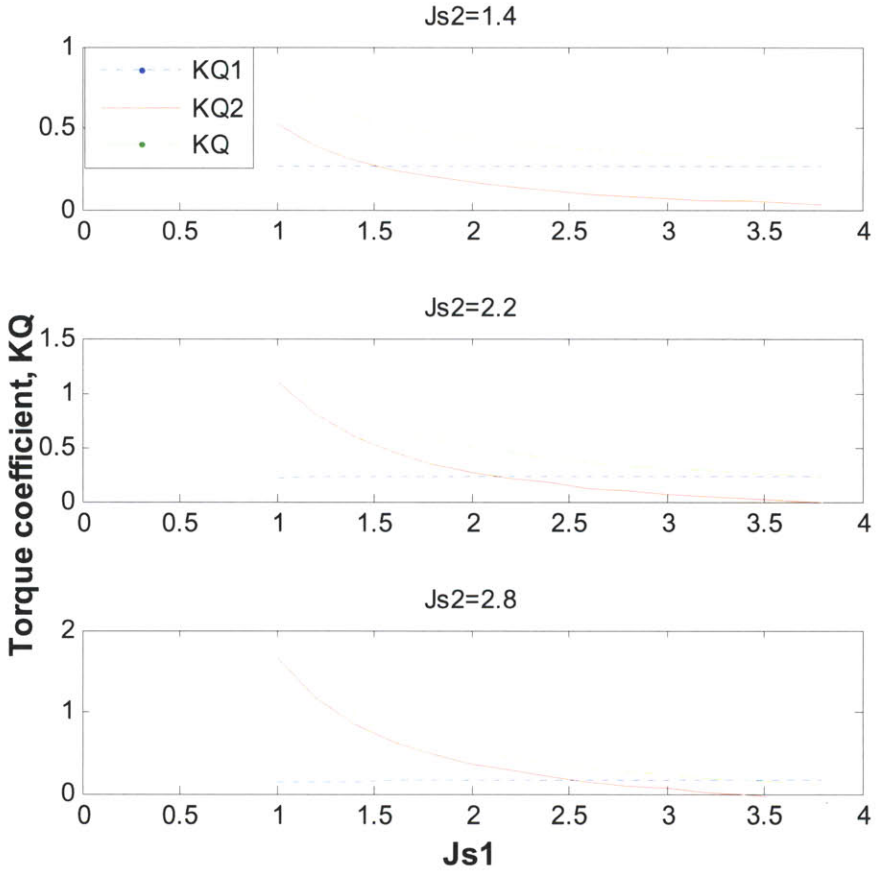

Figure 3-18: Contra-rotating torque coefficient (KQ)

The total propeller thrust and torque coefficients for the full range of advance coefficients are presenting in the next figures (3-19, 3-20). In contrast to the single propeller open water diagram, it can be seen from the figures that the trend of the curves increases with the combinations of smaller advance ratios and decreases with the opposite, with contrast to the SR propeller ,which in, the curves tendency decreases for the all range of advance ratios.

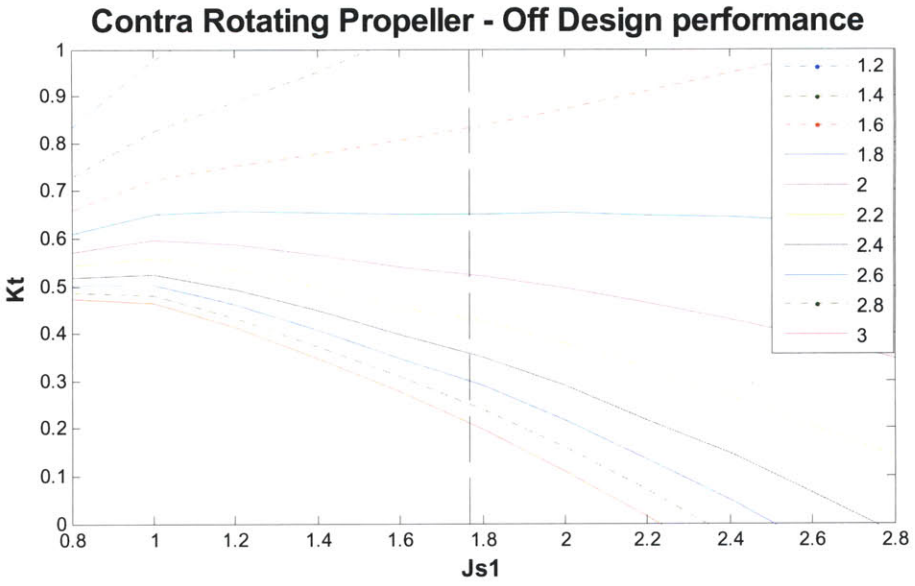

Figure 3-19 : Total propeller thrust coefficient

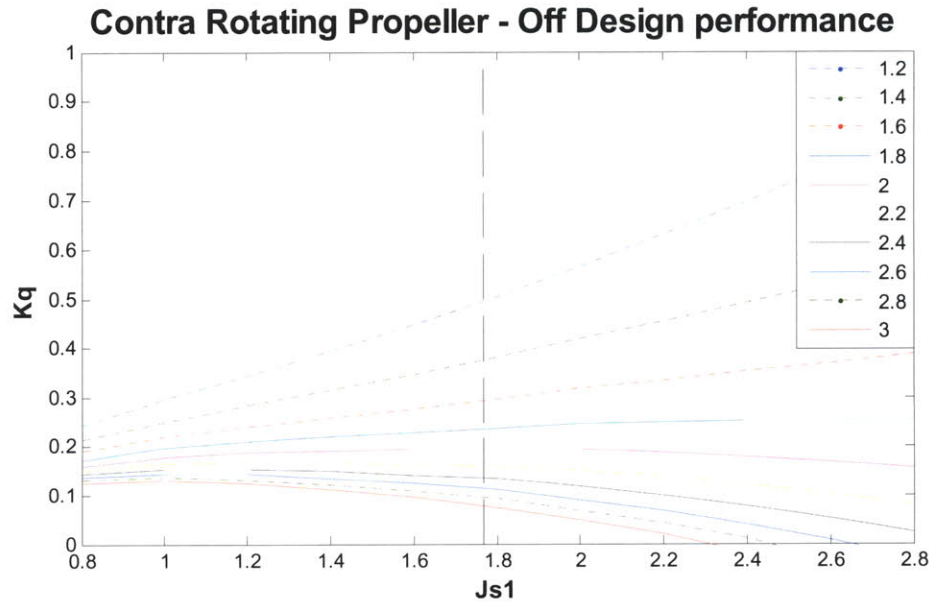

Figure 3-20 : Total propeller torque coefficient

3.5.2.3 Hub drag coefficient

The hub drag coefficient equations were introduced in chapter two (2.18 and 2.19).The hub drag is formed as a result of a concentrated hub vortex. However, the problem of the hub drag can be overcome with the contra-rotating propeller at the design process; if the circulation distribution is well designed, than the hub drug force can be eliminated. Figure 3-22 shows precisely this predicted phenomenon for the DDG-51 contra-rotating designed propeller. The hub drag coefficient at the design point is negligible, however, at some off-design states it has to be account. This shows that the CRP optimizer well computed the circulation distribution over the propellers' blades.

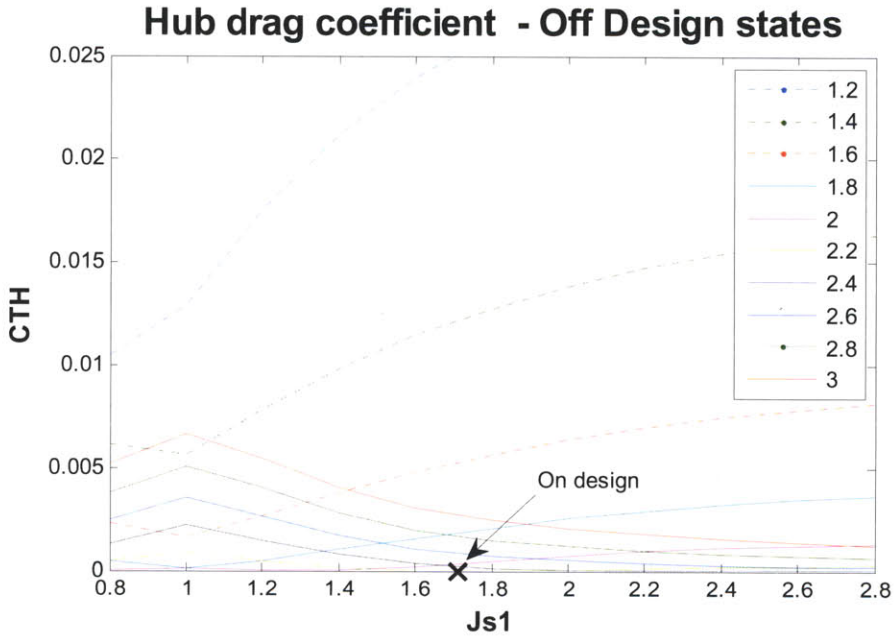

Figure 3-21: CRP Hub drag coefficient

3.5.2.4 CRP efficiency

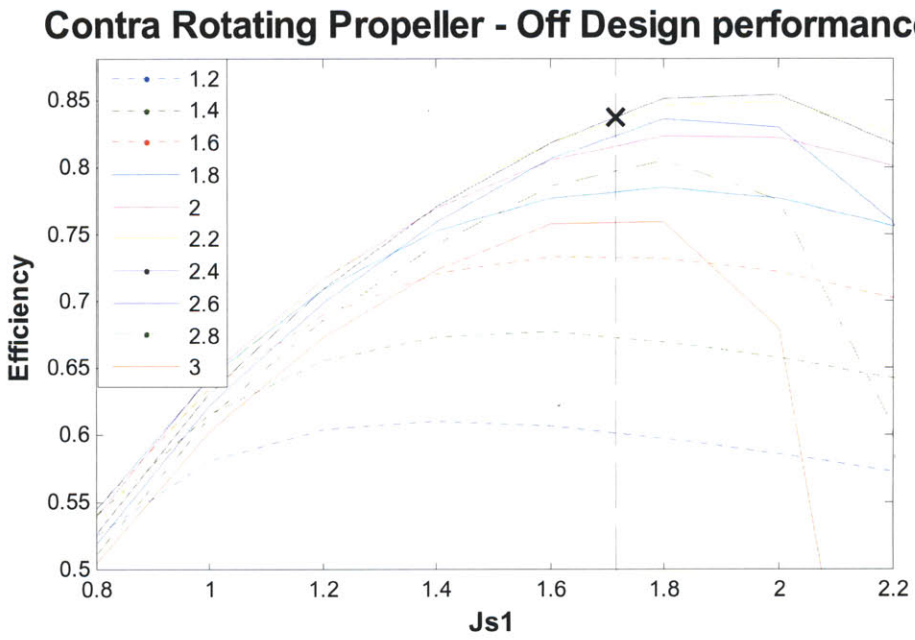

Figure 3-22 : CRP efficiency for different aft propeller advance ratios (Js2) curves.

As we already mentioned for the CRP open water diagram, the x axis is (J_{S1}), and the y axis is the propeller efficiency (η_O) for different curves of(J_{S2}). The X point represents the on design efficiency. It can be seen that in the vicinity of the on design spot, the efficiency increases with the increase of J_{S2}.This phenomena ,at first sight, seems wrong since the analyzer is expected to deliver a propeller geometry which produces the maximum efficiency at the design point .However, the input parameters for the analyzer were the ship speed and the required thrust for the design point, as a result the parametric study computed the maximum efficiency for a range of different propeller speed with a constant ship speed. Though, after finding the optimum propellers rotational speeds at the on design state, the efficiency might increase at some off design states where for a given propeller rotational speed the ship velocity increases. At these advance ratios a better efficiency can be found. This phenomenon is similar to the single propeller off design analysis. Additionally, in contrast to the single propeller case, the CRP off design efficiencies, with the way the numerical analysis is formed; it undesirably can increase above unity.

3.5.3 SP and CRP efficiency comparison

In the section 3.3 a parametric study was made to design a single and contra-rotating propeller for the DDG-51. The focus of this section, however, is to conduct a comparison between the two propulsors; single and contra-rotating propellers, with respect of propeller efficiency; the ship fuel consumption comparison will be conduct in the next chapter.

Before continuing, a summary of the final parametric study for both propellers, at the design point, is needed to be presented, and can be seen in table 3-12.

	CRP	SP
DDG-51 design speed [knt]	Vs=20.14	Vs=20.14
Required thrust [lbf]	Tr=97,405	Tr=97,405
Propeller chord length distribution	4148	4148
Propellers diameters [ft]	D1=D2=17	D=17
Propeller speed [rpm]	N1=N2=50	N=120
Hub diameter /prop diameter	3.25/14	3.25/14
Number of blades	Z1=Z2=5	Z=3
Axial separation	Xf=0.5	-
Designed advance coefficient	Js1=Js2=2.3994	Js=0.9998
2D Thickness	NACA 65A010 (modified)	NACA 65A010 (modified)
2D Meanline	NACA a=0.8 (modified)	NACA a=0.8 (modified)
Efficiency	**0.841**	**0.768**

Table 3-12: Design specification for SP and CRP

The contra-rotating propeller efficiency is expected to be superior to the single propeller. The major advantages of the CRP is that it capture the kinetic energy loses from the fore propeller with the aft one. The advantage of CRP over single propeller efficiency is in particular at off design states. As the advance coefficient increase, rotational losses dominate over viscous losses and the efficiency benefit of CRP over conventional single propeller increases. When the aft

propeller in the CRP sets is not constraint to rotate at the same speed as the forward propeller, it can gain even better efficiency, since the aft propeller speed can be designed in such a way to ideally capture the rotational losses at each of the off design states. As the two CRP propellers rotate at different rates the off design analysis is more complicated and it is profoundly discussed in previous chapter. For each of the forward propeller advance coefficient (Js1) there are many combinations for the aft propeller advance coefficient (Js2) to define an off design state, however, there is only one Js2 which produce the optimum efficiency for a given Js1.When joining all these optimum combination configurations, a maximum off design CRP efficiency curve can be plotted. Figure 3-23 illustrates this CRP distinctive characteristic. In this figure, x axis is the forward propeller advance coefficient (Js1) ,y axis is the CRP set total efficiency for a different aft propeller advance coefficient (Js2).The bold red curve represents the maximum efficiency curve and the blue bold circle mark represents the on design point.

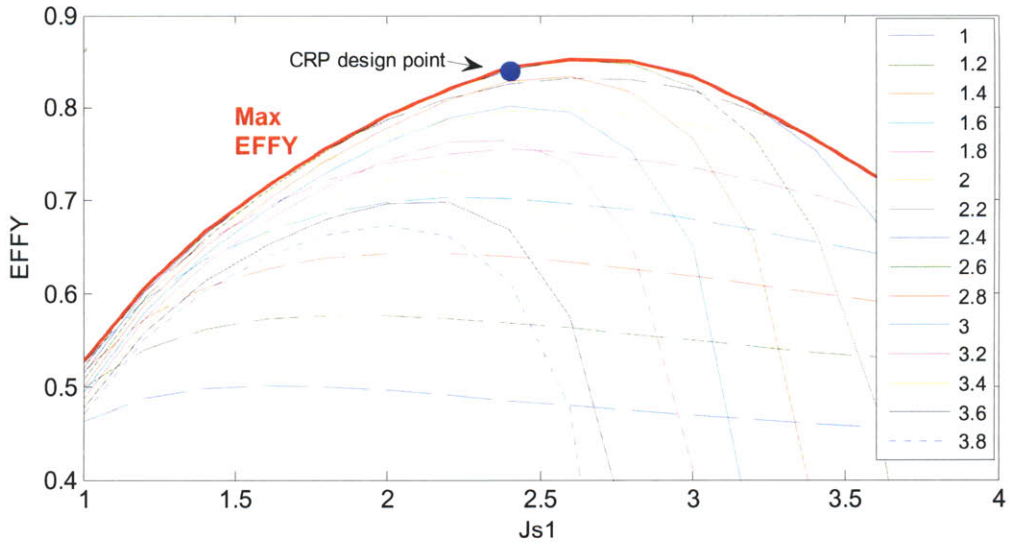

Figure 3-23: CRP maximum off design efficiency curve

The CRP maximum efficiency off design curve depends on the ability to design the aft propeller speed to optimize the efficiency. On the other hand, if both propellers are restricted to rotate at the same speed a reduction of the propeller efficiency is expected especially at high advance coefficients when the aft propeller could not optimally capture the rotational losses .As a result, the off design operational range will decrease as well. Figure 3-24 demonstrates this phenomena; a comparison of two maximum efficiency curves with and without aft propeller

speed constraint limitation. In this figure the red curve describes the maximum off design curve for a CRP set that the aft propeller is not constraint to rotate at the same speed as of the forward propeller, therefore, a greater efficiency range is accomplished, On the other hand, the green curve represents a CRP set which both propellers rotate at the same speed, it can be seen that, as predicted, the efficiencies of the green curve is smaller than the red curve, especially at high advance coefficients. The CR propellers used in this figure is the designed optimum CRP for the DDG-51.

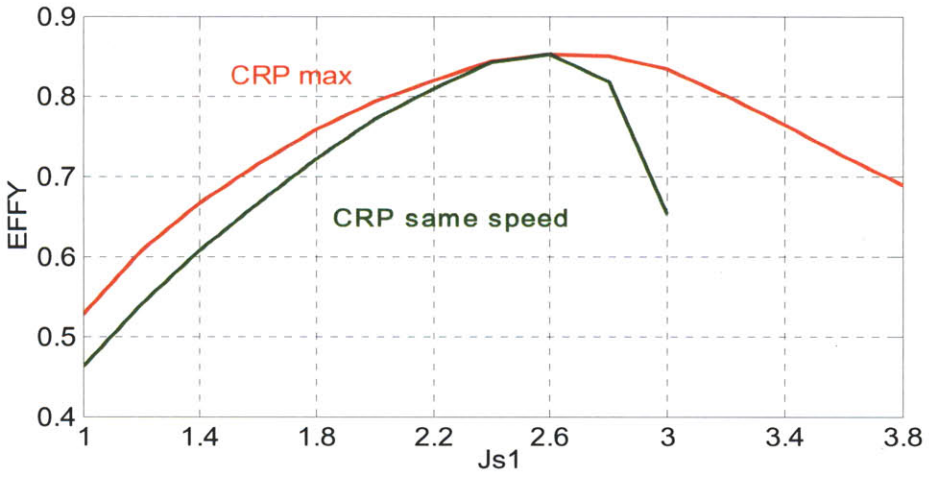

Figure 3-24: CRP Maximum off design curve for same and different propeller speed

To make a fair comparison between the two types of propellers, the best efficiency, which can be achieved, for each case will demonstrate. The maximum efficiency off design curve for the CRP set, and the off design states for the single propeller; both were derived from the parametric study to optimize the design state .The advantages of the CRP set are clearly seen in figure 3-25, this graph is a slightly confusing; notice the x axis scale difference for each propeller, the upper x axis refer to the SP advance coefficient (black) while the lower axis refers to the forward propeller advance coefficient (red).

A number of major advantages of the CRP set with comparison to the single propeller can be derived from this graph:

1. The CRP design point efficiency is about 8.7% higher than the single propeller design point (84.15% and 76.8%, respectively).

2. **The operational range**, is defined as the off design states with efficiency larger than 50%.The CRP operational range is 75% larger than of the SP operational range. (2.8, 0.7 respectively).

3. **The optimum range**, is defined as the off design states with efficiency larger than 70%. It is in 83% greater for the CRP set. (2.2, 0.37, respectively).

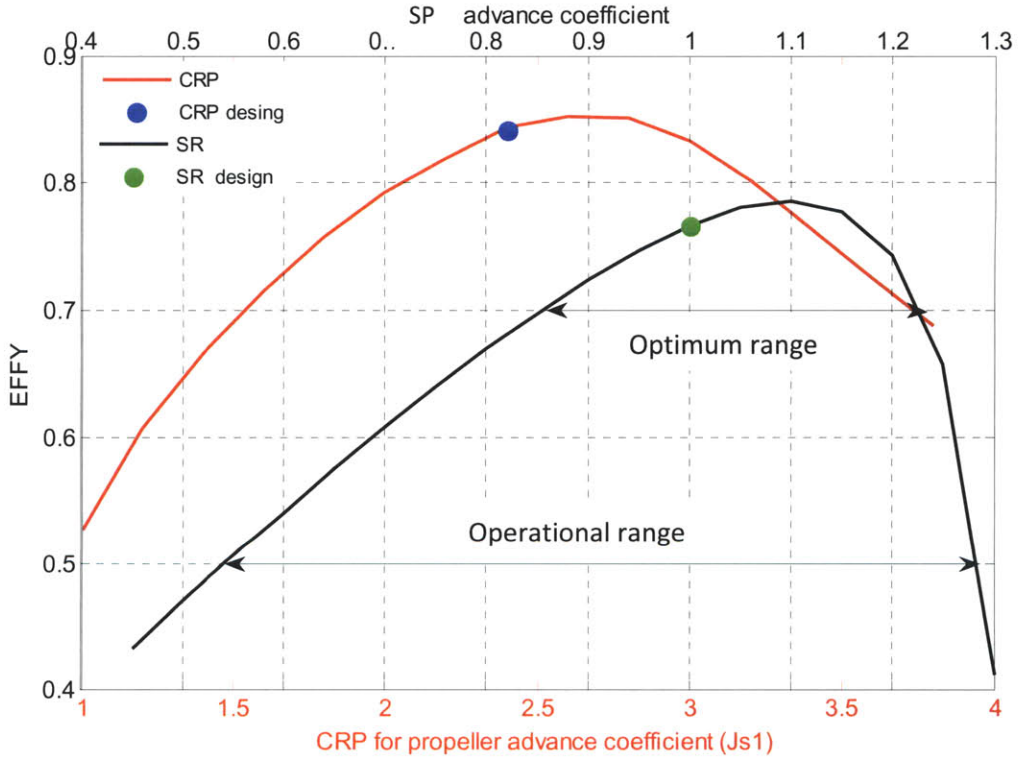

Figure 3-25: Single and Contra-rotating propellers efficiency comparison

Figure 3-26 summarizes the efficiency comparison described in this section. First, the CRP off design maximum efficiency curve is established for the CRP set from a different aft propeller advance coefficient at a certain Js1.The off design single propeller curve is than added to the graph.

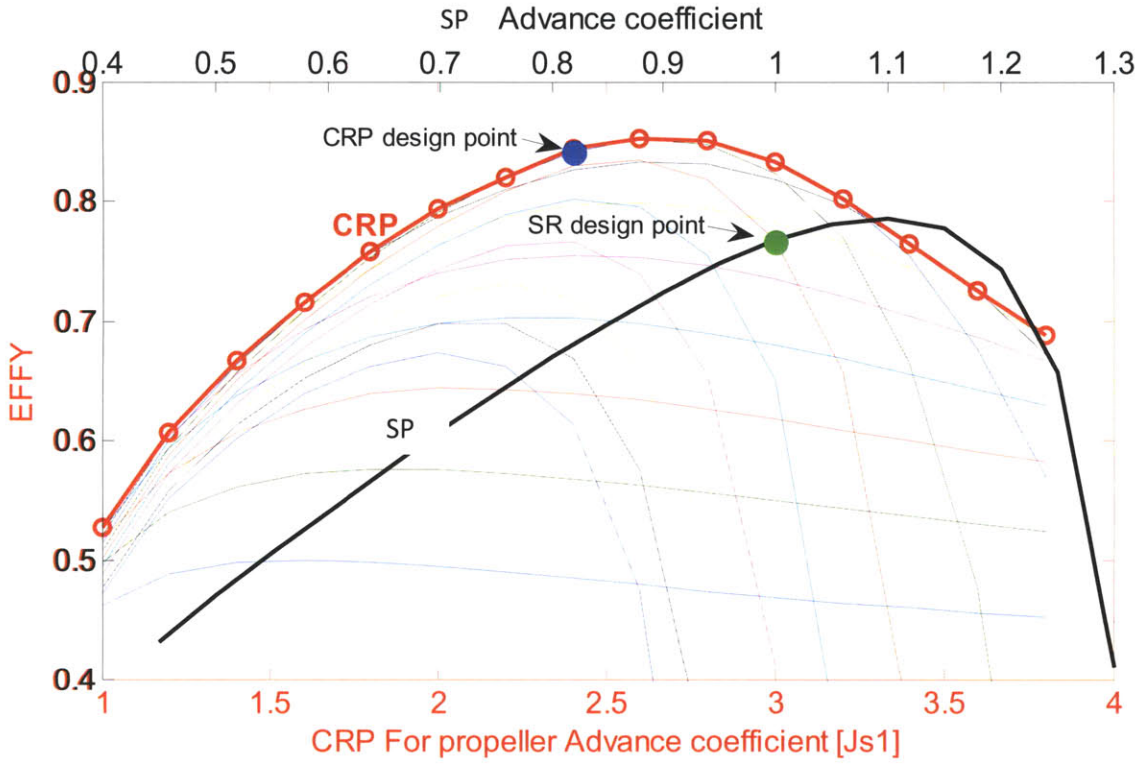

Figure 3-26 : Single propeller and CRP on and off - design efficiencies with maximum curves

In the next section the propeller comparison with respect to the DDG-51 fuel consumption will analyzed.

This page intentionally left blank

Chapter 4 - Fuel consumption comparison

So far the open water propeller efficiency was discussed. This efficiency is the most commonly term for propeller designers since it accounts only the propeller performances as computed on propeller design codes and tested in propeller tanks without considering the influence of the ship. However, for the naval architect point of view the open water efficiency is only one of a diverge efficiencies exists in the propulsion plant chain. A major difference of the propeller performance exists if it is tested in a propeller tank; where the inflow speed is almost uniform or assumed to be one, to where it is located at the aft of the ship hull where the inflow speed is from being uniform and so the ship wake fraction is added to the equations. Furthermore, the ship hull resistance as valued from ship model experiments in towing tanks is not considered the added resistance when adding the propeller and other appendages.

These affects, and more, which leads to the fuel consumption calculation will present in this section. The procedure used herein to estimate ship powering requirements follows that described in the OPENPROP v.2.4 Theory Document (Epps, 2010b).

4.1 From hull resistance to required thrust power

Translation the hull in the water requires a force. This force is called resistance: it is the force that is required to tow the ship at a specified speed (without propulsors).The thrust developed by the propulsion system has to overcome this resistance. The ship resistance is not the main subject of this thesis and it is well study in many sources. However, when investigating propulsion systems and fuel consumption this term has to be introduced. The total resistance consists of three main components: frictional resistance, form or pressure resistance and wave resistance.

The power required to overcome ship resistance at a certain speed is called effective power and is define,

$$P_{EFF} = R \cdot V_S \tag{4.1}$$

R is the ship resistance at ship speed Vs.

The power of a propeller in water moving at velocity of advance V_a with useful thrust T is called the thrust power,

$$P_T = T \cdot V_a \tag{4.2}$$

To compute the velocity of advance (V_a), the Taylor wake fraction should familiarized. This fraction is used to account for the difference between the velocity of the ship and the average flow velocity at the propeller disk. The wake fraction (w), equals one minus the ratio of the average water velocity relative to the ship at the propeller disk to the ship velocity. The advance velocity can so be calculate,

$$V_a = (1 - w) \cdot V_s \tag{4.3}$$

The required thrust delivered by the propulsion plant is generally exceeds the ship resistance, which is scaled up from a towing test of a model without propulsors. The main reason for this difference is that the propulsors draws its water along the hull and rudders and thus creates added resistance. This difference in the propeller thrust delivered by all propellers and the ship resistance as a fraction of the total propeller thrust is called the thrust deduction factor.

$$t = \frac{K_P \cdot T - R}{K_P \cdot T} = 1 - \frac{R}{K_P \cdot T} \tag{4.4}$$

t is the thrust deduction factor , K_P is the number of propellers.

As a result of the thrust deduction factor and the wake fraction the sum of the thrust power P_T of all the propellers does not equal the effective power P_E.The hull efficiency is defined as the ratio between the effective power and the total delivered thrust power,

$$\eta_H = \frac{P_E}{K_P \cdot P_T} = \frac{R \cdot V_S}{K_P \cdot T \cdot V_a} \tag{4.5}$$

The hull efficiency is often higher than unity. This is caused by the total thrust ($K_P \cdot T$) is normally exceeding the ship resistance on one hand, and the velocity of advance is being lower than the ship speed on the other hand (this is why the propeller locate behind the ship).Adding equations 4.3 and 4.4 to equ.4.5 the hull efficiency can be written as,

$$\eta_H = \frac{1 - t}{1 - w} \tag{4.6}$$

The hull efficiency can be estimated using the resistance and the wake fraction obtained from a model tests in the towing tank, and an estimation of the thrust deduction factor based on the propulsion plant configuration. The required thrust power of each propeller can then be calculated using equ.4.5 and 4.6.

$$P_T = \frac{P_E}{K_P \cdot \eta_H} = \frac{P_E \cdot (1-w)}{K_P \cdot (1-t)} \tag{4.7}$$

4.2 From open water power to required thrust power

In the previous section the ship required thrust power to overcome the ship resistance was calculated. In order to deliver the ship thrust power at certain ship speed, power must be delivered to the propeller as torque and rotational speed.

$$P_O = Q \cdot w_P = 2\pi \cdot n_P \cdot Q \tag{4.8}$$

where P_O is the open water power, Q is the open water delivered torque, w_P is the rotational speed. The propeller is usually tested in open water tank or tunnel in which the inflow in front of the propeller is uniform. During the test the well-known open water efficiency is calculated,

$$\eta_0 = \frac{P_T}{P_O} = \frac{T \cdot V_a}{2\pi \cdot n_P \cdot Q} \tag{4.9}$$

In reality, the torque M_P and thus the power P_P delivered to the propeller operating behind a hull (highly disturbed flow) is generally slightly different to that of the same propeller operating in open water (uniform flow).

$$P_P = M_P \cdot w_P = 2\pi \cdot M_P \cdot n_P \tag{4.10}$$

The relative rotational efficiency (η_R) is a factor used to account for this difference, and is defined as the ratio between the open water power and the actually delivered power.

$$\eta_R = \frac{P_O}{P_P} = \frac{Q}{M_P} \tag{4.11}$$

The relative rotational efficiency is normally does not differ much from unity; values are in the range of 0.98 to 1.02.

It is common practice to define the total propulsive efficiency (η_D) to embrace all effects concerning hull and propeller discussed up to now. The propulsive efficiency is defined as the effective power delivered to the hull (the power require to overcome the ship resistance) divided by the total power actually delivered to all propellers.

$$\eta_D = \frac{P_E}{P_D} = \frac{P_E}{K_P \cdot P_P} \tag{4.12}$$

Adding the definition for hull, open water and relative efficiencies from equ.4.7, 4.9 and 4.11 the propulsive efficiency can be written as,

$$\eta_D = \eta_H \cdot \eta_0 \cdot \eta_R \tag{4.13}$$

As a result of the propeller-hull interaction, the propulsive efficiency (η_D) of the propeller operating behind the ship can be better than the open water efficiency (η_0) as measured in the open water tests. For calculations of the ship fuel consumption in general and in particular for the DDG-51 case, the propulsive efficiency is essential, since it takes into account all the losses during the energy conversion process. The final thrust power required from all propellers to overcome the ship resistance can be calculated by considering all the energy loses from the effective power,

$$p_D = \frac{P_E}{\eta_H \cdot \eta_0 \cdot \eta_R} \tag{4.14}$$

4.3 Propulsion efficiency chain

After calculating the required thrust power (p_D) delivered by all the propellers in the ship, the equivalent required engine brake power (p_B) is now can be calculated. In the conventional propulsion plant configuration there is a shafting and probably a gear box between the prime mover and the propulsor which in our case an engine and a propeller, respectively. This transmission is responsible for power loses caused by friction in the stern tube bearing and shaft bearings .Shaft loses are expressed in terms of shaft efficiency η_S , which is define as,

$$\eta_S = \frac{P_P}{P_S} \tag{4.15}$$

Where P_P is the required power delivered to the propeller which calculated in equation 4.14, and P_s is the power delivered to the shaft defined as,

$$P_S = 2\pi \cdot n_S \cdot M_S \tag{4.16}$$

n_S is the shaft rotational speed , and M_S is the delivered shaft torque.

The gear box efficiency is defined as the ratio between the shaft power to the total required brake power.

$$\eta_{GB} = \frac{P_S}{K_e P_B} \tag{4.17}$$

K_e is the number of engines delivered power to the shaft. P_B is the engine brake power.

Substitute equation 4.15 to 4.17 we can get,

$$P_B = \frac{P_P}{K_e \eta_{GB} \eta_S} = \frac{P_P}{K_e \eta_{TR}} \tag{4.18}$$

where η_{TR} defines as the transmission efficiency.

4.4 Matching the designed propellers to DDG-51

In Chapter three, two types of propellers were designed for the DDG-51; single and contra-rotating propellers. The outcome of the design is the open water diagrams for propeller efficiency, propeller load and torque coefficients. The propeller performances are graphed as a function of the propeller advance coefficient. The advance coefficient is the ratio between the ship speed and the propeller rotational speed; as a result there are two degree of freedom for each state on the propeller performance open water diagram; ship speed and propeller rotational speed. This becomes even more complicated when the contra-rotating propeller is discussed where each point on the open water diagrams is defined by two advance ratios; for the forward and aft propellers. Accordingly, there are three degrees of freedom; ship speed and forward and aft propellers' rotational speeds.

The propeller is designed for a given characteristics; the ship required thrust at a specified speed. At the design process, the ship characteristics are not taking into account and this is the motive for generalizing the performance with the advance coefficients and produce the required propeller speed to be self-determination .In the process of matching a propeller to a specific ship load, the exact propeller required thrust is define; resulting to eliminate the propeller speed freedom to only one distinct speed which provides the required ship thrust for this specified ship speed. This process is presented in the following sections. First, matching the single propeller performance to the DDG-51 load curve, and then, repeat the procedure to the CRP case.

4.4.1 Matching single propeller to DDG-51 load curve

The DDG-51 required thrust was measured during the performance trials conducted by the Naval Surface Warfare Center (Tsai,1994).The ship thrust coefficient vs. the ship speed is presented in figure 4-1.On the other hand, the single propeller (open water) thrust coefficient as a function of the advance ratio is presented in figure 4-2. In order to match the propeller curve to the ship load curve an interpolation is necessity from the ship speed to the propeller advance coefficient. The interpolation process is implemented in the **Fuel_Consumption.m** script file. This script can be found in appendix C.2.

The interpolation process can be explained by the dotted green lines. For example, required thrust coefficient of 0.45 the ship speed is ~28 knt (figure 4-1).Next, from the propeller thrust coefficient curve (Fig. 4-2) the associated advance coefficient at the same thrust coefficient can be found, which in this example is ~0.96. The required propeller speed can be calculated using the definition of the advance ratio (J_S),

$$J_S = \frac{V_S}{n_p \cdot D} \tag{4.19}$$

The subscript s in the advance ratio relates to the ship speed with contrast to J_A which defined as the ratio of the advance speed (equ.4.3) and the propeller speed. n_P is the propeller rotational speed.

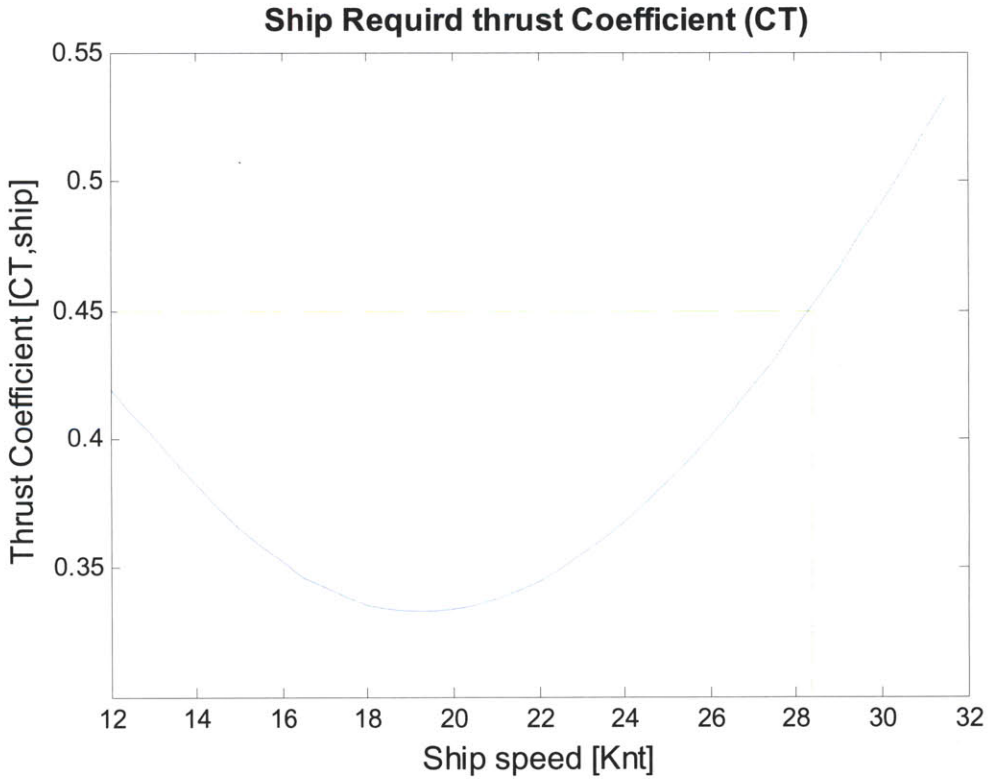

Figure 4-1 : DDG-51 Thrust coefficient vs. ship speed

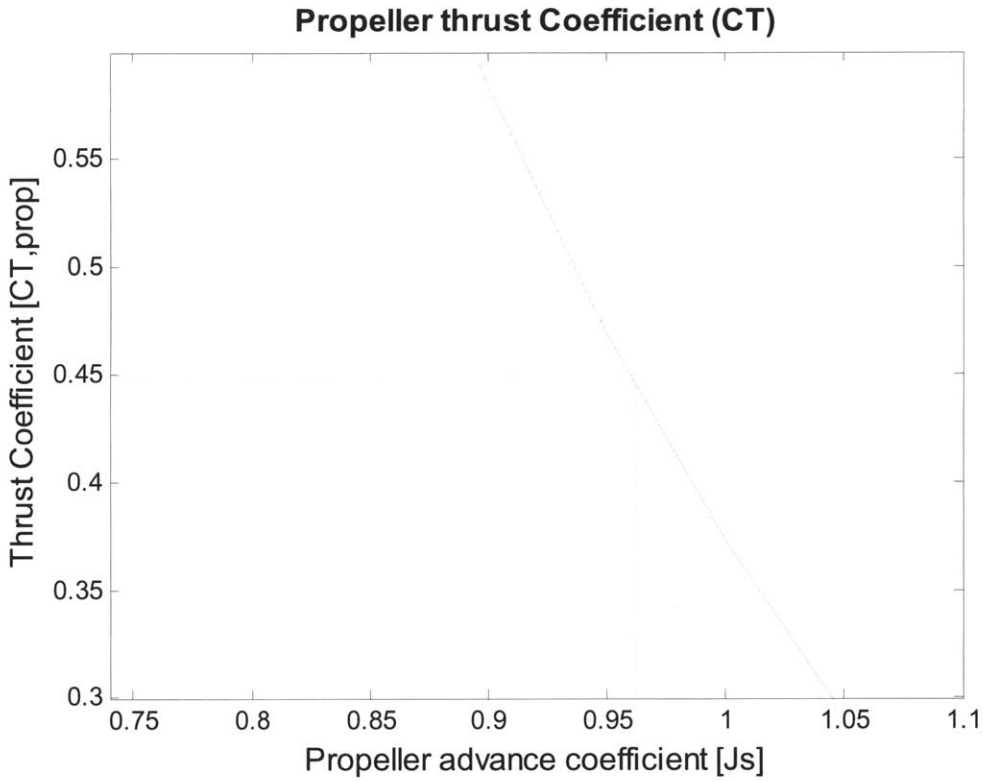

Figure 4-2 : Single Propeller Thrust coefficient vs. advance ratio

The single propeller thrust coefficient values, as illustrated in figure 4-2, are only the values that match the ship required thrust. The full range single propeller thrust coefficient can be seen in figure 3-1 (chapter three).

4.4.2 Matching CRP to DDG-51 load curve

As already mentioned, matching the CRP propeller open water performance to the required ship load is more complicated from the single propeller case ,since for each ship load there are several matching combination of forward and aft propellers' advance ratios, as illustrated in figure 4-3.

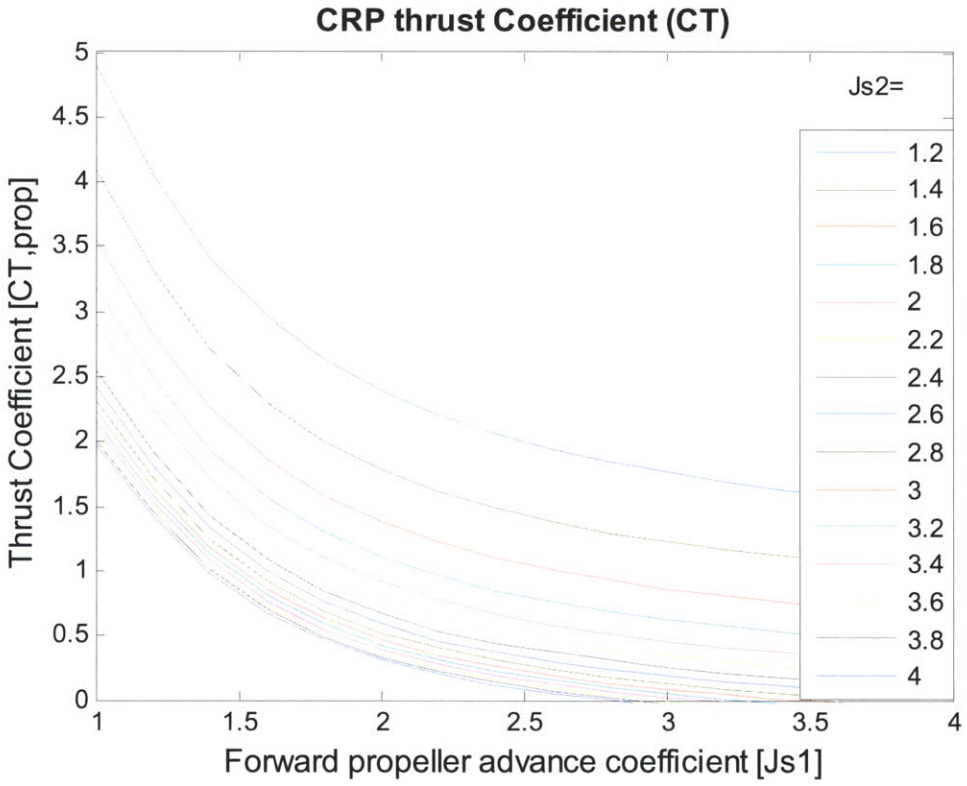

Figure 4-3 : CRP Thrust coefficient vs. for propeller advanced coefficient

To reduce the multiple advance ratios combination to only one, a constraint must be added. Such a constraint should product a particular advance ratio combination which takes into account one of the follow:

1. Optimize the CRP set efficiency.
2. Equal torque at each propeller.
3. Reducing propeller cavitation vulnerability.

For consistent with the efficiency comparison (3.5), the advance ratio's combination, which produces the best efficiency at each point, was selected.

The propeller thrust coefficient curve for these combinations is presented in figure 4-4.

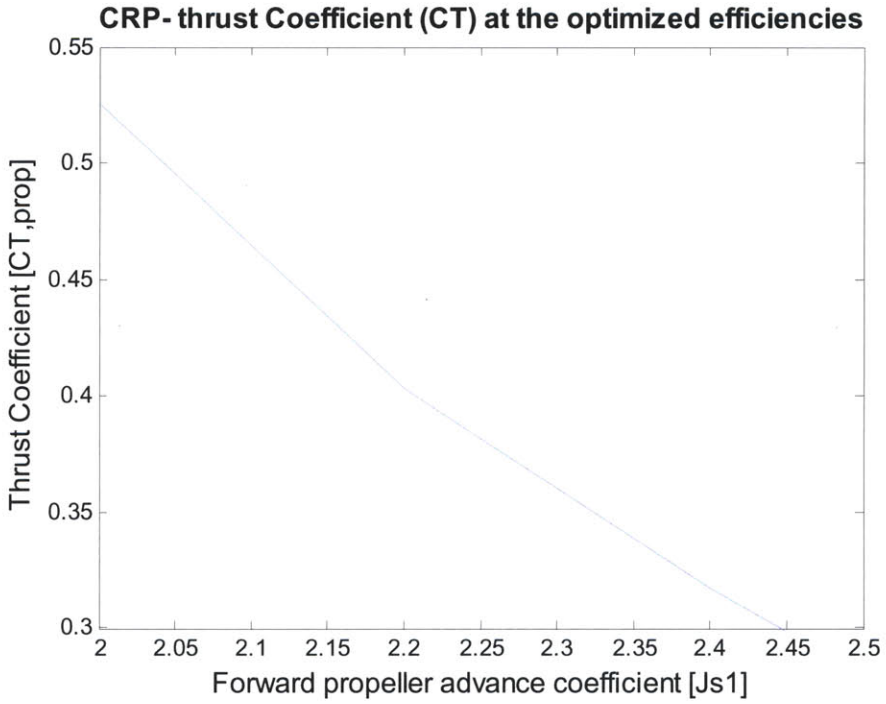

Figure 4-4: CRP thrust coefficient at advance ratio combinations which produce max efficiency

Again, the thrust coefficient values which presented in figure 4-4 are only those that match with the ship required load coefficient. Now, the same interpolation procedure as done for the single propeller case can be made to match each ship load to the associated propeller performance.

4.5 Fuel Consumption

4.5.1 From propeller thrust coefficient to required engine brake power

The outcome of the interpolation of the propeller thrust coefficient with the required ship load is the required advance ratio at each specified ship speed, for both cases; single and contra-rotating propeller. The next step is to evaluate the open water required torque Q at these advance ratios. After the open water required torque is found, the shaft required torque M_P could be calculated using equation 4.11 ,which take into account the differences between the propeller operating in open water to the same propeller operating behind the ship (η_R). The shaft required power is computed with equation 4.10.When considering the shaft and gear box loses, the required engine brake power is, then, calculated threw equ.4.18. The results of this procedure will introduce next for the single and contra-rotating propellers.

Single propeller:

The propeller torque coefficient at the required advance ratios can be found from the single propeller open water diagram (figure 3-14).The open water required torque is calculated,

$$Q = K_Q \rho \cdot n_P^2 \cdot D^5 \tag{4.20}$$

From this point, the process for estimating the engine brake power for the designed single propeller is the same as described at the beginning of this section. Several assumptions were made during these calculations:

1. The required load is does not differ from the one measured during the DDG-51 trials, regardless the type of the propulsor (means that the thrust deduction factor is the same and equal to 0.055.
2. The relative efficiency for the designed propeller is the same as for the exciting DDG-51 and is equal to 0.985, regardless the propulsor type.
3. The advance velocity equals the ship speed.
4. The DDG-51 propulsion configuration is two engines (Ke=2) per one shaft, with total of two shafts in the ship. (Kp=2).

5. The transmission efficiency equal to 0.95.

Contra-rotating propeller:

The advance ratios combinations which produce the most effective propeller were interpolated to match to the ship required thrust coefficient.

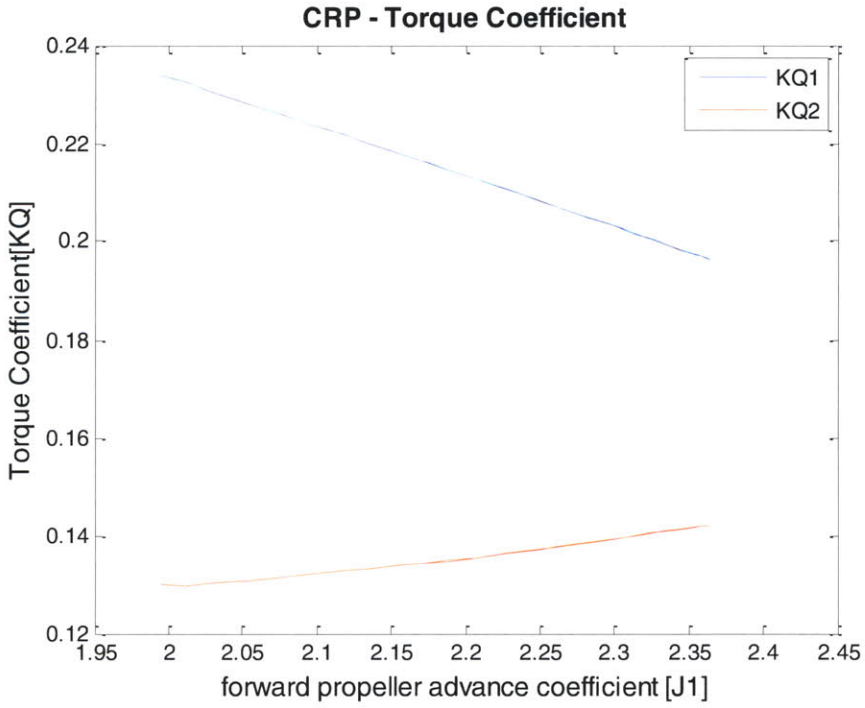

Figure 4-5 : CRP required interpolated torque coefficient

The open water required torque for each propeller is calculated next,

$$Q_{(k)} = K_{Q(k)}\ \rho \cdot n_{P1}^2 \cdot D^5 \tag{4.21}$$

where k=1,2 relates to the fore and aft propeller, respectively. In the CRP code the aft propeller torque is normalized by the fore propeller rotational speed, therefore, the aft torque coefficient is multiplying by the fore propeller speed.

The real torque M_P (i.e., behind the ship) is calculated using equation 4-12.The required thrust power is computed next,

$$P_P = Q_1 \cdot w_1 + Q_2 \cdot w_2 \tag{4.22}$$

where w_1 and w_2 are the fore and aft propeller rotational ratio, respectively, which are interpolated from the required ship speed and the related advance ratios.

From this point the rest of the calculation process for the required CRP engine brake power is the same as the single propeller.

The required ship brake power, for the single and CR propellers, is presented in figure 4-6.

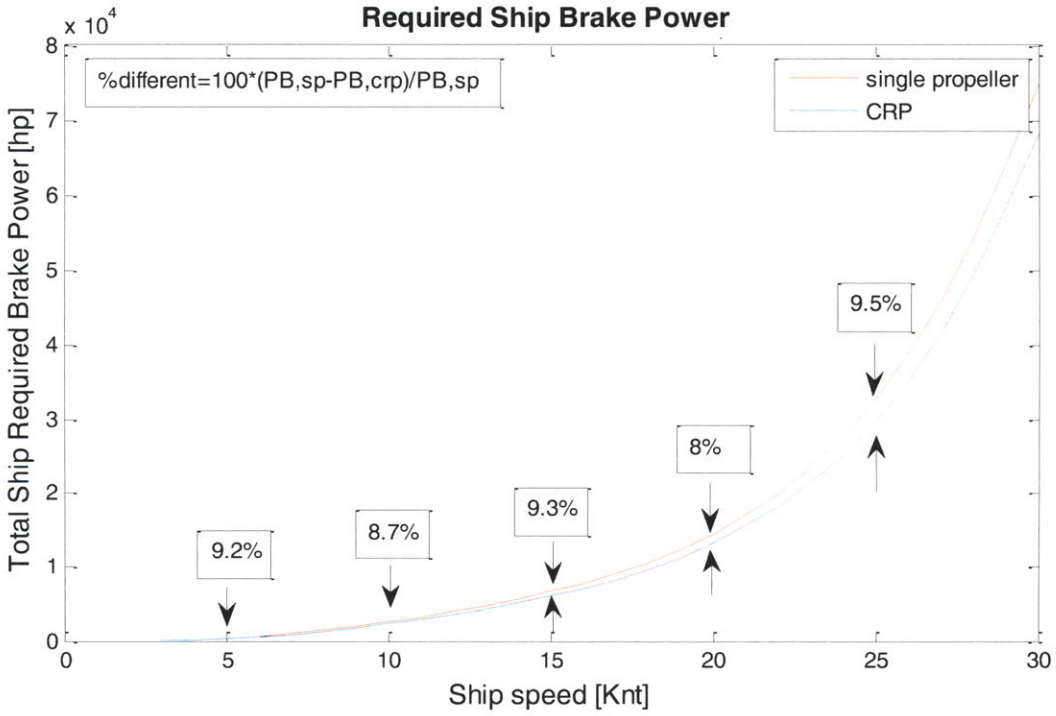

Figure 4-6 : Estimated required engine brake power for the DDG-51

The CR propeller is more effective the off design states, it can be seen from figure 4-6 that at the on design (20 knts); the percentage in the required ship brake power is the minimum (8%).The average power saving with the CRP propulsion is 8.8%.

4.5.2From engine brake power to fuel consumption

The ship fuel consumption is determined by a number of parameters; the ship or engine specific fuel consumption, the required engine brake power to overcome the ship resistance and the operational profile, i.e., how much time the ship travel at each speed. When designing a ship the operational profile is estimated by the profile of the same type existing ships and so, the propeller design point will be, probably, the one where the ship travels the most. The engine specific fuel consumption is defined by the engine manufacturer. However, the actual operational profile is, in general, slightly different from the estimated one therefore the actual fuel consumption is also altered from the predictable one. The actual specific fuel consumption is also slightly different from the one given by the manufacturer when the engine was tested in optimum condition in the manufacturer lab. These are the reasons for the fuel consumption calculation, at this work; the actual specific fuel consumption and the actual operational profile were selected.

Data from actual DDG-51 class ships were recorded and averaged to produce the actual operational profile for this class (Surko and Osborne, 2005).This data is also used in this work to compute the fuel consumption for the DDG-51 equipped with single and contra-rotating propellers, the DDG-51 operational profile is shown in figure 4-7.The data is also given in appendix D.

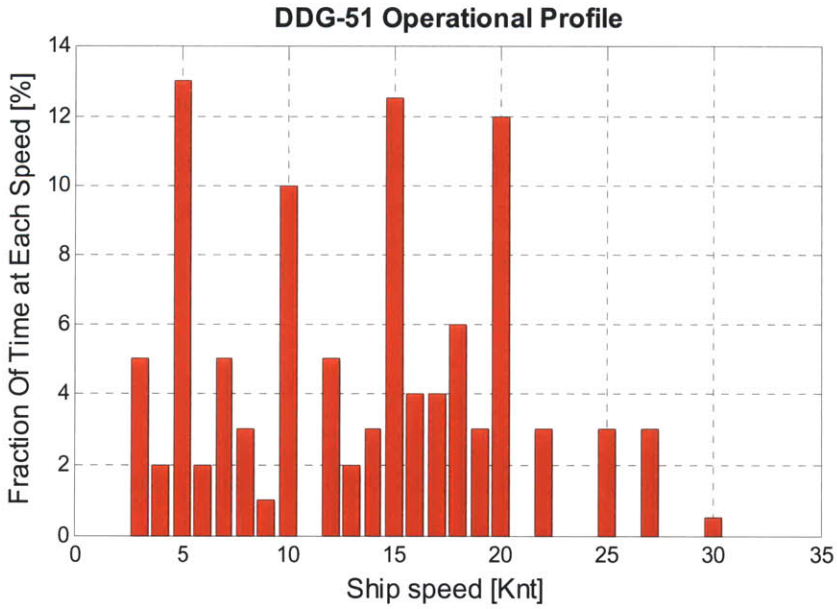

Figure 4-7 : DDG-51 actual operational profile data took from (Surko and Osborne, 2005)

The ship actual specific fuel consumption was recorded and analyzed during the ship performance trials (Tsai, 1994) and is presented in figure 4-8.

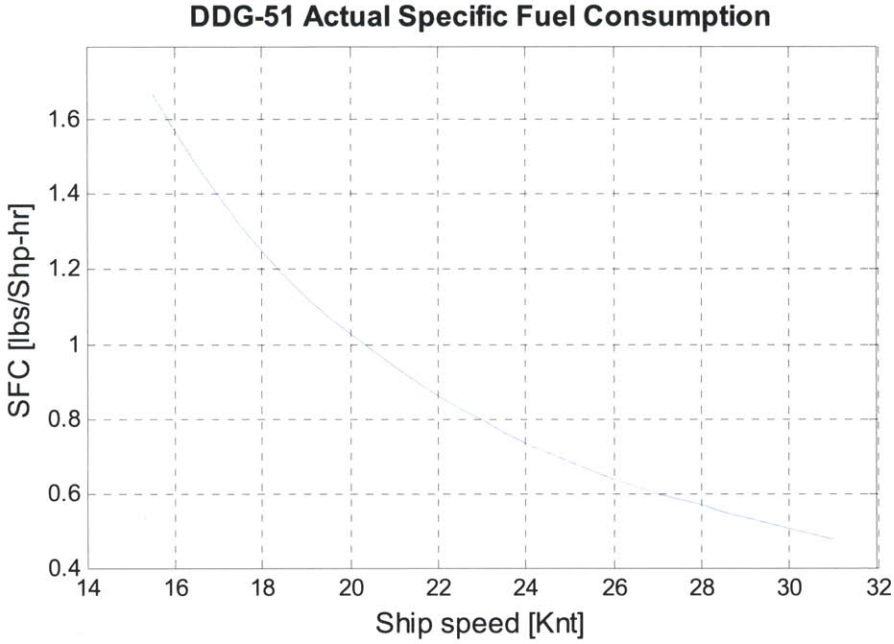

Figure 4-8 : DDG-51 actual specific fuel consumption data took from (Tsai, 1994)

The actual specific fuel consumption is already accounts for the number of engines connecting to the shaft at each ship speed and also it accounts for the number of propellers required to operate at each speed. For example, at low ship speeds not all the engines brake power is required, so by the mission operational methodology is decided whether to use one engine at half load with one shaft or two engines with 25% load connect to each shaft. The actual specific fuel consumption is already taking into account these configurations.

Once the required engine brake power, the specific fuel consumption and the operational profile were determined, the ship estimated fuel consumption W_{fuel} [lbs] can be calculated,

$$W_{fuel} = P_{B,ship} \cdot (sfc) \cdot (time) \tag{4.23}$$

Here $P_{B,ship}$ is the total brake power delivered by all engines at each speed. $time$ is the total hours the ship stay at each ship during a deployment of six month, which is the average deployment period for this ship class, assuming the ship does only one deployment a year.

The DDG-51 annually fuel consumption (assuming one deployment of six month a year) for each type of the optimum designed propulsors; single or contra-rotating propellers is presented in figure 4-9.

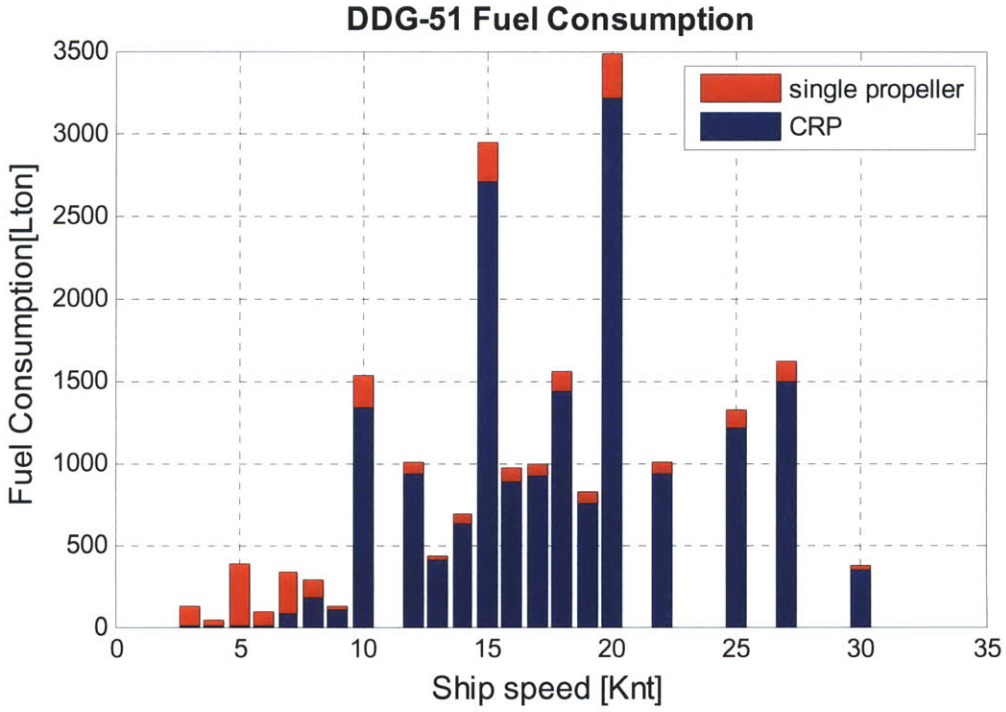

Figure 4-9 : DDG-51 annually fuel consumption calculated for the designed SP and CR propellers

The total annually estimated saving for one DDG-51 destroyer propelled by a contra-rotating propeller in contrast to the same ship propelled by single propeller assuming one deployment of six month a year is 2548 [Lton].

Total annual DDG-51 estimated fuel consumption:

SP = 19,733 [Lton]

CRP = 17,998 [Lton]

Difference = 1,734 [Lton].

Percent difference = 8.8%

The computing of the DDG-51 fuel consumption is implemented in the MATLAB script, **Fuel_Consumption.m**. This script is added in appendix B.3

This page intentionally left blank

Chapter 5 – Prototype Manufacturing

Once the design process for the single and contra-rotating propellers for the DDG-51 is completed, we can move forward to the next step; modeling and manufacturing the propellers prototypes. The propellers' hub was designed to fit to a specific electric motor designed and developed by an electrical engineering team working with Sea grant collage at MIT. This motor is currently under evaluation tests.

The production of a these propellers as well as making a test plan for future experiments are the subject of the following sections .

5.1 Modeling the propellers

5.1.1 Full scale propeller selection

Table 3-9 summarizes the most efficient DDG-51 CR propeller for a various number of blades configuration. The CRP set with five blades for both propellers was found to be the most efficient configuration. In this chapter, however, the concept which leads the experimental set up was to make the CRP model as simple as possible with respect to manufacturing aspects. Therefore, the CRP configuration of 3 blades for the fore propeller and four blades for the aft one was chosen to be the suitable set for the experiments. As for the single propeller, since the most effective propeller already with the minimum number of blades it was the one who was selected for the performance comparison validation between the two propulsors type. Moreover, another set of CR propeller was designed, to detect the influence of the axial separation between the two components. The assumption of the CRP code is that the slipstream does not contract downstream, therefore the aft component diameter is not required to be smaller than the fore one .Based on this assumption the aft propeller geometry is computed with consideration of its axial space from the fore propeller. Validation of this assumption with respect to the axial separation will be tested by the additional propeller.

The propeller performances of the last propeller are very similar to the first CRP set (with different axial separation), which is expected by the assumptions of the code. The comparison between the real performances of the two CRP sets is very important with respect to the code assumptions validation.

The characteristics of the three model propellers are shown in table 5-1,

	Single Propeller	CRP1	CRP2
Diameter [in]	D_m=14	$D1_m$= $D2_m$ =14	$D1_m$= $D2_m$ =14
Hub Diameter [in]	D_{hub}=3.25	D_{hub}=3.25	D_{hub}=3.25
Number of blades	Z=3	Z1=3,Z2=4	Z1=3,Z2=4
Axial separation/R1	-	Xf=0.5	Xf=0.75
2D drag coefficient	0.01	0.01	0.01
On design advance coefficient	Js=0.9928	Js1=1.702, Js2= 2.3828	Js1=1.702, Js2= 2.3828
Thrust coefficient	Kt=0.1485	Kt=0.4363	Kt=0.4363
Torque coefficient	Kq=0.0307	Kq=0.1668	Kq= 0.1669
Efficiency	0.7647	0.8264	0.8260

Table 5-1: Propeller models main characteristics

5.1.2 Similitude analysis

The model propeller outer diameter was selected to be large enough for better accuracy with the full scale prop performance .The maximum diameter is, however, restricted by the following : tow tank or propeller tunnel geometry , the maximum allowable torque delivered by the motor, and by the max thrust limit of the load sensors. The model diameter was therefore chosen to be 14 inch. For fluid continuity, the outer hub diameter set to be the same as the electric motor diameter. The non-dimensional propeller performances; Kt, Kq, Js1, Js2 for both; full scale and model scale, are equal at all states.

The constraints for set up the test plan arise from tow tank and motor characteristics are summarized in table 5-2.

No.	Characteristic	Value	Limitation item
1.	Max Thrust	100lbf	Dynamometer/load sensors
2.	Inflow speed	3-12 ft/sec	Tow tank/Propeller tunnel
3.	Max Torque	9 N-m	Motor
4.	Moment ratio [q]	1	Motor

Table 5-2: Similitude analysis limitation

As already explained in chapter two, each off design state has a multiple combination of potential advance ratios because both propellers are free to rotate in different speeds. However, with the limitation of the torque ratio delivered by the motor is equal to one (q=1), only one combination of advance ratios (Js1, Js2) defines an off design state. The propellers torque coefficient at the off design for the CRP1 set (Xf=0.5) as well as the points with the equal torque (green line) are presented in figure 5-1.

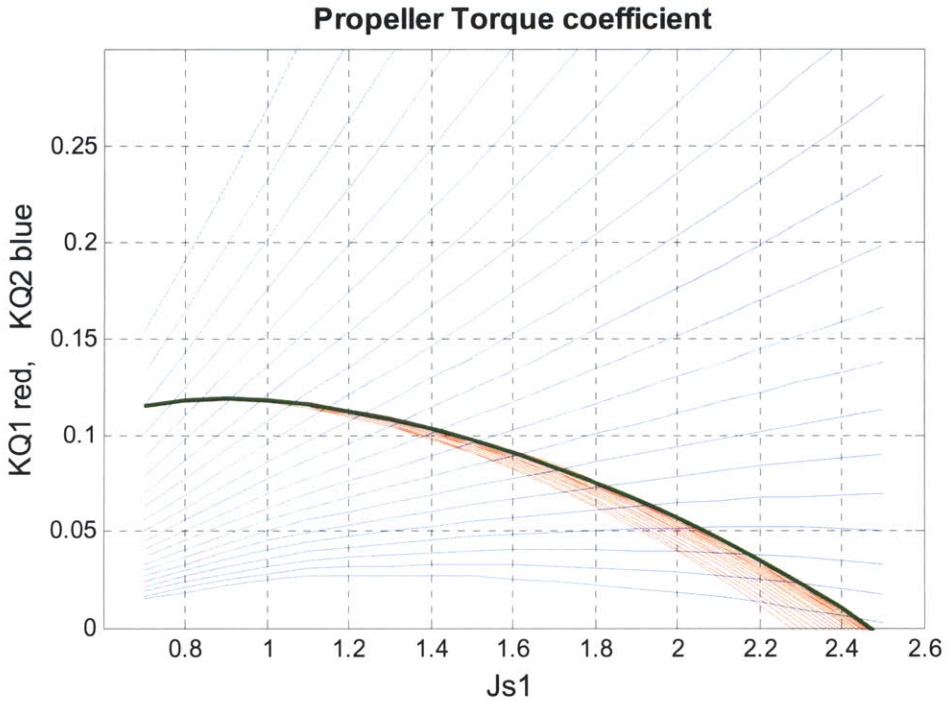

Figure 5-1: CRP1 Torque coefficient, the green line represent the equal torque coefficient

5.2 Propeller design with Solid Works

Once the propeller was optimized and designed using the CRP code, the geometry function can produce a model scale propeller .This function produces a file of a single designed blade coordinates in a text file (using **MakeSolidworks.m** function). This file could transfer to STL files if using Solid Works as the CAD program, by the Solid Works macro. In this work Solid Works was used as the CAD program design tool. Next, the propeller blade is being transformed from surface to object. After the full blade is accomplished in the CAD program, it is copied to the required number of blades. A detailed design can now be made like designing the suitable hub and other desired propeller features such as; fillets at the hub, fairings, slots for screw connections, etc. In the final stage a practical CRP model set which perfectly fitting on the electric motor shafts can be produced by a 3D printer.

The final propellers geometry which produced by the Matlab codes are presented in figures 5-2. .

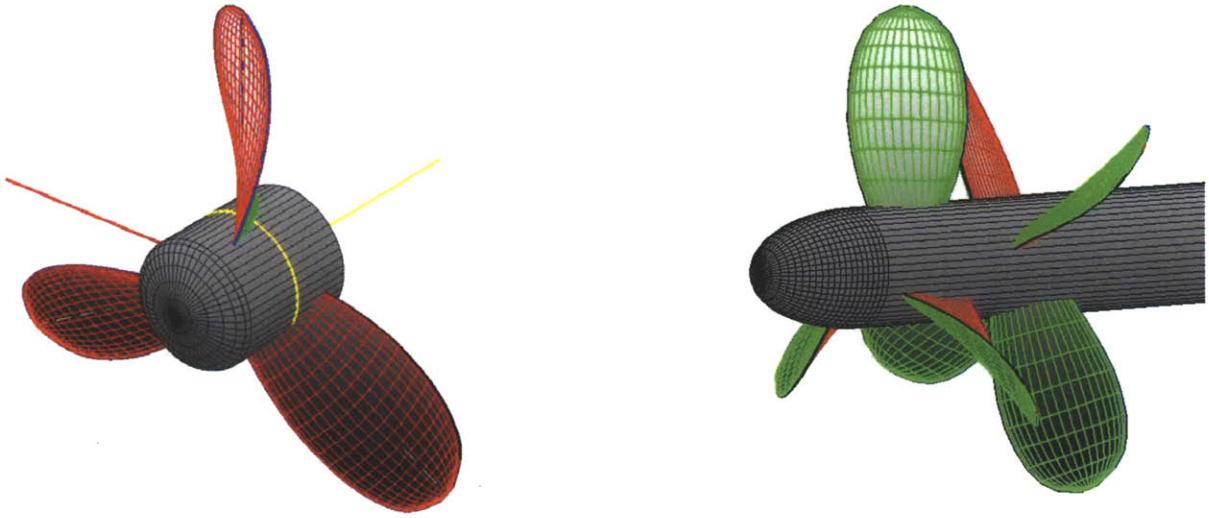

Figure 5-2: single and contra-rotating propeller (CRP1) geometry as produced by the Matlab code.

The final Solid Works design for CRP1 is shown in figure 5-3.

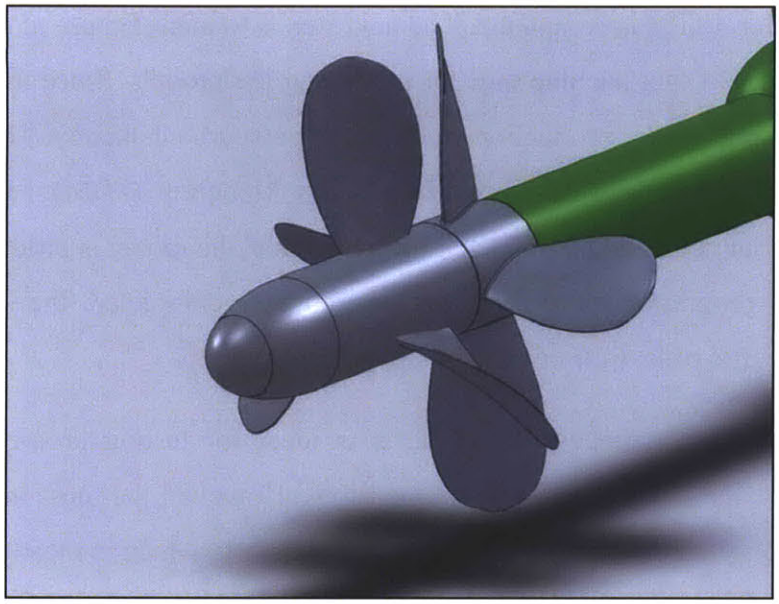

Figure 5-3: CRP1 as designed by Solid works

The designed contra-rotating propeller as attached to the electric motor is presented in figure 5-4.

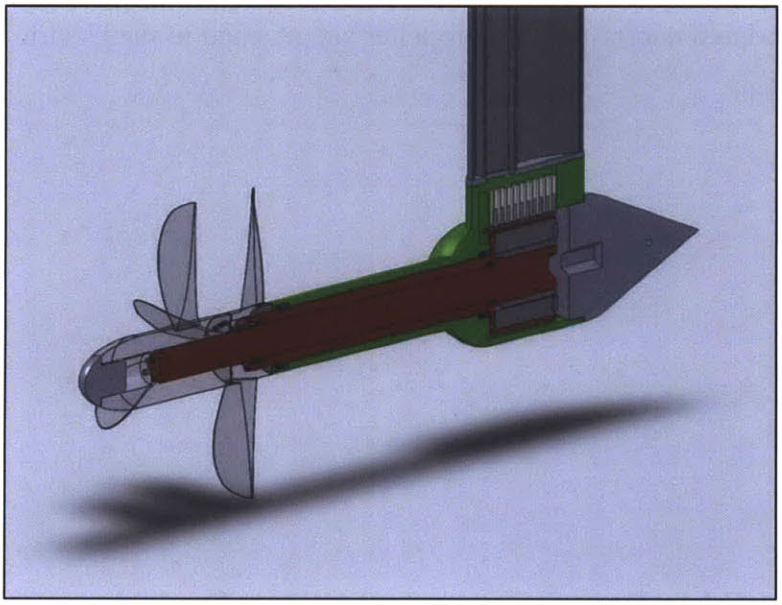

Figure 5-4: The electric motor equipped with the CRP set

5.3 The prototypes production- FDM process

Once the propeller design is completed. The next step is to manufacture it; one way to do so is by using a 3D printer as the machine tool for producing the models. Since the MIT printers are limited to 9 inch diameter, the production made by an outsource company. The process selected for production our models was the Fused Deposition Modeling (FDM). In this process, a thermoplastic material is melted and injected from a nozzle, the model is produced layer by layer based on the solid program. One the model production is completed, the support material is removed with a specific base. (http://www.quickparts.com).

The advantages of this process are: first, it is ideal for testing prototypes. Second; this process can produce the required propeller dimensions, However, the most important advantage is that it has an impressive production tolerance of 0.005 inch, which is mostly important in case of propeller where the produced model should be similar to the designed one, to get the same performance.

The material which used in the FDM process to produce the models is a blend of ABS (Acrylonitrile butadiene styrene) called ABS-M30.

The complete 3D printed contra-rotating propeller set attached to the electric motor can be seen in figures 5-5 and 5-6.

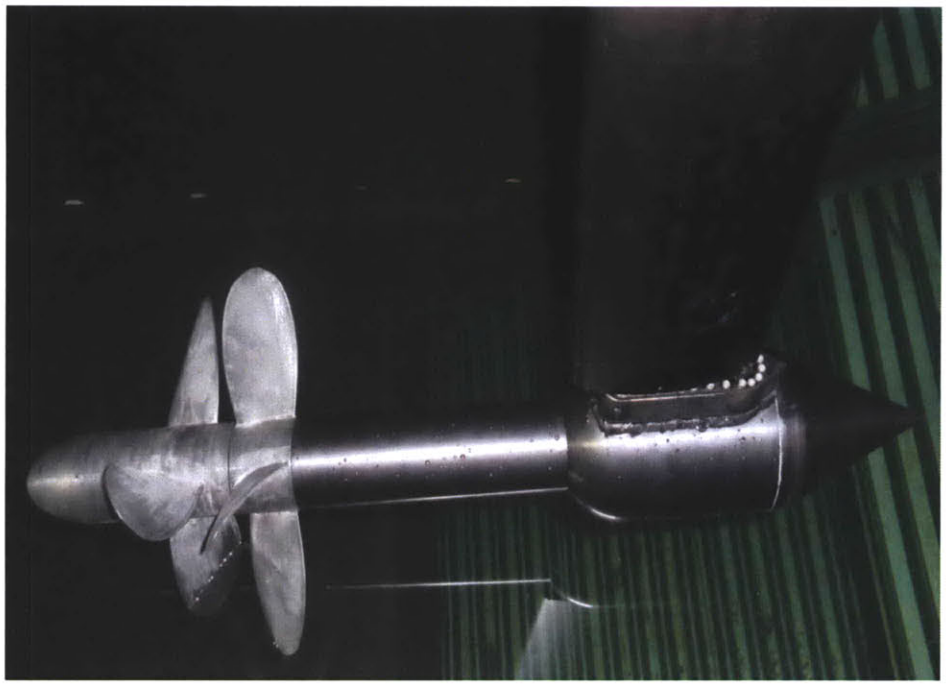

Figure 5-5: Picture of the CRP1 set connected to the electric motor at the preliminary tests

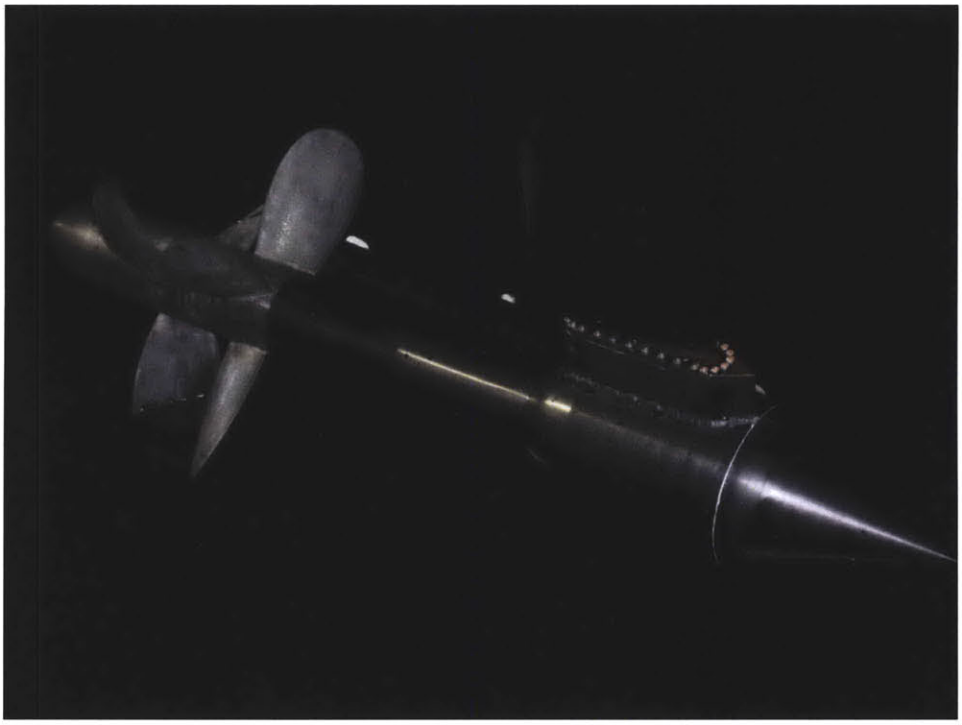

Figure 5-6: Picture of the CRP1 set connected to the electric motor at the preliminary tests

5.4 Experimental set up

As soon as the propellers models were produced and the electric motor was ready for inspection, the next level towards the future experiments can be prepared. Since the MIT propeller tunnel is limited to propeller model diameter up to 10 inch another location for assembly the preliminary tests is required. This place decided to be the US Naval Academy towing tank.

5.4.1 Naval Academy towing tank

The facility in the towing tank at the US Naval academy was found to be suitable for the preliminary experiments. The 380-Foot Towing Tank is shown in figure 5-7,

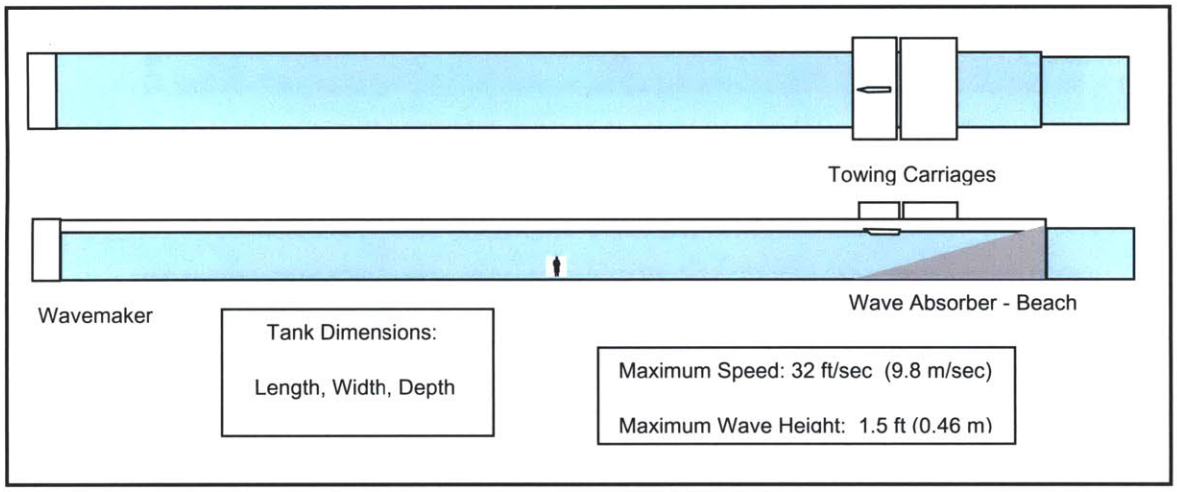

Figure 5-7: US Naval Academy 380 foot towing tank

This 380-foot towing tank is a world class facility that is large enough to test ship models up to 25 feet in length and weighing several thousand pounds. A large tank is required to overcome scaling problems when testing models fitted with propellers, rudders and other scaled appendages. The long tank length allows testing at high speeds. The tank is outfitted with two towing carriages and specialized equipment for measuring resistance.

Carriage:

1) High speed – 15' x 34' wide aluminum box truss; 11,000 lbs.
2) Low speed – 19' x 34' wide aluminum deep-web box truss; 21,000 lbs.

Drive system:

1) Shore mounted motors pulling pre-loaded wire rope cable.

2) 200 hp motors with 400% overload capability equal to total of 1,600 hp.

Instrumentation:

16 bit PC data acquisition systems on carriage with digital wireless data transmission network, fiber optic trailing cable for video transmission, dynamometers for measurement of multiple axis forces on surface and submerged vehicles, propeller thrust and torque dynamometers, full range of sensors for measurement of force, displacement, angle, angular rate, acceleration, pressure, wave elevation; acoustic Doppler velocimeters, 3-D video motion analysis system.

5.4.2 Test plan

The objective of the preliminary tests is to check the motor apparatus and the fairing connected to the motor to properly attach to the carriage which can deliver in the future reliable results. In addition, the concept of the electric motor is inspected for appropriately driving the contra-rotating propellers. The motor was not ready at this point to make full sets of experiments to validate the CRP code but these preliminary tests were a further step to rich this goal.

After running the carriage in several speeds in the range of 3-15 ft/sec the apparatus and the propellers were found to be able with conducting full sets of experiments with regards to vibrations, and power delivering. The electric motor, on the other, requires more developments and improvements.

The implementation of the test set up plan in the Matlab code, **Test_plan.m** script can be found in appendix B.3.

This page intentionally left blank

Chapter 6 – Summery

The development of this thesis was in a deliberate instruction. First, the history of contra-rotating propellers and the design theory behind the contra-rotating code was introduced in chapter one .A CRP preliminary design for an existent ship, the DDG-51, with comparison to single propeller performances was performed in chapters two. Once the efficiency superiority of the contra-rotating propeller over the conventional single propeller was studied in chapter two, the consequence with respect to the ship fuel consumption was investigated in chapter three. Next, the CRP off design analysis; theory and implementation in MATLAB function was introduced in chapter four. The propeller final design and the propeller model design and manufacturing procedures was described in chapter five, at the end of the same chapter a preliminary tests and a progress toward future experiments was presented. All the supplementary calculations as well as the Matlab codes are shown in the appendices for a full completion of this work.

6.1 Conclusions

1. The contra-rotating propeller found to be, as expected, superior to the traditional single propeller to propel the DDG-51 class destroyer. The propeller efficiency at the on-design point is about 8.7% higher than the single propeller design point (84.15% and 76.8%, respectively).This fact match with other

2. Some new definitions which describe the off design attributes were familiarized in this thesis:

   The operational range, is defined as the off design states with efficiency larger than 50%.The CRP operational range is 75% larger than of the SP operational range,(2.8, 0.7 respectively).

   The optimum range, is defined as the off design states with efficiency larger than 70%. It is in 83% greater for the CRP set. (2.2 and 0.37, respectively).

3. If considering the same propulsion plant as for the exciting DDG-51 and assuming equal propulsive coefficients $t-w-\eta_R$ and transmission efficiency of 0.95, the annually fuel consumption saving for one DDG-51 ship with one deployment of six months a year can reach up to 2548 [Lton] which is 12.7% less than when equipped with the single propeller.

6.2 Recommendation for Future Work

1. As soon as the evaluation tests of the electric motor will complete, a set of experiments should be conducted to validate the CRP on and off design code. A portion of this thesis was to manufacture three propeller models based on the full scale DDG-51 design; contra-rotating propeller with axial separation between component of Xf=0.5; another set of contra-rotating propeller with the same characteristics but with an axial separation of Xf=0.75;and a single propeller. The apparatus for attaching the motor to the carriage at a towing tank was manufactured as well. The experiments should be based on the matrix test plan as perform in appendix D. The results should be compared to the open water diagram which can be formed with the **Test_plan.m** Matlab script.

2. Due to mutual interaction between forward and aft propeller, the prediction of cavitation performance is much more difficult for CRP than for SP propeller. The aft propeller induces a velocity field in the forward propeller plane which is mainly axially directed and nearly uniform. On the contrary, the forward propeller induces a strongly inhomogeneous velocity field in the aft propeller plane. Therefore, one blade of the aft propeller experiences an unsteady inflow not only depending on its own angular position but also on the forward propeller position; this leads to unsteady cavitation patterns on the aft blade. Laskos (2010) wrote a Matlab code to predict cavitation inception on the propeller blade of the CRP set. Further experiments in a cavitation tunnel should conduct to validate this code. The model propellers as well as the electric motor could be used for these experiments.

3. In the design process at this thesis, the propeller vibrations were not took into account. The frequencies of propeller in the water induced forces, moments and pressures on the ship structure these frequencies shall not be disturbed over a wide range. In order to keep the CRP set, especially with different number of blade, within certain limits these affects

should be considered during the design process and could be added as a complementary function to the CRP code.

4. The propeller designed point is currently determined by the ship operational profile. A Matlab code that calculates this point by means of reducing the ship full consumption for the full operational profile could be added to the OPENPROP codes.

Finally, all the above future recommendations mentioned above shows that even that this thesis was another step of understanding and designing a contra-rotating propeller further investigation on this field is required.

This page intentionally left blank

References

Abbott, I. & vonDoenhoff, A., 1959. *Theory of wing sections, including a summary of airfoil data,*, New York: Dover Publications.

Betz, A., 1919. Schraubenpropeller mit geringstem Energieverlust. *Nachrinchten der K. Gesellschaft der Wissenschaften zu Göttingen, Math-Phys.*, 193-217.

Breslin, J.P. & Andersen, P., 1994. *Hydrodynamics of Ship Propellers*, Cambridge University Press.

Burrill, L.C. Calculation of marine propeller performance characteristics. *Trans.NECIES*, 60,1944.

Caponnetto, M., Rolla, P. & Porro, M., 1997. A New Propeller Design Method for Fast Planing Boat Application. In FAST '97:Fourth International Conference on Fast Sea Transportation, July 21-23, 1997. Sydney, Australia: Baired Publications, pp. 175-185.

Caponnetto, M., 2000. Optimisation and Design of Contra-Rotating Propellers. In SNAME Propellers/Shafting Symposium. Virginia Beach, Virginia, pp. 3-1 to 3-9.

Carlton, J., 2008. *Marine Propeller and Propulsion*, Second edition.

Caster, E.B. & LaFone, T.A., 1975. *A Computer Program for the Preliminary Design of Contrarotating Propellers.*, Washington, D.C.: David W. Taylor Naval Ship Research and Developement Center.

Chung, H., 2007. *An Enhanced Propeller Design Program Based on Propeller Vortex Lattice Lifting Line Theory*. S.M. Thesis. Massachusetts Institute of Technology.

Coney, W., 1989. *A method for the design of a class of optimum marine propulsors*. Ph.D. Thesis. Cambridge, MA: Massachusetts Institute of Technology.

Conway, J., 1995. Analytical solutions for the actuator disk with variable radial distribution of load. *Journal of Fluid Mechanics*, 297, 327-55.

Conway, J., 1998. Exact actuator disk solutions for non-uniform heavy loading and slipstream contraction. *Journal of Fluid Mechanics*, 365, 235-67.

Cox, B. & Reed, A., 1988. Contrarotating Propellers-Design Theory and Application. In *Propellers '88 Symposium, September 20 and 21, 1988*. Virginia Beach, Virginia: Jersey City N.J.:Society of Naval Architectects and Marine Engineers, pp. 15.1-29.

Drela, M., 1989. XFOIL: An Analysis and Desing System for Low Reynolds Number Airfoils. In *Proceedings of the Conference,Notre Dame, Indiana, USA,5-7 June 1989*. Low 94 Reynolds number aerodynamics. Springer-Verlag.

Eckhardt,M.K.,Morgan,W.B.A propellerdesign method.*Trans.SNAME*,63,1955

Epps, B. et al., 2009. OpenProp: An open-source parametric design and analysis tool for propellers. In *Grand Challenges in Modeling & Simulation Conference (GCMS'09)*. Instabul, Turkey: Society for Modeling and Simulation International.

Epps, B.P., 2010a. *An impulse framework for hydrodynamic force analysis:fish propulsion, water entry of spheres, and marine propellers*. Ph.D. Thesis. Cambridge, MA: Massachusetts Institute of Technology.

Epps, B.P., 2010b, "OpenProp v2.4 Theory Document," MIT Department of Mechanical Engineering Technical Report, December 2010.

Froude,W. On the elementary relation between pitch, slip and propulsive efficiency.*Trans.RINA*,19,1878.

Glover, E., 1987. Propulsive Devices for Improved Propulsive Efficiency. In *Trans. Institute of Marine Engineers*. London: Published for the Institute of Marine Engineers by Marine Management (Holdings) Ltd., pp. 23-31.

Hough, G. & Ordway, D., 1965. Generalized actuator disk. *Developments in Theoretical and Applied Mechanics*, 2, 317-336.

Hans.K & Douwe.S., 2008. *Propulsion and Electric Power Generation Systems*.IMarEST.

Hsin, C., 1987. *Efficient Computational Methods for Multi-Component Lifting Line Calculations*. S.M. Thesis.

John Erricsson 1803-1899. *RINA* Affairs, October 2004.

Kerwin, J., 2001. "Hydrofoils and Propellers". In *Course 2.23 Lecture Notes*. Cambridge, MA: Massachusetts Institute of Technology.

Kerwin, J.E., and Hadler, J.B., "Principles of Naval Architecture Series: Propulsion," SNAME, 2010.

Kerwin, J., Coney, W. & Hsin, C., 1986. Optimum Circulation Distributions for Single and Multi-Component Propulsors. In *Twenty-First American Towing Tank Conference (ATTC)*. Washington, D.C.: National Academy Press, pp. 53-62.

Kerwin, J. & Lee, C., 1978. Prediction of Steady and Unsteady Marine Propeller Performance by Numerical Lifting-Surface Theory. In *Trans. SNAME, Vol.86*. pp. 218-253.

Kerwin, J. & Leopold, R., 1964. A Design Theory for Subcavitating Propellers. In *Trans. SNAME, Vol.72*. pp. 294-335.

Kerwin, J.E., 1986. MARINE PROPELLERS. In Annual Review of Fluid Mechanics. Palo Alto, CA, USA: Annual Reviews Inc, pp. 367-403.

Kimball R.W. and Epps B.P., "OpenProp v2.3 propeller/turbine design code," http://openprop.mit.edu, 2010.

Laskos, D., 2010. *Design and Cavitation Performance of Contra-rotating Propeller*. S.M. Thesis. Massachusetts Institute of Technology

Lerbs, E., 1955. *Contra-Rotating Optimum Propellers Operating in a Radially Non-Uniform Wake*, Ft. Belvoir: Defense Technical Information Center.

Lerbs, E., 1952. Moderately loaded propellers with finite number of blades and arbitrary distribution of circulation. In *Trans. SNAME, Vol.60*. New York, N.Y.: SNAME, pp. 73-123.

Morgan, W., 1960. The Design of Counterrotating Propellers Using Lerbs' Theory. In *Trans. SNAME, Vol.68*. New York, NY: SNAME, pp. 6-38.

Morgan, W., Silovic, V. & Denny, S., 1968. Propeller lifting-surface corrections. In *Trans. SNAME, Vol.76*. New York, N.Y.: SNAME, pp. 309-347.

Morgan, W. & Wrench, J., 1965. Some Computational Aspects of Propeller Design. In *Methods in Computational Physics*. New York: Academic Press, pp. 301-31.

NAVSEA website, http://www.navsea.navy.mil.

Pien,P.C. The calculation of marine propellers based on lifting surface theory *.J. Ship Res.*,5(2),1960

Rankine,WJ. On the mechanical principles of the action of propellers.*Trans.*Rina,6,1865.

Sasaki, N. et al., 1998. Design system for optimum contra-rotating propellers. *Journal of Marine Science and Technology*, 3(1), 3-21.

Surko, S and Osborne,M. Operating Speed Profiles and the Ship Design Cycle. *Naval Engineers Journal*, pages 79–85, 2005

Taggart,R. *Marine propeller*. Principle and Evolution. Gulf Publishing,Texas,1969.

Tsai ,S,J, Bret, R,Hopkins, R and Stenson, *Comparison of Powering Performance Between DDG-51 and Conventional Combatant Hull Forms*. Naval Engineers Journal,1994, pages 88-89.

Wang, M., 1985. *Hub effects in propeller design and analysis*. Ph.D. Thesis. Cambridge, MA: Massachusetts Institute of Technology.

Wrench, J., 1957. *The Calculation of Propeller Induction Factors*, Washington, DC, United States: David Taylor Model Basin, Navy Department.

This page intentionally left blank

Appendix A-Circumferential induced velocity

A.1 Self-induced velocity

Hsin (1987) compared several methods for the calculation of the self-induced velocity .He found that the asymptotic formula developed by Lerbs-Wrench to be both the fastest and most accurate of the method. The final set of equations formulated by this method is presented in this section. The axial and tangential velocities induced by Z helical vortex lines of unit strength can be expresses as follows:

For $r_c \le r_v$

$$\bar{u}_a = \frac{Z}{4\pi\lambda}(1-2Z\frac{r_v}{\lambda}F_1), \qquad \bar{u}_t = \frac{Z^2}{2\pi r_c}\cdot\frac{r_v}{\lambda}F_1 \tag{A.1}$$

For $r_c \le r_v$

$$\bar{u}_a = -\frac{Z^2}{2\pi}\cdot\frac{r_v}{\lambda^2}F_2, \qquad \bar{u}_t = \frac{Z}{4\pi r_c}(1+2Z\frac{r_v}{\lambda}F_2) \tag{A.2}$$

Were:

$$F_1 \approx -\frac{1}{2Zy_0}(\frac{1+y_0^2}{1+y^2})^{0.25}\{\frac{1}{U^{-1}-1}+\frac{1}{24Z}[\frac{9y_0^2+2}{(1+y_0^2)^{1.5}}+\frac{3y^2-2}{(1+y^2)^{1.5}}]\ln(1+\frac{1}{U^{-1}-1})\} \tag{A.3}$$

$$F_2 \approx -\frac{1}{2Zy_0}(\frac{1+y_0^2}{1+y^2})^{0.25}\{\frac{1}{U-1}-\frac{1}{24Z}[\frac{9y_0^2+2}{(1+y_0^2)^{1.5}}+\frac{3y^2-2}{(1+y^2)^{1.5}}]\ln(1+\frac{1}{U-1})\} \tag{A.4}$$

$$U = \{\frac{y_0(\sqrt{1+y^2}-1)}{y\ (\sqrt{1+y_0^2}-1)}\exp(\sqrt{1+y^2}-\sqrt{1+y_0^2})\}^Z \tag{A.5}$$

$$y = \frac{r_c}{r_v \tan\beta} \quad , \quad y = \frac{1}{\tan\beta} \tag{A.6}$$

Here, r_c, r_v are the radii locations of the control point and vortex, respectively. λ is the strength of the trailing vorticity.

These influence functions are only for a single helical element of trailing vorticity. The total influence function induced by the complete vortex horseshoe is solitary due to the two free trailing vortices, since the bound vorticity induces no velocities on the lifting lines. The total axial and tangential influence function induced on control point on the lifting line can be written as:

$$\bar{u}_a^*(m,p) = \bar{u}_a(m,p) - \bar{u}_a(m,p+1) \tag{A.7}$$

$$\bar{u}_t^*(m,p) = \bar{u}_t(m,p) - \bar{u}_t(m,p+1) \tag{A.8}$$

A.2 Circumferential mean velocities

A2.1 Axial interaction velocities:

In the calculation of the axial velocity, only the free trailing helical vortices are taken into account since there is no contribution from the bound vorticity. Following Coney's notation, the local axial velocity induced at the m_{th} control point of component j by the p_{th} trailing vortex with unit strength of component l is given by:

$$\bar{u}_{a\,j,l}(m,p) = \frac{Z1}{\pi r_{v,l}(p)\tan(\beta_i(p))} C1 \tag{A.9}$$

Where,

$$C1 = \begin{cases} \pi + \dfrac{X_f}{2\sqrt{r_{c,j}(m) r_{v,l}(p)}} Q_{-\frac{1}{2}}(q) + \dfrac{\pi}{2}\Lambda_0(s,t), & r_{c,j}(m) \le r_{v,l}(p) \\ \dfrac{X_f}{2\sqrt{r_{c,j}(m) r_{v,l}(p)}} Q_{-\frac{1}{2}}(q) - \dfrac{\pi}{2}\Lambda_0(s,t), & r_{c,j}(m) > r_{v,l}(p) \end{cases} \tag{A.10}$$

The parameter included the definition of C1 are determined by:

$$q = 1 + \frac{X_f^2 + (r_{c,j}(m) - r_{v,l}(p))^2}{2 r_{c,j}(m) r_{v,l}(p)}$$

$$s = \sin^{-1}\left[\frac{X_f}{\sqrt{X_f^2 + (r_{c,j}(m) - r_{v,l}(p))^2}} \right]$$

$$t = \sqrt{\frac{4 r_{c,j}(m) r_{v,l}(p)}{X_f^2 + (r_{c,j}(m) - r_{v,l}(p))^2}}$$

Here, X_f is the axial separation between components. $Q_{-\frac{1}{2}}$ is the Lagendre function of the second kind and half integer order. And Λ_0 is the Heumann's Lambda function.

As same as for the self-induced velocity, the influence function derived at equation A.9 is for a single trailing vortex. The total axial velocity induced by the complete horseshoe vortex is therefore,

$$\bar{u}^*_{aj,l}(m,p) = \bar{u}_{aj,l}(m,p) - \bar{u}_{aj,l}(m,p+1) \qquad \text{(A.11)}$$

A2.2 Tangential interaction velocities

Contrary to the axial velocity component, both the bound and the trailing vorticity contribute to the tangential induced velocity. Hough's and Ordway's formula for the total tangential velocity shows that it vanishes everywhere outside the slipstream of the horseshoe vortex and is proportional to the bound circulation values and inversely proportional to the radial distance from the propeller hub. The resulting expression for this velocity is the same as the one obtained by a direct application of Kelvin's theorem using a circular path about the propeller shaft axis. Based on the notation used by Coney, a horseshoe vortex of strength Γ with lattice points at radii $r_{v,l}(p-1)$ and $r_{v,l}(p)$ of one component will induce a tangential circumferential mean velocity on a control point $r_{c,j}(m)$ of the other component, of:

$$\bar{u}_{t\ j,l}(m,n) = \begin{array}{lll} 0 & S > 0 & \infty < X_f \le \infty \\ 0 & S \le & X_f < 0 \\ \dfrac{-Z\Gamma}{2\pi r_{c,j}(m)} & S < 0 & X_f > 0 \end{array} \tag{A.12}$$

where

$$S = (r_{v,j}(p-1) - r_{c,j}(m))(r_{v,j}(p) - r_{c,j}(m)) \tag{A.13}$$

Appendix B –Matlab codes

B.1 CRP_Analyzer.m

```
% ========================================================================
% ========================================================= Analyze Function
%
% This function computes the "states" of a given Contra-rotating Propeller
"design"
% at given off-design advabcesd coefficient.
%
% Reference:
% B.P. Epps et al, "OpenProp: An Open-source Parametric Design and
% Analysis Tool for Propellers", Grand Challenges in Modeling and
% Simulation conference, Istambul, Turkey, July 2009.
%
% B.P. Epps et al, "OpenProp: An Open-source Design Tool for Propellers and
% Turbines", SNAME Propellers and Shafting conference, 2009.
%
% Author: Eyal Kravitz
% Last modified: 10/22/2010 by Kravitz Eyal
% ------------------------------------------------------------------------
function  [CT1,CQ1,CP1,KT1,KQ1,EFFY1,CT2,CQ2,CP2,KT2,KQ2,EFFY2,CT ,CQ, CP,
KT, KQ, EFFY,CTH, KTH]=...

CRP_Analyzer(Mp,M1,M2,Z1,Z2,RC1,RC2,RV1,RV2,VAC1,VTC1,VAC2,VTC2,C1oD1,C2oD1,G
1,G2,Xf,TANBIC1,TANBIC2,TANBIV1,TANBIV2,CL1,CL2,CD,Hub_Flag,Rhub_oR1,...

UAHIF11,UTHIF11,UAHIF12,UTHIF12,UAHIF22,UTHIF22,UAHIF21,UTHIF21,UASTAR1,UTSTA
R1,UASTAR2,UTSTAR2,VSTAR1,VSTAR2,VMIV1,VMIV2,...
                        Rhv,DR1,DR2,Js1,Js2)

% ------------------------------------------------------------------------
% '------ Computational inputs ------'
ALPHAstall  = 8*pi/180;
ITER        = 30;
dCLdALPHA   = 2*pi;
om1 = pi/Js1;              % om1 == omega1 * R1 / Vs
```

```
om2 = pi/Js2;%/R2oR1;      % om2 == omega2 * R1 / Vs
%The subscript X"o" refere to On Design point.
% ------------------------------------------- Record on-design variables

G1          = G1';                  % [1 x Mp] circulation distribution
G2          = G2';                  % [1 x Mp] circulation distribution
CL1o        = CL1;                  % [1 x Mp]On design lift coefficient
propeller 1
CL2o        = CL2;                  % [1 x Mp]On design lift coefficient
propeller 2
CD          = CD*ones(size(RC1));   % [1 x Mp] Section drag coefficient
(The input is scalar)
CDo         = CD;                   % [1 x Mp]On design Section drag
coefficient both propellers(?)

BetaIC1o    = atan(TANBIC1);        % [rad]
BetaIC2o    = atan(TANBIC2);        % [rad]

% '------ Initial 2D section performance ------'

ALPHA1      = zeros(size(RC1));   % [1 x Mp], [deg] alpha -alphaIC1 (At the
design point alpha -alphaIC)
ALPHA2      = zeros(size(RC2));   % [1 x Mp], [deg] alpha -alphaideal

% ------------------------------------------------------------------------
    % ========================================================================
    % ==   FIND STATE OF SYSTEM USING NEWTON SOLVER:
    % ==  iterate to solve residual equations for unknowns
    N_iter   = 1;
    ERROR    = 1;
    ERRORtol = 0.005;

    while N_iter <= ITER & any((ERROR) > ERRORtol )          % (WHILE LOOP
N1)

        disp(['------- Newton iteration: ',num2str(N_iter)]),  % status
message
```

```
        disp(' '),

        % ---------------------------------- Store last state of the system
        %Propeller 1:
        VSTAR1last =  VSTAR1;
        alpha1last =  ALPHA1;
        CL1last    =  CL1;
        G1last     =  G1;
        UASTAR1last=  UASTAR1;
        UTSTAR1last=  UTSTAR1;
        %Propeller 2:
        VSTAR2last =  VSTAR2;
        alpha2last =  ALPHA2;
        CL2last    =  CL2;
        G2last     =  G2;
        UASTAR2last=  UASTAR2;
        UTSTAR2last=  UTSTAR2;


        %Update UASTAR1,UASTAR2,UTSTAR1,UTSTAR2 for the residual vector

        [UASTAR1temp,UTSTAR1temp,UASTAR2temp,UTSTAR2temp] =
Induced_Velocity_CRP(M1,M2,G1,G2,UAHIF11,UTHIF11,UAHIF12,UTHIF12,UAHIF22,UTHI
F22,UAHIF21,UTHIF21);

        %Start "for" loop to update all blade sections with Newton solver
        for m = 1:Mp

                % -------------- Initialize linear system of equations
matrices
            R  = zeros(12,1);            % R  = vector of residuals
            A  = zeros(12,12);            % A  = matrix of derivatives
            DX = zeros(12,1);            % DX = vector of change in unknowns
            X  = zeros(12,1);            % X  = vector of unknowns

            X(1)  =  VSTAR1(m);          % X1
            X(2)  =  ALPHA1(m);          % X2
```

```
            X(3)  =     CL1(m);          % X3
            X(4)  =      G1(m);          % X4
            X(5)  = UASTAR1(m);          % X5
            X(6)  = UTSTAR1(m);          % X6
            X(7)  =  VSTAR2(m);          % X7
            X(8)  =  ALPHA2(m);          % X8
            X(9)  =     CL2(m);          % X9
            X(10) =      G2(m);          % X10
            X(11) = UASTAR2(m);          % X11
            X(12) = UTSTAR2(m);          % X12

            % ------------------------------------------------------------
----------

            % ------------------------------------------------------ Evaluate
residuals
            %disp('Evaluating residuals vector, R1...'),
            % disp(' '),
            %Residual vector propeller 1

            R(1) =  VSTAR1(m) - sqrt((VAC1(m)+UASTAR1(m)).^2 +
(pi*RC1(m)/Js1+VTC1(m)+UTSTAR1(m)).^2); % R1

            R(2) =  ALPHA1(m) - (BetaIC1o(m) - atan(TANBIC1(m)));
% R2

            R(3) =  CL1(m) -
CLCD_vs_ALPHA(ALPHA1(m),ALPHAstall,CL1o(m),CDo(m),dCLdALPHA);              %
R3

            R(4) =  G1(m) - (1/(2*pi))*VSTAR1(m)*CL1(m)* C1oD1(m);
% R4

            R(5) =  UASTAR1(m)-UASTAR1temp(m);
% R5
```

```
            R(6) =  UTSTAR1(m)-UTSTAR1temp(m);
% R6

            R(7) =  VSTAR2(m) - sqrt((VAC2(m)+UASTAR2(m)).^2 +
(pi*RC2(m)/Js2+VTC2(m)+UTSTAR2(m)).^2); % R7

            R(8) =  ALPHA2(m) - (BetaIC2o(m) - atan(TANBIC2(m)));
% R8

            R(9) =  CL2(m) -
CLCD_vs_ALPHA(ALPHA2(m),ALPHAstall,CL2o(m),CDo(m),dCLdALPHA);              %
R9

            R(10) =  G2(m) - (1/(2*pi))*VSTAR2(m)*CL2(m)* C2oD1(m);
% R10

            R(11) =  UASTAR2(m)-UASTAR2temp(m);
%R11

            R(12) =  UTSTAR2(m)-UTSTAR2temp(m);
%R12


            % ------------------------------------------------------------------
----------


            % ------------------------------------- Evaluate residual
derivatives
            %disp('Evaluating residual derivatives matrix, A...'),
            %disp(' '),

            A       =    eye(12,12);  % A(i,i) == 1 for all i = 1:8
            A(1,5)  =  - (VAC1(m)+UASTAR1(m))/sqrt((VAC1(m)+UASTAR1(m)).^2 +
(pi*RC1(m)/Js1+VTC1(m)+UTSTAR1(m)).^2);
```

```
            A(1,6)   =  -
(pi*RC1(m)/Js1+VTC1(m)+UTSTAR1(m))/sqrt((VAC1(m)+UASTAR1(m)).^2 +
(pi*RC1(m)/Js1+VTC1(m)+UTSTAR1(m)).^2);
            A(2,5)   =
(1/(1+(TANBIC1(m))^2))*(1/(pi*RC1(m)/Js1+VTC1(m)+UTSTAR1(m)));
            A(2,6)   =  -
(1/(1+(TANBIC1(m))^2))*(TANBIC1(m)/(pi*RC1(m)/Js1+VTC1(m)+UTSTAR1(m)));
            A(3,2)   =  -
Find_dCLCDdALPHA(ALPHA1(m),ALPHAstall,CL1o(m),CDo(m),dCLdALPHA);
            A(4,1)   =  - (1/(2*pi))*CL1(m)*C1oD1(m);
            A(4,3)   =  - (1/(2*pi))*VSTAR1(m)*C1oD1(m);
            A(5,4)   =  - UAHIF11(m,m);
            A(5,10)  =  - UAHIF12(m,m);
            A(6,4)   =  - UTHIF11(m,m);
            A(6,10)  =  - UTHIF12(m,m);
            A(7,11)  =  - (VAC2(m)+UASTAR2(m))/sqrt((VAC2(m)+UASTAR2(m)).^2 +
(pi*RC2(m)/Js2+VTC2(m)+UTSTAR2(m)).^2);
            A(7,12)  =  -
(pi*RC2(m)/Js2+VTC2(m)+UTSTAR2(m))/sqrt((VAC2(m)+UASTAR2(m)).^2 +
(pi*RC2(m)/Js2+VTC2(m)+UTSTAR2(m)).^2);
            A(8,11)  =
(1/(1+(TANBIC2(m))^2))*(1/(pi*RC2(m)/Js2+VTC2(m)+UTSTAR2(m)));
            A(8,12)  =  -
(1/(1+(TANBIC2(m))^2))*(TANBIC2(m)/(pi*RC2(m)/Js2+VTC2(m)+UTSTAR2(m)));
            A(9,8)   =  -
Find_dCLCDdALPHA(ALPHA2(m),ALPHAstall,CL2o(m),CDo(m),dCLdALPHA);
            A(10,7)  =  - (1/(2*pi))*CL2(m)*C2oD1(m);
            A(10,9)  =  - (1/(2*pi))*VSTAR2(m)*C2oD1(m);
            A(11,4)  =  - UAHIF21(m,m);
            A(11,10) =  - UAHIF22(m,m);
            A(12,4)  =  - UTHIF21(m,m);
            A(12,10) =  - UTHIF22(m,m);




          [dUAHIF11dB1,dUTHIF11dB1] =
Find_Self_dHIFdBetaIC(Z1,TANBIV1,RC1,RV1,Hub_Flag,Rhub_oR1,m);
```

```
                A(5,2)   = G1(m)*dUAHIF11dB1;
                A(6,2)   = G1(m)*dUTHIF11dB1;
            [dUAHIF12dB2,dUTHIF12dB2] = Find_Int_dHIFdBetaIC
(Z2,TANBIV2,RC1,RV2,-Xf,Hub_Flag,Rhub_oR1,m);
                A(5,8)   = G2(m)*dUAHIF12dB2;
                A(6,8)   = G2(m)*dUTHIF12dB2;
            [dUAHIF21dB1,dUTHIF21dB1] = Find_Int_dHIFdBetaIC
(Z1,TANBIV1,RC2,RV1,Xf,Hub_Flag,Rhub_oR1,m);
                A(11,2) = G1(m)*dUAHIF21dB1;
                A(12,2) = G1(m)*dUTHIF21dB1;
            [dUAHIF22dB2,dUTHIF22dB2] =
Find_Self_dHIFdBetaIC(Z2,TANBIV2,RC2,RV2,Hub_Flag,Rhub_oR1,m);
                A(11,8) = G2(m)*dUAHIF22dB2;
                A(12,8) = G2(m)*dUTHIF22dB2;


            % ------------------------------------------------------------
------


            % ------------------------------------------------- Solve for
delta X
            %disp('Solving linear system of equations...'),
            %disp(' '),
            DX = linsolve(A,-R);


            % ------------------------------------------------------------
------


            % ------------------------------------------------- Update
variables
            %disp('Updating variables...'),
            %disp(' '),


            % ---------------------------- Update Newton solver vector of
unknowns
            relax = 0.9;
            X = X + relax*DX;
```

```
            % -------------------------- Extract unknowns from Newton system
vector


             VSTAR1(m) = X(1);    % X1
             ALPHA1(m) = X(2);    % X2
                CL1(m) = X(3);    % X3
                 G1(m) = X(4);    % X4
            UASTAR1(m) = X(5);    % X5
            UTSTAR1(m) = X(6);    % X6
             VSTAR2(m) = X(7);    % X7
             ALPHA2(m) = X(8);    % X8
                CL2(m) = X(9);    % X9
                 G2(m) = X(10);   % X10
            UASTAR2(m) = X(11);   % X11
            UTSTAR2(m) = X(12);   % X12

        end   % ---------------------------------- END Newton solver for
VSTAR,ALPHA,CL,G at each blade section for both propellers

        % ----------------- Update unkowns not implemented in the Newton
solver
        % ---------------------------------------- Compute induced
velocities
        %The initial influence functions adjust to on-design point
         %disp('Update unkowns not implemented in the Newton solver'),
        % disp(' ')



    % ------------------- Compute tan(BetaI) for the new induced velocities
    [TANBIC1,TANBIV1] =
find_tan_BetaI(VAC1,VTC1,UASTAR1,UTSTAR1,RC1,RV1,Js1);
    [TANBIC2,TANBIV2] =
find_tan_BetaI(VAC2,VTC2,UASTAR2,UTSTAR2,RC2,RV2,Js2);
```

```
    %disp('Beginning to update {UAHIF,UTHIF,URHIF}'),
    % ------------------- Compute the vortex Horseshoe Influence Functions
    [UAHIF11,UTHIF11] = Horseshoe_self(M1    ,Z1,TANBIV1,RC1,RV1,
Hub_Flag,Rhub_oR1); % influence of 1 on 1
    [UAHIF12,UTHIF12] = Horseshoe_int( M1,M2,Z2,TANBIV2,RC1,RV2,-
Xf,Hub_Flag,Rhub_oR1); % influence of 2 on 1 (2 assumed downstream of 1)
    [UAHIF22,UTHIF22] = Horseshoe_self(M2,    Z2,TANBIV2,RC2,RV2,
Hub_Flag,Rhub_oR1);  % influence of 2 on 2
    [UAHIF21,UTHIF21] = Horseshoe_int(
M2,M1,Z1,TANBIV1,RC2,RV1,Xf,Hub_Flag,Rhub_oR1);  % influence of 1 on 2

    % disp('Done updating {UAHIF,UTHIF,URHIF}'),

     %Updating variables in the Newton Solver:




        % ------------------------------------------------ End update
variables

        % ---------------------------------------- Evaluate normalized
residuals


        % ---------------------------------------- END evaluate normalized
residuals

        ERROR=[ abs(VSTAR1-VSTAR1last   ), ...
                abs(ALPHA1-alpha1last   ), ...
                abs(CL1-CL1last         ), ...
                abs(G1-G1last           ), ...
                abs(UASTAR1-UASTAR1last ), ...
                abs(UTSTAR1-UTSTAR1last ), ...
```

```
                abs(VSTAR2-VSTAR2last   ), ...
                abs(ALPHA2-alpha2last   ), ...
                abs(CL2-CL2last         ), ...
                abs(G2-G2last           ), ...
                abs(UASTAR2-UASTAR2last ), ...
                abs(UTSTAR2-UTSTAR2last )];



            % ------------------------------------ Prepare for the next
iteration
        N_iter  = N_iter + 1;             % iteration in the N loop

        if N_iter-1 < 10
            disp(['The max error for iteration  ',num2str(N_iter-1),' is:
',num2str(max(abs(ERROR)))]),

        else
            disp(['The max error for iteration ' ,num2str(N_iter-1),' is:
',num2str(max(abs(ERROR)))]),

        end

        if N_iter > ITER
            disp('WARNING: While loop N1 did NOT converge.'),
        end
    end                                                 % (END WHILE LOOP
N1)

    % ================================================ END NEWTON SOLVER
    % ======================================================================

  %% Calculate forces:
```

```
  %DR1 = diff(RV1);           % (difference in rv1) / R1
  %DR2 = diff(RV2);           % (difference in rv2) / R1
  %R2oR1=R2/R1;
  %om1 =  pi/Js1;             % []om1 == omega1 * R1 / Vs
  %om2 = (pi/Js2)/R2oR1;      % []om2 == omega2 * R1 / Vs

    G1=G1';
    G2=G2';
    CD1=zeros(size(CL1));
    CD2=zeros(size(CL2));
   %Updating sectional drag coefficient for each propellers section:

     for m = 1:Mp
        [CL1(m),CD1(m)] =
CLCD_vs_ALPHA(ALPHA1(m),ALPHAstall,CL1o(m),CDo(m),dCLdALPHA);
        [CL2(m),CD2(m)] =
CLCD_vs_ALPHA(ALPHA2(m),ALPHAstall,CL2o(m),CDo(m),dCLdALPHA);
    end

    [CT1,CQ1,CP1,KT1,KQ1,EFFY1,CT2,CQ2,CP2,KT2,KQ2,EFFY2,CT ,CQ, CP, KT, KQ,
EFFY,CTH, KTH] = Off_Design_CRP_Forces(VAC1,VAC2,VTC1,VTC2,om1,om2,...

UASTAR1,UASTAR2,UTSTAR1,UTSTAR2,G1,G2,RC1,RC2,...

DR1,DR2,C1oD1,C2oD1,CD1,CD2,Z1,Z2,VMIV1,VMIV2,Hub_Flag,Rhv);




    disp(' '),
    %disp(['Forces for state:  J= ',num2str(LAMBDA_some(i)),' , Js =
',num2str(pi/LAMBDA_some(i))]),
    disp(['CT1    = ',num2str(CT1)]),
    disp(['CQ1    = ',num2str(CQ1)]),
    disp(['KT1    = ',num2str(KT1)]),
    disp(['KQ1    = ',num2str(KQ1)]),
```

```
    disp(['EFFY1 = ',num2str(EFFY1)]),
    disp(' ')
    disp(' ')
    disp(' ')
    disp(['CT2   = ',num2str(CT2)]),
    disp(['CQ2   = ',num2str(CQ2)]),
    disp(['KT2   = ',num2str(KT2)]),
    disp(['KQ2   = ',num2str(KQ2)]),
    disp(['EFFY2 = ',num2str(EFFY2)]),
    disp(' ')
    disp(' ')
    disp(['Js1 = ',num2str(Js1)]),
    disp(['Js2 = ',num2str(Js2)]),
    disp(['EFFY = ',num2str(EFFY)]),
end
```

B.2 Fuel_Consumption.m

```
%FUEL_CONSUMTION Summary of this function goes here:
%This function calculate the DDG-51 fuel consumption for the single and
%contra-rotating propeller, for each propeller you need to load the analyze
%date from the code analyzer



clc;clear all; close all
rho = 1025;                 %[Kg/m^3] Row water density.
D   = 5.1816;               %[m] propeller diameter [m] = [ft] * [0.3048 m/ft]
R   = D/2;                  %[m] Propeller Radius

%% DDG-51 data from Comparison of Powering performance Between DDG-51 and
% conventional combatant hull forms (Tsai1)

Vreq    = (12:0.5:31.5)*0.514444444;%[m/s] required ship speed
CTreq   =
[0.4198,0.4105,0.4010,0.3914,0.3822,0.3735,0.3655,0.3583,0.3519,0.3464,0.3419
,0.3382,0.3355,0.3337,0.3327,0.3327,0.3335,0.3351,
0.3376,0.3408,0.3448,0.3495,0.3550,0.3611,0.3678,0.3752,0.3832,0.3918,0.4009,
0.4106,0.4208,0.4315,0.4427,0.4543,0.4664,0.4789,...
          0.4918,0.5051,0.5188,0.5329];

Tn      = 0.5*rho.*Vreq.^2*pi*D^2/4.*CTreq;%[N]Ship required thrust
Tlbf    = Tn*0.224808;                     %[lbf]Propeller required thrust
effyr   = 0.985;                           %[]Relative efficiency for DDG-51
efftrm  = 0.95;                            %[]Transmosion efficiency
Ke      = 2;                               %number of shaft for DDG-51 Ke=2.
Kp      = 2;                               %[]Number of propellers installed.
i       = 1;                               %[] gear retio
LM      = 26250;                           %[Hp]LM2500 max brake power.

%DDG-51 Operational Profile Data(Surko 2005)
VOPF = 3:1:30;                             %[Knots] ship speed
%Operational profile
POPF = [5 2 13 2 5 3 1 10 0 5 2 3 12.5 4 4 6 3 12 0 3 0 0 3 0 3 0 0 0.5]/100;
                                           %[] Surko 2005
```

```
year = 365/2*24;                                    %[hr] number of hours in a
year(assuming deployment of 6 month a year)
time = POPF*year;                                   %[hr] Percentage time in
hours the DDG-51 stay in each speed.

%Specific fuel consumption (from Tsai)
SFCV    = 15.5:0.5:31;                              %[Knots] speeds in which
the SFC data for the DDG-52 is given (Tsai1)
SF      = [1.672478 1.570743 1.478968 1.395935 1.32055 1.251875 1.19 1.13
1.078 1.0288 0.983 0.940384 0.900511 0.863183 0.8282 0.7954 ...
          0.764657 0.735874 0.70897 0.683867 0.6605 0.638784 0.618629 0.6
0.582488 0.566 0.55069 0.53578 0.521 0.50611 0.49 0.473305];%[lbf/Shp-Hr]DDG-
52 SFC data (Tsai1)
sfc     = pchip(SFCV,SF,VOPF);                      %[lbf/Shp-Hr] DDG-52,
interpolate the given SFC data(from 15.5-31) to the all ship speed range
(12:31.5)
sfc(1:4)= 3.7;                                      %[lbf/Shp-Hr] sfc
correction for low ship speeds

%%Single propeller fuel consumption calaculation:

load('C:\Users\Eyal\Desktop\MATLAB\Last
Version\COMPARISON\Single_prop_Final(Z=3,N=120,4148).mat')
%Unpacked data structure from single propeller openprop analysis
D       =  pt.input.D;
CTsr    =  pt.states.CT;
Jsr     =  pt.states.Js;
EFFYsr  =  pt.states.EFFY;
KTsr    =  pt.states.KT;
KQsr    =  pt.states.KQ;
CQsr    =  pt.states.CQ;



%Jrsr    = interp1(CQsr,Jsr,CQpreq);                %[] Interpolate to find the
ship advance coefficient matching with the DDG-51 data.
Jrsr    = interp1(CTsr,Jsr,CTreq);                  %[] Interpolate to find the
ship advance coefficient matching with the DDG-51 data.
```

```
np      = Vreq./(Jrsr*D);                                   %[rps] The propeller
required speed which deliver the required thrust for a given ship speed
wp      = 2*pi*np;                                          %[] w=2*pi*n
KQrsr   = interp1(Jsr,KQsr,Jrsr);                           %[] Required torque
coefficient given by one propeller
CTrsr   = interp1(Jsr,CTsr,Jrsr);                           %[] Required thrust
coefficient given by one propeller
Qsr     = KQrsr.*rho.*(np).^2*D^5;                          %[N-m]Calculate required
torque given by one propeller
Nsr     = 60*np;                                            %[rpm]
Msr     = Qsr/effyr;                                        %[N-m]The real torque
behind the ship is larger then the open water torqe Q ,Q=Mreq*relative
eff(Mp>Q)
Ppsrw   = wp.*Msr/1000;                                     %[Kw] Propulsion power, the
power required by the one shaft to overcome the resistance at certain speed
Ppsrhp  = Ppsrw*1.340;                                      %[Hp] Propulsion
power,1KW=1.34hp
Pbsr    = Ppsrhp/(efftrm*Ke);                               %[Hp] Required brake power
per engine to overcome the ship resistacne at certain speed.
Pbtot1  = Pbsr*Ke*Kp;                                       %[Hp] Total ship required
brake power.(each shaft has Ke=2 engines ,with total Kp shafts)
Pbtot   = pchip(Vreq/0.5144444444,Pbtot1,VOPF);             %[Hp] Total ship required
brake power.(interpolate to 3:1:31 S for the operational profile for fuel
consumpsion calculation)

%To find the exact fuel consumption in lbs Wfsr=mf*time= sfc*Pbtot*time
MFsr=ones(size(VOPF));
for k=1:length(VOPF)
   MFsr(k)=sfc(k).*Pbtot(k).*time(k)*0.00044642857143;    %[Lton]ship fuel
consumption per year with single propeller 1lb=0.00044642857143 Lton
end

%% Calculating Fuel Consumption for the CRP CASE.
%load('C:\Users\Eyal\Desktop\Thesis\MATLAB\Last
Version\Kravitz_CRP\CR_OffDesign_FINAL.mat') % CD=0.01
load('C:\Users\Eyal\Desktop\MATLAB\Last
Version\COMPARISON\comparison_study_final_diff.mat')%CD=0.008 (This is the
file I worked in my thesys).
```

```
% Find Js2 such that EFFY is maximized for given Js1

ind = find(EFFY < 0 | EFFY > 1 | KT < 0 | KQ < 0);
KT(ind)   = NaN;
KQ(ind)   = NaN;
EFFY(ind) = NaN;

[EFFYmax,index]=max(EFFY);
Js2e=Js2(index);
Js1e=Js1;

for i=1:length(Js1)

KQe(i) = KQ(i, index(i));                    %Find the propeller
performance for the advance ratio combination which produce the best
efficiency curve.
CTe(i) = CT(i, index(i));
CQe(i) = CQ(i, index(i));
KTe(i) = KT(i, index(i));
KQ1e(i)= KQ1(i, index(i));
KQ2e(i)= KQ2(i, index(i));

end

%J1     = interp1(CQe,Js1e,CQreq);            %[] Interpolate to find the
ship for propeller advance coefficient matching with the DDG-51 data for CRP
case.
J1     = interp1(CTe,Js1e,CTreq);            %[] Interpolate to find the
ship for propeller advance coefficient matching with the DDG-51 data for CRP
case.
J2     = interp1(Js1e,Js2e,J1);              %[] Interpolate to find the
ship aft propeller advance coefficient matching with the DDG-51 data for CRP
case.
n1     = Vreq./(J1*D);                       %[rps] The for propeller
required speed which deliver the required thrust for a given ship speed
```

```
n2      = Vreq./(J2*D);                                 %[rps] The aft propeller
required speed which deliver the required thrust for a given ship speed
w1      = 2*pi*n1;                                      %[] w=2*pi*n for propeller
w2      = 2*pi*n2;                                      %[] w=2*pi*n aft propeller
CTcrp   = interp1(Js1e,CTe,J1);                         %[] Required load
coefficient given by for propeller
KQ1crp = interp1(Js1e,KQ1e,J1);                         %[] Required torque
coefficient given by for propeller
KQ2crp = interp1(Js1e,KQ2e,J1);                         %[] Required torque
coefficient given by aft propeller
Q1crp   = KQ1crp.*rho.*(n1).^2*D^5;                     %[N-m]Calculate required
torque given by one propeller
Q2crp   = KQ2crp.*rho.*(n1).^2*D^5;                     %[N-m]Calculate required
N1      = 60*n1;                                        %[rpm]
N2      = 60*n2;                                        %[rpm]
M1crp   = Q1crp/effyr;                                  %[N-m]The real torque behind
M2crp   = Q2crp/effyr;                                  %[N-m]Assuming the relative.
Ppcrpw = ((w1.*M1crp)+(w2.*M2crp))/1000;                %[Kw] Propulsion power, the
Ppcrphp= Ppcrpw*1.340;                                  %[Hp] CRP Propulsion Pbcrp
certain speed assuming trim efficiency is the same as the SR case.
Pbtcrp1= Pbcrp*Ke*Kp;                                   %[Hp] Total ship required
brake power CRP.(each shaft has Ke=2 engines ,with total Kp shafts)
Pbtcrp = pchip(Vreq/0.5144444444,Pbtcrp1,VOPF);         %[Hp] Total ship required
brake power for CRP.(interpolate to 3:1:31 S for the operational profile for
fuel consumpsion calculation)
Pbtcrp(1:4)=0.0235;                                     %[Hp] power correction
(positive the negative values
%To find the exact fuel consumption in lbs WEIGHT=mf*time= sfc*Pbtot*time
for k=1:length(VOPF)
   MFcrp(k)=sfc(k).*Pbtcrp(k).*time(k)*0.00044642857143;   %[Lton]ship fuel
consumption per year with single propeller 1lb=0.00044642857143 Lton
end
%Total fuel consumption for a 6 month deployment
Fsr  = sum(MFsr)
Fcrp = sum(MFcrp)
Fdif = Fsr-Fcrp
```

B.3 Test_Plan.m

```
%This script male the test plan for future experiments with the
%manufacturind 3 propeller sets; CRP1(13V2) and CRP2 (14V2)
close all,clear all,clc

%Load props 13v2 (Xf=0.5) and 14v2 (Xf=0.75)data
load('C:\Users\Eyal\Desktop\MATLAB\CRPv101108\ESRDC 13v2 CRP (Dm=14, Xf=0.50,
Z12=3,4)\CRP13_off_design.mat');
load('C:\Users\Eyal\Desktop\MATLAB\CRPv101108\ESRDC 13v2 CRP (Dm=14, Xf=0.50,
Z12=3,4)\CRP13_new.mat');

%Eliminate the negative values for the performance curves
ind = find(EFFYa < 0 | EFFYa > 1 | KTa < 0 | KQa < 0);

  KTa(ind) = NaN;
  KQa(ind) = NaN;
EFFYa(ind) = NaN;

% Find Js2 == Js2qs such that KQ2 == qe * KQ1 (i.e. q === KQ2/KQ1 == qe)
%   q == torque ratio Q2/Q1 == KQ2/KQ1, since
%   KQ1 == Q1 / (rho*n1^2*D1^5)
%   KQ2 == Q2 / (rho*n1^2*D1^5)   (BE CAREFUL!)

qe = 1;
Vf=[3,6,9,12];% [ft/s] Velocities of the carridge
Js1e = Js1all;
Js2e = zeros(size(Js1all));

for i = 1:NJ1

    Js2l = min(Js2all(:));
    Js2r = max(Js2all(:));
    Js2c = 0.5*(Js2l+Js2r);

    while Js2r - Js2l > 0.0001

        if     interp1(Js2a(i,:),KQ2a(i,:),Js2c) < qe *
interp1(Js2a(i,:),KQ1a(i,:),Js2c)
               Js2r = Js2c;
        elseif interp1(Js2a(i,:),KQ2a(i,:),Js2c) > qe *
interp1(Js2a(i,:),KQ1a(i,:),Js2c)
               Js2l = Js2c;
        else
            break
        end
              Js2c = 0.5*(Js2l+Js2r);
    end
              Js2e(i) = Js2c;
end
%Initialyzing the propeller performance characteristics
 KQ1e = zeros(size(Js1all));
 KQ2e = zeros(size(Js1all));
  KQe = zeros(size(Js1all));
 KT1e = zeros(size(Js1all));
 KT2e = zeros(size(Js1all));
```

```
  KTe = zeros(size(Js1all));
EFFYe = zeros(size(Js1all));

for i = 1:NJ1
    KQ1e(i) = interp1(Js2a(i,:),KQ1a(i,:),Js2e(i));
    KQ2e(i) = interp1(Js2a(i,:),KQ2a(i,:),Js2e(i));
     KQe(i) = interp1(Js2a(i,:), KQa(i,:),Js2e(i));
     T1e(i) = interp1(Js2a(i,:),KT1a(i,:),Js2e(i));
    KT2e(i) = interp1(Js2a(i,:),KT2a(i,:),Js2e(i));
     KTe(i) = interp1(Js2a(i,:), KTa(i,:),Js2e(i));
   EFFYe(i) = interp1(Js2a(i,:), EFFYa(i,:),Js2e(i));
end

%Plotting the off design states with equal moment Kq1=Kq2

figure(1), hold on, grid on, box on,
%On design point
plot(Js1,KQ,'.')
xlabel('Js1'), ylabel('KQ')
%off design curves for different Js2
plot(Js1a,KQa,'k')
%Curve for points where Kq1=Kq2
plot(Js1e,KQe,'.m')

figure(2), hold on, grid on,box on
%plot(Js1,KQ,'.')
xlabel('Js1'), ylabel('KQ1 red.KQ2 blue')
%off design curves for different Js2
plot(Js1a,KQ1a,'r')
plot(Js1a,KQ2a,'b')
%Curve for points where Kq1=Kq2
plot(Js1e,KQ1e,'.m')


%%Finding the model test matrix (lay out)
%% Design experiment:

rhom = 1000;          % [kg/m^3] model water density
Tmax = 100 * 4.448 ; % [N]  max allowable thrust
Qmax = 8.75;          % [Nm] max allowable torque  (max continuous is 8.75 N-
m, peak is a bit less than 30 (limited by the drive) )
NVf  = length(Vf);
Vm   = Vf/3.2808;     % [m/s]

for i=1:NJ1
    for j=1:NVf
nm1(i,j) = Vm(j)/(Js1e(i)*Dm); % [RPM]
nm2(i,j) = Vm(j)/(Js2e(i)*Dm); % [RPM]
Tm1(i,j) = KT1e(i) * rhom * Dm^4 * nm1(i,j).^2; % [N]
Tm2(i,j) = KT1e(i) * rhom * Dm^4 * nm2(i,j).^2; % [N]
Qm1(i,j) = KQ1e(i) * rhom * Dm^5 * nm1(i,j).^2; % [N-m]
Qm2(i,j) = KQ1e(i) * rhom * Dm^5 * nm2(i,j).^2; % [N-m]
    end
end
Nm1  = 60*nm1;          % [RPM]
Nm2  = 60*nm2;          % [RPM]
```

```
Nrel = Nm1+Nm2;
Tm   = Tm1 + Tm2;
Qm   =(Qm1 + Qm2)/2;
Tm_lb = Tm * 0.2248;    % [lb]
Qm_lb = Qm / 1.3558;    % [ft-lb]

for i = 1:NJ1
    for j = 1:NVf
        if (Tm(i,j)< 0) || (Tm(i,j) > 2*Tmax)
            Nm1(i,j)   = NaN;
            Nm2(i,j)   = NaN;
            Nrel(i,j)  = NaN;
            Tm(i,j)    = NaN;
            Qm(i,j)    = NaN;
            Tm_lb(i,j) = NaN;
            Qm_lb(i,j) = NaN;
        end
    end
end
Js1e
Js2e
Nm1
Nm2
Nrel
Tm
Tm_lb
Qm
Qm_lb

REm = VmALL*(0.2311*Dm).*(sqrt(pi*0.7./JmALL+1))/10^-6;

% ---------------------------------------- Output experimental test plan
b=length(find(Qm <= Qmax)); % number of experiments
```

Appendix C – Naval propellers properties

	4119			4381			4148		
r/R	c/D	t/D	t/c	c/D	t/D	t/c	c/D	t/D	t/c
0.20	0.3200	0.0658	0.2056	0.1740	0.0434	0.2494	0.1600	0.0329	0.2056
0.30	0.3625	0.0563	0.1553	0.2290	0.0358	0.1562	0.1818	0.0282	0.1551
0.40	0.4048	0.0478	0.1181	0.2750	0.0294	0.1068	0.2024	0.0239	0.1181
0.50	0.4392	0.0396	0.0902	0.3120	0.0240	0.0768	0.2196	0.0198	0.0902
0.60	0.4610	0.0321	0.0696	0.3370	0.0191	0.0566	0.2305	0.0160	0.0694
0.70	0.4622	0.0250	0.0541	0.3470	0.0146	0.0421	0.2311	0.0125	0.0541
0.80	0.4347	0.0183	0.0421	0.3340	0.0105	0.0314	0.2173	0.0091	0.0419
0.90	0.3613	0.0120	0.0332	0.2800	0.0067	0.0239	0.1806	0.0060	0.0332
0.95	0.2775	0.0090	0.0324	-	-	-	0.1387	0.0045	0.0324
1.00	0.0020	0.0000	0.0000	-	-	-	0.0010	0.0000	0.0000

After
modification:

1.00	0.0250	0.0029	0.1143	0.0250	0.0029	0.1143	0.0250	0.0029	0.1143

The blade thickness and chordlength tip modification were made for better printing the propeller models (3D printing).This is the reason for dissimilarity of the propeller maximum predicted efficiencies between the propeller before and after this change.

Appendix D – DDG-51 operational profile

Ship speed [knt]	Traveling time [%]	Ship speed [knt]	Traveling time [%]
3	5.0%	**17**	4.0%
4	2.0%	**18**	6.0%
5	13.0%	**19**	3.0%
6	2.0%	**20**	12.0%
7	5.0%	**21**	0.0%
8	3.0%	**22**	3.0%
9	1.0%	**23**	0.0%
10	10.0%	**24**	0.0%
11	0.0%	**25**	3.0%
12	5.0%	**26**	0.0%
13	2.0%	**27**	3.0%
14	3.0%	**28**	0.0%
15	12.5%	**29**	0.0%
16	4.0%	**30**	0.5%